Ph.D. Dissertation of Medicine

Study on mechanisms of cell-cycle arrest and apoptosis induced by *Toxoplasma gondii* dense granule protein 16 (GRA16) in cancer cells

암세포에서 톡소포자충 과립 단백질 16 (GRA16)이 유도하는 세포주기 억제와 세포사멸에 대한 기전 규명 연구

February 2023

Graduate School of Medicine
Seoul National University College of Medicine
Tropical Medicine and Parasitology

Seung-Hwan Seo

Study on mechanisms of cell-cycle arrest and apoptosis induced by *Toxoplasma gondii* dense granule protein 16 (GRA16) in cancer cells

Doctoral advisor: Professor Eun-Hee Shin

Submitting a Ph.D. Dissertation of Medicine

October 2022

Graduate School of Medicine
Seoul National University College of Medicine
Tropical Medicine and Parasitology

Seung-Hwan Seo

Confirming the Ph.D. Dissertation written by Seung-Hwan Seo

January 2023

Chair _____(Seal)

Vice Chair _____(Seal)

Examiner _____(Seal)

Examiner _____(Seal)

Examiner _____(Seal)

Abstract

Study on mechanisms of cell-cycle arrest and apoptosis induced by *Toxoplasma gondii* dense granule protein 16 (GRA16) in cancer cells

Seung-Hwan Seo
Department of Tropical Medicine and Parasitology
The Graduate School
Seoul National University College of Medicine

Anticancer research focused on the mechanisms induced by parasites is a novel approach to enhancing the anticancerous therapeutic effects. Based on previous studies, the relationship between parasites and cancer is unclear. *Toxoplasma gondii* (*T. gondii)* is one of the anticancer parasites and has been shown to inhibit cancer growth; however, the mechanisms involved have not yet been elucidated. Based on the previous studies, *T. gondii* and *T. gondii* lysate antigens inhibit cancer growth, and *T. gondii* dense granule protein 16 (GRA16) binds to Herpesvirus Associated Ubiquitin Specific Protease (HAUSP) and Protein Phosphatase 2A-regulatory subunit B55 (PP2A-B55) in the host cells. Therefore, I selected GRA16 as a crucial protein for studies evaluating the anticancer effect and analyzed the signaling mechanisms that could inhibit cancer growth when GRA16 was expressed in various cancer cells. First, it was demonstrated that GRA16 in hepatocellular carcinoma cells (HepG2) inhibited the proliferation of cancer cells by binding to HAUSP, increasing Phosphatase and TENsin homolog (PTEN) nuclear localization and P53 activity, and inhibiting p-AKT(S473). Second, in non-small cell lung carcinoma cells (H1299), GRA16 activated PP2A-B55 and inhibited p-AKT(T308). Also, GRA16 inhibited NF-kB nuclear translocation. Furthermore, the NF-kB inhibition of GRA16 supplemented the efficacy of a commercially available anticancer drug (Irinotecan), and the anticancer effects were further increased when GRA16 and

irinotecan were used in combination. Based on the above results, it was identified that GRA16 in cancer cells could induce cell-cycle arrest and apoptosis via the HAUSP/PTEN/AKT/P53 and PP2A-B55/AKT/NF-kB pathways, thereby increasing the sensitivity of anticancer drugs. In cancer cells, AKT increases the activity of hTERT, a catalytic subunit of telomerase, allowing the perpetual growth of cancer cells. Two previous studies allowed me to focus on how GRA16 inhibited AKT. Third, I confirmed how GRA16 can regulate the expression and activity of hTERT and how it affects telomere shortening before apoptosis. In colorectal carcinoma cells (HCT116), GRA16 inhibited hTERT expression and phosphorylation, inhibited telomerase activity, and induced telomere shortening. Using target protein/gene inhibition (protein inhibitor and siRNA gene silencing), I revealed that the central mechanism regulating hTERT expression and activity of GRA16 is HAUSP/PTEN/AKT/STAT3/E2F1/c-Myc pathway. Through these studies, I found that *T. gondii*-derived GRA16, which binds to HAUSP and PP2A-B55, regulates PTEN, NF-kB, AKT, and hTERT in cancer cells and induces cell-cycle arrest, telomere shortening, and apoptosis. I suggested that these findings may reveal a novel role of GRA16 in host cancer cells.

*** This dissertation is based on the previously published articles.**

1. Seung-Hwan Seo, et al. (2020) *International Journal of Molecular Sciences*, 21.18: 6642.
2. Seung-Hwan Seo, et al. (2022) *Biomedicine & Pharmacotherapy*, 153: 113366.

Keyword : *Toxoplasma gondii* GRA16, PTEN, NF-kB, AKT, hTERT, Anticancer effect

Student Number : 2018-32737

Contents

Abstract i

Content iii

List of Figures iv

List of Tables vi

Abbreviations vii

1. Introduction 1

2. Materials & Methods 6

3. Results 21

3.1. Study−I. Inhibitory effect of *Toxoplasma gondii* GRA16 on host NF−kB pathway and parasitic enhancement of anticancer effect in combination with drug. 21

3.2. Study−II. Telomerase inhibition and telomere shortening of *Toxoplasma gondii* GRA16 in cancer cell 47

4. Discussion 81

5. Bibliography 87

Abstract in Korean 92

List of Figures

Study-I. Inhibitory effect of *Toxoplasma gondii* GRA16 on host NF-kB pathway and parasitic enhancement of anticancer effect in combination with drug

Figure 1. Ectopic expression of GRA16 in H1299 cells and confirmation of binding between GRA16 and PP2A-B55.

Figure 2. Anticancer effect in xenograft mice transplanted with H1299 GRA16 cells.

Figure 3. IC_{50} determination of irinotecan in H1299 cells and its effects on NF-kB pathway and chemoresistance markers.

Figure 4. Inhibition of GWL and CyclinB1 and dephosphorylation of ENSA, AKT, and ERK by the augmentation of PP2A-B55 in H1299 GRA16 cells.

Figure 5. Effects of GRA16 and irinotecan on the induction of apoptosis and cell-cycle arrest in H1299 cells.

Figure 6. NF-kB inhibition induced by GRA16 in H1299 cells regardless of irinotecan treatment.

Figure 7. LB-100 (PP2A inhibitor) reversed the reduced cell viability, AKT dephosphorylation, and NF-kB inactivation induced in H1299 GRA16 cells.

Study-II. Telomerase inhibition and telomere shortening of *Toxoplasma gondii* GRA16 in cancer cell

Figure 8. Production of GRA16 expressing HCT116 cells and expression of signaling molecules involved in hTERT transcription and decrease in hTERT-expression and -phosphorylation in HCT116 GRA16 cells.

Figure 9. Increase in the nuclear localization of PTEN and decrease in the nuclear localization of NF-kB p65 in HCT116 GRA16 cells.

Figure 10. Comparison of DNA damage (γ-H2A.X-stained nucleus),

nucleus size, and telomerase activity among the experimental groups of HCT116 cells.

Figure 11. Cell-cycle arrest and apoptosis were increased in HCT116 GRA16 cells.

Figure 12. Identification of signaling pathway to induce hTERT inactivation in HCT116 GRA16 cells using inhibitors of PTEN and PP2A-B55 (SF1670 and LB-100, respectively).

Figure 13. Changes in hTERT-related signaling molecules in HCT116 GRA16 cells transfected with PTEN siRNA or PP2A-B55 siRNA.

Figure 14. Increase in DNA damage (γ-H2A.X-stained nucleus) and inactivation of hTERT in *T. gondii*-infected HCT116 cells.

Figure 15. Summary of this study.

List of Tables

Table 1. Primer sequences used in conventional PCR and real-time qPCR.

Table 2. Antibodies used in immunofluorescence and western blotting.

Abbreviations

ABCG2: ATP binding cassette super family G member 2
ARHGEF7: Rho guanine nucleotide exchange factor 7
ATP5A1: ATP synthase F1 subunit alpha
BAX: BCL-2 associated x protein
BCL-2: B cell lymphoma-2
BRCA1: Breast cancer type 1
CDC2: Cell division cycle 2
c-Myc: Cellular-myelocytomatosis
CIN: Chromosomal instability
CITED2: Cbp/p300 interacting transactivator 2
COPD: Chronic obstructive pulmonary disease
CRC: Colorectal cancer
CREB1: CAMP responsive element binding protein 1
CTCF: CCCTC binding factor
CTNNAL1: Catenin alpha like 1
DSBs: Double stranded DNA breaks
ENSA: Endosulfine alpha
ERK: Extracellular signal regulated kinase
E2F1: E2 promoter binding factor 1
FACS: Fluorescenc activated cell sorting
FOXO3A: Forkhead box class O 3A
GADD45A: Growth arrest and DNA damage inducible alpha
γ-H2A.X: Gamma-histone 2A family member X
GAPDH: Glyceraldehyde 3 phosphate dehydrogenase
GRA16: Granule protein 16
GWL: Greatewall
HA: Hemagglutinin
HAUSP: Herpesvirus associated ubiquitin specific protease
HCC: Hepatocellular carcinoma
HIF-2α: Hypoxia inducible factor-2 alpha
hTERT: Human telomerase reverse transcriptase
IgG: Immunoglobulin G
IkBα: Inhibitor of kappa B alpha
IKKβ: Inhibitory kappa B kinase beta
IL-12: Interleukin-12
MAD1: Mitotic arrest deficient 1
MDM2 : Mouse double minute 2
MIC: Macrophage inhibitory cytokine
MyD88: Myeloid differentiation primary response 88
MYR1: Myc regulation 1
NF-kB: Nuclear factor-kappa light chain enhancer of activated B
NOXA: Phorbol-12-myristate-13-acetate induced protein 1

NSCLC: Non-small cell lung cancer
PCR: Polymerase chain reaction
PI: Propidium iodide
PI3K: Phosphoinositide 3 kinase
PKCα: Protein kinase C alpha
POT1: Protection of telomeres 1
PP2A-B55: Protein phosphatase 2A-regulatory subunit B55
PTEN: Phosphatase and tensin homolog
PV: Parasitophorous vacuole
PVM: Parasitophorous vacuole membrane
PUMA: P53 upregulated modulator of apoptosis
P21: Cyclin dependent kinase inhibitor 1A (= CDKN1A)
RAP1: Repressor activator protein 1
ROP: Rhoptry protein
RTA: Relative telomerase activity
SIRT3: Sirtuin3
SP-1: Specificity protein-1
STAT3: Signal transducer and activator of transcription 3
TELO2: Telomere maintenance 2
TFAP4: Transcription factor activating enhancer binding protein 4
TIN2: TRF1 interacting nuclear factor 2
T. gondii: *Toxoplasma gondii*
Topo-I: Topoisomerase-I
TRF1: Telomeric repeat binding factor 1
Wnt3A: Wnt family member 3A

1. Introduction

Recently, studies on the relationship between parasites and cancer have been increasing. Therefore, understanding how these parasites activate or inactivate oncogenesis in humans could serve as novel strategies for anticancer research and drug development [1]. In this study, I introduced the characteristics of *Toxoplasma gondii* (*T. gondii)*, a parasite that suppresses cancer, and molecules derived from *T. gondii* that control the host cells. Although they have not yet been identified, I introduced a new molecule that can induce cancer cell suppression through this study.

T. gondii is an apicomplexa belonging to protozoa, with a feline as its final host. It is known to regulate various biological processes, including chronic immune and metabolic mechanisms in the host cells, through infection [2]. *T. gondii* is a widespread parasite that infects several animal species, including mammals and birds, and causes diseases in warm-blooded hosts, including domestic animals and humans [3]. During host cell invasion by *T. gondii*, three types of secretory organelles, micronemes, rhoptries, and dense granules, participate in establishing a successful infection in the host cell by discharging several secretory proteins [4]. Organelle proteins with high pathogenicity and immunogenicity are secreted from micronemes, rhoptries, and dense granules in two infective stages of *T. gondii*, namely tachyzoites and bradyzoites, as previously explained in a systematic review on *T. gondii* antigens [5]. Macrophage inhibitory cytokine (MIC)1 and MIC5 as microneme antigens; rhoptry protein (ROP)5, ROP8, ROP16, ROP17, ROP19, ROP38, and ROP48 as rhoptry antigens; and GRA2, GRA4, GRA10, GRA12, and GRA15 as dense granule antigens are expressed in two infection stages, and they have pathogenicity and strong immunogenicity in the host cell cytoplasm [5]. In addition, some dense granule proteins secreted by *T. gondii* can cross the parasitophorous vacuole membrane (PVM) and migrate into the host nucleus (GRA16, GRA24, and GRA28). These granule proteins regulate host cell immunity, signaling, and invasion mechanisms [6].

In the host cell nucleus, GRA24 activates myeloid differentiation primary response 88 (MyD88)-independent p38 mitogen-activated protein kinase (MAPK) and triggers the production of interleukin-12 (IL-12), which induces host protective immune response [7]. Meanwhile, GRA28 is released by the Myc regulation 1 (MYR1) secretory pathway and cooperates with the host chromatin remodeling machine in the host cell nucleus to promote the chemotactic migration of infected macrophages [8]. Unlike other GRAs, I discovered a new biological activity of GRA16, which will be discussed in this study. In brief, GRA16 binds to herpes virus-associated ubiquitin-specific protease (HAUSP) and protein phosphatase 2A B55 regulatory subunit (PP2A-B55) in host cells, which are essential components in the cell proliferation and cell-cycle regulation [9].

Cancer is initiated, progressed, and suppressed by various chemical, physiological, biological, and environmental factors [10]. Recently, Statistics Korea has reported that the cancer mortality rates in Korea since 2016 are the highest in the order of lung cancer, liver cancer, and colon cancer [11]. Based on these statistics, while various anticancer treatment methods are being developed, the anticancer effects of parasites are also attracting attention [12].

In particular, preclinical studies have reported that *T. gondii* has a cancer-suppressing effect by inhibiting the development of cancer tumors and the formation of new blood vessels, which are essential elements for cancer proliferation and metastasis [13]. *T. gondii* is a new approach to research on anticancer and more detailed research is required to discover anticancer-inducing molecules and to identify the anticancer mechanisms of the molecules [14-16]. According to a recent study, GRA8 is phosphorylated by protein kinase Cα (PKCα) in colorectal cancer cells and binds to SIRTuin3/ATP synthase F1 subunit alpha (SIRT3/ATP5A1) in mitochondria to induce deacetylation of ATP5A1. It regulates the activity of mitochondria and induces metabolic resuscitation that contributes to antiseptic activity in vivo, thereby increasing the

antitumor activity of colon cancer cells [17].

Based on the previous studies, I chose *T. gondii* GRA16 as a potential suppressor for cancer. HAUSP and PP2A-B55 are essential molecules that regulate the activation and suppression of cancer cells, and *T. gondii* GRA16 can bind them, but how GRA16 regulates them has not yet been identified [9]. HAUSP deubiquitinates the tumor suppressor phosphatase and tensin homolog (PTEN) and promotes localization from the nucleus to the cytoplasm of PTEN. HAUSP increases degradation and limits the transcriptional activity of PTEN and P53 [18-20]. Therefore, negative regulation of HAUSP, which is highly expressed in cancer cells, is essential for therapeutic intervention for tumor suppression [21, 22]. PP2A-B55 is a serine/threonine phosphatase that plays an essential role in cell-cycle regulation as a gatekeeper of exit in mitotic entry [23]. PP2A-B55 deficiency is highly associated with poor prognosis of cancer [23]. Since PP2A regulates nuclear factor-kappa light chain enhancer of activated B (NF-kB), a transcriptional factor activated in cancer cells, therapeutic strategies targeting PP2A are becoming increasingly important [24, 25]. The properties of these two molecules provide a rationale for GRA16's ability to modulate the activity and suppression of various cancer cells. In a previous study, together with Kim, S.G. (co-first author) and colleagues, I investigated the effects of GRA16 on HAUSP/PTEN/P53 and the anticancer mechanism using *nf-kb* null hepatocellular carcinoma cells (HepG2) [26]. In this study, I investigated the anticancer mechanism of GRA16 related to PP2A-B55/NF-kB, using *p53* null non-small cell lung cancer cells (H1299). Finally, I used colorectal carcinoma cells (HCT116) to elucidate the role and mechanism of GRA16 on telomerase, which induces telomere length maintenance and increases cancer cell viability. In a previous study, the HepG2 cells are *hausp* and *p53* gene wild-type but have gene deficiency for *relA (p65)* and *p50*, constitute NF-kB. Therefore, the NF-kB signaling pathway function according to the binding of PP2A-B55 is impossible [9, 27]. Based on the information, HepG2 was selected as a suitable

cell for analyzing the regulatory mechanism through binding to HAUSP in HepG2 cells according to GRA16 expression, and the mechanism of action of GRA16 and HAUSP was analyzed using the corresponding cancer cells regardless of the binding of GRA16 and PP2A-B55 [26]. When GRA16 was expressed in HepG2 cells, it was confirmed that it binds to HAUSP, and cell viability and proliferation were reduced by GRA16 expression [26]. In addition, with the increase in PTEN expression, which occurs when HAUSP is suppressed, the distribution of PTEN in the nucleus is significantly increased. Accordingly, it was confirmed that the expression of tumor suppressor P53 increased [26]. This phenomenon resulted from an increase in cancer cell apoptosis according to the action of GRA16 and a decrease in tumor size in the cancer cell transplantation mice [26]. Through this, I demonstrated that GRA16 inhibits the function of HAUSP by binding to HAUSP in cancer cells and increases the distribution of PTEN in the nucleus, thereby inducing stabilization of P53 and inhibiting the cancer activator protein kinase B (AKT), eventually promoting the death of cancer cells [26].

Following the previous studies that confirmed the anticancer effects of *T. gondii* GRA16 via the HAUSP/PTEN/P53/AKT pathway, in study-I, I examined the changes in essential factors related to PP2A-B55 when GRA16 binds to PP2A-B55, another binding protein different from HAUSP, and compared it with commercially available anticancer drug (Irinotecan) that has a different anticancer mechanism. Through these results, I suggested establishing a new anticancer mechanism related to GRA16/PP2A-B55 and irinotecan. In the following study (study-II), among the two signaling pathways of GRA16, the central signaling pathway that directly regulates activated telomerase and maintains telomere length in cancer cells was identified. Through this study, I focused on P53, NF-kB, AKT, and telomerase, essential factors regulating cancer activity. I showed that *T. gondii* GRA16 could trigger cancer cell-cycle arrest and apoptosis by stabilizing PTEN, activating P53 via the GRA16/HAUSP/AKT pathway and inhibiting NF-kB via the

GRA16/PP2A-B55/AKT pathway. In addition, it was confirmed that these effects could supplement the efficacy of commercially available anticancer drugs. In cancer cells, positive regulation of PTEN and PP2A-B55 by GRA16 induced AKT inactivation. AKT increases telomerase activity, which causes continuous cancer cell proliferation, and it was newly identified that GRA16 inhibits telomerase and shortens telomere length via AKT inhibition. This mechanism is induced via the GRA16/HAUSP/PTEN pathway. These data suggested that GRA16 has potential anticancer effects via PTEN activation, NF-kB inactivation, and hTERT inactivation and that GRA16 can complement the efficacy of anticancer drugs.

2. Materials & Methods

2.1. Cell Culture

The human non-small cell lung cancer (NSCLC) H1299 cell was purchased from ATCC (Manassas, VA, USA). The human colorectal cancer (CRC) HCT116 cell and human foreskin fibroblast (HFF) cell were purchased from Korean Cell Line Bank (Seoul, Korea). Retrovirus packaging Platinum-A cell was purchased from Cell Biolabs (San Diego, CA, USA). H1299 cell and HCT116 cell were cultured in complete RPMI 1640 medium (WELGENE Inc., Gyeongsan, Korea). HFF cell and Platinum-A cell were cultured in high glucose DMEM medium (WELGENE Inc.). All medium were contained 10% fetal bovine serum (FBS; WELGENE Inc.) and 1% antibiotic-antimycotic solution (WELGENE Inc.) at 37℃ in a 5% CO_2 incubator.

2.2. *Toxoplasma gondii*

T. gondii RH strain was purchased from ATCC (Manassas). The *T. gondii* was serially passaged in HFF cells before infecting HCT116 cells. The multiplicity of infection (MOI) of *T. gondii* tachyzoites to HCT116 cells was determined 10:1 (MOI10) for appropriate dose of cell infection.

2.3. Plasmid and transfection

T. gondii gra16 gene (1,518 bp) (ToxoDB database, Gene ID: TGGT1_208830) harboring the restriction sites for *EcoRI (GAATTC)* and *SalI (GTCGAC)* was amplified by PCR using the cDNA of *T. gondii* RH strain. The sequence of each primer is listed in Table 1. PCR was performed under the following conditions: 95℃ for 5 min, followed by 35 cycles at 95℃ for 30 s, 58℃ for 40 s, and 72℃ for 1.5 min, and a final extension at 72℃ for 3 min. pBABE-HAII-*gra16* plasmid was constructed by cloning *gra16* gene into pBABE-HAII retroviral vector (Addgene, Watertown, MA, USA). The PCR product of *gra16* gene and pBABE-HAII plasmid (Addgene) were digested using restriction enzymes (*EcoRI* and

SalI) and ligated with T4 DNA Ligase (Sigma-Aldrich, St. Louis, MO, USA). The pBABE-HAII-*gra16* plasmid was confirmed by gene sequencing (Cosmogenetech Co. Ltd., Seoul, Korea). Retrovirus packaging cells (Platinum-A) (Cell Biolabs) were transfected with either pBABE-HAII plasmid vector only or pBABE-HAII-*gra16* plasmid using a Lipofectamine 3000 transfection kit (Life Technologies, Carlsbad, CA). Supernatants containing *gra16* gene expressing retrovirus were centrifuged at 2,000 rpm for 10 min at 4℃ and filtered (0.45 μm). To produce a stably GRA16 expressing cancer cells (H1299 or HCT116) supernatants of *gra16* expressing retrovirus were treated with 1 μg/ml of polybrene (Santa Cruz Biotechnology, Santa Cruz, CA, USA) and incubated for 48 h. After then, 2 μg/ml of puromycin (Santa Cruz Biotechnology) was treated to select only vector or GRA16 expressing cells. The *gra16* gene expression in H1299 cells or HCT116 cells was analyzed by PCR using pBABE-HAII vector only primers or *gra16* gene specific primers, including the primer sequences listed in Table 1. Total RNA was extracted using HiGene™ Total RNA Prep Kit (BIOFACT, Daejeon, Korea) and cDNA was reverse-transcribed using Reverse-Transcription Master Premix Kit with oligo d(T)15 primers (ELPIS Biotech, Daejeon, Korea). The cDNA was used in PCR to validate *gra16* gene expression using SureCycler 8800 Thermal Cycler (Agilent Technologies, Santa Clara, CA, USA). PCR products were visualized by 1% agarose gel electrophoresis using the Gel Doc XR+ Gel Documentation System (Bio-Rad Laboratories, Hercules, CA, USA).

2.4. Determination of half maximal inhibitory concentration (IC_{50}) using chemicals

In Study-I experiment, to determine the IC_{50} values of irinotecan (CPT-11; LC Laboratories, Woburn, MA, USA) and LB-100 (Selleckchem, Houston, TX, USA), 3×10^3 of starved H1299 cells were incubated for 24 h in RPMI 1640 medium containing 10% FBS. Subsequently, irinotecan or LB-100 was added at concentrations of 0-100 μM, and the cells were incubated for 48 h.

In Study-II experiment, to determine the IC_{50} values of SF1670 (Selleckchem) and LB-100 (Selleckchem), 1×10^4 of starved HCT116 cells were incubated for 24 h in RPMI 1640 medium containing 10% FBS. SF1670, LB-100, or both (SF1670 and LB-100) was added to the cells at various concentrations of 0-100 μM, and then the cells were incubated for 48 h. All cell viabilities were investigated using the CCK-8 assay (Dojindo, Rockville, MD, USA). 10 μL of CCK-8 was added to each well and incubated for 1 h at 37℃. Optical density was measured at 450 nm using the Infinite M200 PRO microplate reader (Tecan, Männedorf, ZH, Switzerland). The IC_{50} value of each chemical was calculated using GraphPad Prism 5 (GraphPad, San Diego, CA, USA).

2.5. Cell viability and proliferation

In Study-I experiment, after starving the H1299 cells in RPMI 1640 medium containing 1% FBS, 3×10^3 of cells were seeded and incubated for 0, 24, 48, and 72 h. Cell viability was analyzed using the CCK-8 assay. Optical density was measured at 450 nm using Infinite M200 PRO microplate reader (Tecan). Also, to investigate cell numbers, 1×10^4 of H1299 stable cells were seeded and incubated for 0, 24, 48, and 72 h. At each time point, cell numbers were monitored by counting using Trypan Blue solution (Sigma-Aldrich) and hemocytometer (Paul Marienfeld, Lauda-Königshofen, Germany).

In Study-II experiment, HCT116 cells in each experimental group were starved in RPMI 1640 medium containing 1% FBS. To investigate cell viability, 1×10^3 HCT116 stable cells were seeded and incubated for 0, 24, 48, 72, 96, and 120 h. Optical density was measured at 450 nm by Infinite M200 PRO microplate reader (Tecan) using CCK-8 assay kit. To investigate cell numbers, 1×10^4 of HCT116 stable cells were seeded and incubated for 0, 24, 48, 72, 96, and 120 h. At each time point, cell numbers were monitored by counting using Trypan Blue solution (Sigma-Aldrich) and hemocytometer (Paul Marienfeld).

2.6. Real-Time qPCR

For real-time qPCR, total RNA from each H1299 stable cells HCT116 stable cells were extracted using the HiGene™ Total RNA Prep Kit (BIOFACT) and reverse-transcribed to cDNA using Reverse-Transcription Premix (Elpis Biotech). The primer sequences are listed in Table 1. Real-time qPCR was performed using the CFX96 Touch Real-Time PCR Detection System (Bio-Rad Laboratories) with TOPreal™ qPCR 2X PreMIX (SYBR Green with low ROX) (Enzynomics, Daejeon, Korea). Amplification reactions were performed under the following conditions: 95℃ for 15 min, followed by 40 cycles at 95℃ for 20 s, 59℃ for 20 s, and 72℃ for 30 s. SYBR green fluorescent signals were analyzed using the iQTM5 optical system software (Bio-Rad Laboratories). In inhibitors (SF1670, LB-100, or Both) treated HCT116 GRA16 cells, the relative expression of target genes was compared to that of the nontreated GRA16 cells group after normalizing to Ct values of *GAPDH*. Other relative expressions of target genes were compared to that of the control group (H1299 control cells or HCT116 control cells) after normalizing to Ct values of *GAPDH*.

2.7. Western Blotting

Total proteins from cells were extracted using the M-PER™ mammalian protein extraction reagent (Thermo Fisher Scientific, Waltham, MA, USA), and cytoplasmic and nuclear fractions of cells were extracted using the NE-PER™ nuclear and cytoplasmic extraction reagent (Thermo Fisher Scientific). The extracted proteins were quantified using the Pierce™ BCA protein assay kit (Thermo Fisher Scientific). Each protein was separated by 10% SDS-PAGE gel at 110 V for 1.5 h at room temperature (RT) and transferred on to PVDF membrane (Merck Millipore, Burlington, MA, USA)at 100 V for 1 h at 4℃ or cold condition using Mini Trans-Blot® electrophoretic transfer cell instrument (Bio-Rad Laboratories). The membranes were blocked with 5% BSA in TBS-T (Tris-buffered saline with 0.1% Tween-20) for 1 h at RT. The blocked membranes were incubated with primary antibodies for 16

h at 4℃. The primary antibodies were listed in Table 2. Next, the membranes were washed three times with TBS-T and incubated with horseradish peroxidase (HRP) conjugated secondary antibodies for 1 h at RT. Target proteins on the membrane were visualized using Pierce™ ECL western blotting substrate (Thermo Fisher Scientific). The images were captured using Amersham Imager 600 (GE healthcare, Chicago, IL, USA), and signal intensities were calculated using ImageJ (Free software provided by the National Institutes of Health).

2.8. Cell-cycle analysis via fluorescence activated cell sorting (FACS)

In Study-I experiment, FACS analysis was used to analyze cell-cycle transitions. For cell-cycle analysis, the H1299 cells were starved in RPMI1640 medium containing 1% FBS and were fixed with ice-cold 70% ethanol. The fixed cells were stored at -20℃ for 24 h. After washing with PBS, propidium iodide (PI) solution including 50 μg/mL of PI (Sigma-Aldrich), 3.8 mM sodium citrate (Sigma-Aldrich), and 100 μg/mL of RNase A (Sigma-Aldrich) was added to the cells and incubated for 20 min in dark condition at RT. Cell-cycle phases were analyzed using FACS Calibur-P (Becton Dickinson, Franklin Lakes, NJ, USA). Data were acquired by linear amplification of FL2-A and analyzed for proportions of cells in the Sub-G_1, G_1, S, and G_2/M phases using BD CellQuest (Becton Dickinson). The cell-cycle FACS data were visualized using the FlowJo 7.6.2 software.

In Study-II experiment, cell-cycle using HCT116 cells was analyzed at the 5th passage intervals during 20 passages. The experimental passages are P1, P5, P10, P15, and P20. Denomination for passage was determined as P1 when 2×10^5 cells were seeded in 100 mm cell culture dishes and cultured for 3 days to reach 90% confluence. The analysis of cell-cycle FACS was performed using BD FACSCanto™II (Becton Dickinson) in the same method as described above. The sequential phases of cell-cycle (sub-G_1, G_1, S, and G_2/M phase) were analyzed using the BD

FACSDiva Software (Becton Dickinson). The cell-cycle FACS data were visualized using the FlowJo 7.6.2 software.

2.9. Apoptosis analysis via fluorescence activated cell sorting (FACS)

In Study-I experiment, FACS analysis was used to analyze apoptosis transitions. For apoptosis analysis, H1299 cells were incubated for 72 h in RPMI 1640 medium containing 10% FBS. The cells were harvested and resuspended with 100 μL of annexin V binding buffer (BD Pharmingen, Holbrook, NJ, USA), followed by staining with both annexin V-APC (Biolegend, San Diego, CA, USA) and 50 μg/mL of PI solution (BD Pharmingen). The cells were incubated for 20 min at RT in the dark condition. The apoptosis FACS was analyzed using FACS Calibur-P (Becton Dickinson). Data were analyzed based on the proportions of cells in annexin V-APC (X-axis) and PI (Y-axis) using BD CellQuest (Becton Dickinson). The apoptosis FACS data were visualized using the FlowJo 7.6.2 software.

In Study-II experiment, apoptosis FACS using HCT116 cells was analyzed. The HCT116 cells at the experimental time line of passage were harvested and resuspended in 200 μL of annexin V binding buffer (BD Pharmingen). Followed by staining with both annexin V-APC (BioLegend) and 50 μg/mL of PI solution (Sigma-Aldrich) for 20 min at RT in the dark condition. The apoptosis FACS was analyzed using FACS Calibur-P (Becton Dickinson). Data were analyzed based on the proportions of cells in annexin V-APC (X-axis) and PI (Y-axis) using BD CellQuest (Becton Dickinson). The apoptosis FACS data were visualized using the FlowJo 7.6.2 software.

2.10. Immunofluorescence

5×10^3 of H1299 stable cells or HCT116 stable cells were seeded and incubated for 24 h. The cells were fixed with 4% paraformaldehyde solution for 10 min at RT gently shaking. After washing with PBS, the cells were permeabilized with

permeabilization solution (PBS with 0.2% Triton X-100) for 15 min at RT gently shaking. Next, the cells were incubated with blocking buffer (PBS with 0.1% Tween-20, 1% bovine serum albumin (BSA), and 22.52 mg/mL glycine) for 1 h at RT. After washing with PBS-T (PBS with 0.1% Tween-20), followed by staining with target specific primary antibody (PBS with 0.1% Tween-20, 1% BSA, and 1:200 diluted primary antibody) for 16 h at 4℃. The primary antibodies are listed in Table 2. After washing with PBS-T, the cells were stained with fluorescent conjugated secondary antibody (PBS with 0.1% Tween-20, 1% BSA, and 1:1,000 diluted secondary antibody) for 1 h at RT in the dark condition. The secondary antibodies are listed in Table 2. After washing with PBS-T, the cells were stained with 5 μg/mL of Hoechst 33342 (Sigma-Aldrich) for 5 min at RT in the dark condition. After washing with PBS-T, each experimental cell group was visualized under a DE/DMI6000B inverted fluorescence microscope (Leica, Wetzlar, HE, Germany).

2.11. Nucleus size measurements

In Study-II experiment, 1×10^5 of HCT116 cells were seeded and incubated for 48 h. After washing with PBS, 5 μg/mL of Hoechst 33342 (Sigma-Aldrich) was added to the cells and incubated for 10 min at RT in dark condition. After washing, immunofluorescence images were visualized under a DE/DMI6000B inverted fluorescence microscope (Leica). The pixel area of each nucleus was tracked and the size was measured using ImageJ.

2.12. Telomere length measurement by qPCR

In Study-II experiment, using the DNeasy® Blood & Tissue Kit (QIAGEN, Hilden, NW, Germany), total genomic DNA from the each HCT116 cell group was extracted. For telomere length measurement using real-time qPCR, primer sequences for telomere (*Tel1* and *Tel2)* and for single-copy gene (*36B4u* and *36B4d)* were designed as described previously [28]. The primer sequences are listed in Table 1. Real-time qPCR was performed using the

CFX96 Touch Real-Time PCR Detection System (Bio-Rad Laboratories) with TOPreal™ qPCR 2X PreMIX (SYBR Green with low ROX) (Enzynomics). First, for the qPCR using telomere primers (*Tel1* and *Tel2)*, the following reaction protocol was followed: 95℃ for 10 min and then 40 cycles of 95℃ for 15 s and 54℃ for 2 min. Second, for the real-time qPCR using single-copy gene primers (*36B4u* and *36B4d)*, the reaction conditions were 95℃ for 10 min and then 40 cycles of 95℃ for 15 s and 58℃ for 1 min. The relative telomere length was measured by comparison of the ratio (T/S) of telomere (T) to single-copy gene (S). The relative T/S ratio (T/S of control sample relative to the T/S of vector or GRA16 sample) is $2^{-\Delta\Delta Ct}$, and $\Delta\Delta Ct = (\Delta Ct^{Telomere} - \Delta Ct^{36B4})$.

2.13. Telomerase activity

In Study-II experiment, telomerase activity was performed using the TeloTAGGG™ telomerase PCR ELISA kit (Roche Diagnostics, Basel, BS, Switzerland). 1×10^5 cells in each experimental group were seeded and incubated for 48 h. Total proteins of the cells were extracted and quantified using the Pierce™ BCA Protein Assay Kit (Thermo Fisher Scientific). 5 μg of the total proteins was transferred into a PCR tube containing 25 μL of the reaction mixture. 5 μg of the positive control cell extract was used as a positive control. For the negative control, 5 μg the total proteins were incubated with 1 μg of RNaseA (NucleoGen, Siheung, Korea) for 20 min at 37℃. Next, sterile water was added to the PCR tubes for adjusting the total volume to 50 μL. PCR was performed under the following conditions: 25℃ for 20 min, 94℃ for 5 min, 30 cycles of 94℃ for 30 s, 50℃ for 30 s, and 72℃ for 1.5 min, and a final extension step of 72℃ for 10 min using the SureCycler 8800 Thermal Cycler (Agilent Technologies). 5 μL of the PCR product was transferred to a new tube containing 20 μL of denaturation reagent and incubated for 10 min at RT. 225 μL of hybridization buffer was added to the tube. Then, 100 μL of the solution was transferred to a precoated microplate well and incubated for 2 h at 37℃ with shaking. After washing, 100 μL of

anti-DIG-POD working solution was added to each well and incubated for 30 min at RT with shaking. After another washing, 100 μL of TMB substrate solution was added and incubated for 20 min at RT. Color development was stopped using 100 μL of stop solution, and absorbance was measured at 450 nm using the Infinite M200 PRO microplate reader (Tecan). The RTA of each sample was calculated using the following formula: RTA = $(A_S - A_{S,0}) / (A_{TS8} - A_{TS8,0}) \times 100$. A_S means absorbance of vector or GRA16 sample. $A_{S,0}$ means absorbance of RNase A-treated vector or GRA16 sample. A_{TS8} means absorbance of control sample. $A_{TS8,0}$ means absorbance of RNaseA (NucleoGen) treated control sample.

2.14. RNA interference (siRNA)-induced gene silencing

In Study-II experiment, GRA16 expressing HCT116 cells (GRA16 stable cells) were seeded at 2×10^5 cells and incubated for 24 h. Then, the cells were transfected with control siRNA (Santa Cruz Biotechnology), PTEN siRNA (Santa Cruz Biotechnology), or PP2A-B55 siRNA (Santa Cruz Biotechnology) using the Lipofectamine 3000 transfection kit (Life Technologies) and Opti-MEM medium (Life Technologies). After 48 h of transfection, total cell proteins were extracted using M-PER™ Mammalian Protein Extraction Reagent (Thermo Fisher Scientific), and concentration of each protein were quantified using the Pierce™ BCA Protein Assay Kit (Thermo Fisher Scientific). After gene silencing, the expressions of PTEN and PP2A-B55 protein were analyzed by western blotting.

2.15. Xenograft tumor formation of GRA16 expressing cancer cells

In Study-I experiment, to induce tumor formation, after 1 week of acclimatization of 5 weeks old BALB/c nude athymic mice (Orient Bio Inc., Seongnam, Korea), 2×10^6 of H1299 cells in 100 μL PBS were mixed with 100 μL Corning Matrigel Basement Membrane Matrix, Phenol Red-free, LDEV-free (Corning, NY, USA). The mixture was subcutaneously injected into the flank of each mouse.

After 12 days, mouse weight and tumor size of the experimental groups (Control, Vector, and GRA16) (n = 16 each group) were measured once every 4 days. At day 44 after transplantation, the mice were sacrificed and tumor sizes were measured. Tumor volumes were calculated as $A \times B^2/2$ mm^2. 'A' means length and 'B' means width [29].

2.16. Ethics Statement

All animal experiments were approved by the Institutional Animal Care and Use Committee (IACUC) at Seoul National University (Approved Number SNU-190603-2). Mice were maintained in an animal facility according to the standards of the Animal Protection Act and the Laboratory Animal Act in Korea. Also, all mice experiments were conducted according to global standards, such as those established by the Association for Assessment and Accreditation of Laboratory Animal Care International. Cloning of *T. gondii gra16* gene using pBABE-HAII plasmid and subsequent retrovirus transduction were performed at biosafety level 2 (BL-2) with the approval of the Institutional Biosafety Committee (IBC) of Seoul National University (Aapproval number SNUIBC-R180523-1).

2.17. Statistical Analysis

In Study-I experiments, one-way analysis of variance (ANOVA) followed by Dunnett's multiple-comparison test was conducted for the data analysis of time-dependent expressions of mRNA and protein in irinotecan treated H1299 cells. Also, One-way ANOVA followed by Turkey's multiple-comparison test was conducted for the data analysis of real-time qPCR and western blotting in experimental groups of H1299 cells (Control, vector, and GRA16). Two-way ANOVA followed Bonferroni post-hoc comparison test was conducted for the data analysis of cell-cycle FACS, apoptosis FACS, cell viability, cell proliferation, and mouse xenograft. All experimental data were expressed as mean ± standard deviation (SD). Significance was indicated as follows: #

Significant difference at each time point after irinotecan treatment ($p < 0.05$). * Significant at $p < 0.05$ between H1299 control cells and H1299 GRA16 cells; † Significant at $p < 0.05$ between H1299 vector cells and H1299 GRA16 cells.

In Study-II experiments, one-way ANOVA followed by Bonferroni post hoc comparison test was conducted for the data analysis of real-time qPCR, western blotting, TRAP assay, and measurement of nucleus size in experimental groups of HCT116 cells (Control, Vector, and GRA16). Two-way ANOVA followed by Bonferroni post hoc comparison test was conducted for the data analysis of cell viability, cell proliferation, cell-cycle FACS, apoptosis FACS, and telomere length measurement using real-time qPCR in experimental groups of HCT116 cells. One-way ANOVA followed by Dunnett's multiple comparison test was conducted for the data analysis of real-time qPCR and western blotting in HCT116 GRA16 cells treated with inhibitors (SF1670 and LB-100) and western blotting of *T. gondii*-infected HCT116 cells. One-way ANOVA followed by Bonferroni post hoc comparison test was conducted for the data analysis of western blotting using siRNA-transfected HCT116 GRA16 cells. Nucleus size measurement data were presented as mean ± standard error (SE). Other experimental data were expressed as mean ± SD. Significance was indicated as follows: * Significant at $p < 0.05$ between HCT116 control cells and HCT116 GRA16 cells; † Significant at $p < 0.05$ between HCT116 vector cells and HCT116 GRA16 cells. § Significant at $p < 0.05$ between noninfected HCT116 control cells and *T. gondii*-infected HCT116 control cells at 24 h time point; ¶ Significant at $p < 0.05$ between uninfected HCT116 cells and *T. gondii*-infected HCT116 control cells at 48 h time point; ‡ Significant at $p < 0.05$ between nontreatment and SF1670 treatment, LB-100 treatment, or treatment with both inhibitors in HCT116 GRA16 cells; and ** Significant at $p < 0.05$ between control siRNA and PTEN siRNA or PP2A-B55 siRNA in HCT116 GRA16 cells.

Table 1. Primer sequences used in conventional PCR and real-time qPCR

Gene	Forward primer sequence	Reverse primer sequence
gra16	ATGTATCGAAACCACTCAGGG	TCACATCTGATCATTTTTCCGC
pBABE-HA II-gra16	CGGAATTCCGATGTATCGAAACCACTCA	CCGTCGACTCACATCTGATCATTTTTCC
pBABE-HA II-Vector	GAGTCGATGTGGAATCCGAC	GGCTTAGGGTGTACAAAGGG
TRF1	ACAGCGCAGAGGCTATTATTC	GAACCCCAAATCATCAGGGC
TRF2	TATGTCCAAGGACCCCACAAC	AGGCAGCGGACTCAGATTTC
TIN2	GGAAGTATAAGGGTCCATACCAGA	GAGGTGAGAGCAAGCAAAGAG
POT1	TGTTTCCGTGTTGATGATGTG	TGGCACCTTTGGACCTCTAC
RAP1	TCGACTCTGTTCGTGAGGGA	CCAGGATGTACTGCGTGGAG
TPP1	GGCAGCTGCTTGAGGTACTA	GGAGATAGAACTCTGCGGGC
HIF-2a	CTGTATGGTCAGCTCAGCCC	GGCTGTCAGACCCGAAAAGA
MAD1	ACTTCATCTCTCAGCGTGTGG	CTGGATGAGGTGGGACTTCG
SP-1	TCATCCGGACACCAACAGTG	TGTTTGGGCTTGTGGGTTCT
c-Myc	CCCTCCACTCGGAAGGACTA	GCTGGTGCATTTTCGGTTGT
CTCF	GTGGTTCACAGCAGCCCTTA	AACATGTGACAGTTCATGTGCAA
β-Catenin	TCTGAGGACAAGCCACAAGATT	TGGGCACCAATATCAAGTCCAA
PP2A-B55	AGCCGGCGCCATTTTGAAAG	GCCGGCAGGATGCTAGATTT
GADD45A	CACTGTCGGGGTGTACGAAG	GTTGATGTCGTTCTCGCAGC
P21	TCCTCATCCCGTGTTCTCCT	CACCCTGCCCAACCTTAGAG
P27	TAAGGAAGCGACCTGCAACC	AGCAAGCTCTTCATACCCCG
Wee1	ACTGAACAATGGGCCTCGTC	CGATCAGGGCGGGACAATTA
CyclinB1	GGTTGTTGCAGGAGACCATGT	GTGCTGCATAACTGGAAGAAGAGA
CDC2	CTGGGGTCAGCTCGTTACTC	TCCACTTCTGGCCACACTTC
FOXO3A	GGAGCAGATTAGTAGGCGGC	CCTCAGCGCCATGGAAAATG
TELO2	CCCGCAGAGATCGTGGATG	CATGTCGTAGGGGACAAACTC
CDC25C	CTCCAGGCTTGAGCTAGGTT	GCAACGTTTTGGGGTTCCTC
HAUSP	GGATACACCAGGGCGAGCAT	TTACCGGGCTGTGGCTCAAA
MDM2	AGGAATCATCGGACTCAGGTACATC	CAGATTTGTGGCGTTTTCTTTGTCG

Table 1. Primer sequences used in conventional PCR and real-time qPCR (Continued)

Gene	Forward primer sequence	Reverse primer sequence
BCL-2	ACTGAGGAGCTTTGTTTCAACCAAG	GCCACGTAAAGCAACTCTCTAAAGG
Survivin	AGTCCCTGGCTCCTCTACTG	TGAAGGTTGGGCTGACAGAC
Wnt3A	AATTTGGAGGAATGGTCTCTCGG	CAGCAGGTCTTCACTTCACAG
PTEN	CCAGTCAGAGGCGCTATGTG	TCGTGTGGGTCCTGAATTGG
P53	CATCTACAAGCAGTCACAGCACATG	AGTCTTCCAGTGTGATGATGGTGAG
PUMA	GTACAATCTCATCATGGGACTCCTG	GAGCACAGGATTCACAGTCTG
NOXA	GATTTCTTCGGTCACTACACAACGT	AGTCTACTGATTTACTGGCCCCAAG
BAX	CTTTTGCTTCAGGGTTTCATCCAGG	ATCCTCTGCAGCTCCATGTTACTG
GAPDH	GGTGAAGTCGGAGTCAACGGA	GAGGGATCTCGCTCCTGGAAGA
Tel1/2	GGTTTTTGAGGGTGAGGGTGAGGGTGAGGGTGAGGGT	TCCCGACTATCCCTATCCCTATCCCTATCCCTATCCCTA
36B4u/d	CAGCAAGTGGGAAGGTGTAATCC	CCCATTCTATCATCAACGGGTACAA

Table 2. Antibodies used in immunofluorescence and western blotting

Primary antibody	Source	Cat. No.
Toxoplasma gondii (TP3)	Santa Cruz Biotechnology	sc-52255
CyclinB1	Santa Cruz Biotechnology	sc-7393
IKKβ	Santa Cruz Biotechnology	sc-271782
IkBα	Santa Cruz Biotechnology	sc-1643
Phospho-IkBα (Ser_{32})	Santa Cruz Biotechnology	sc-8404
GWL	Abcam	ab169767
ENSA	Santa Cruz Biotechnology	sc-81883
Phospho-ENSA (Ser_{67}/Ser_{62})	Affinity	AF4381
Phospho-ERK1/2 (Thr_{202}/Tyr_{204})	Enzo Life Sciences	ADI-900-098
ERK1/2	Enzo Life Sciences	ADI-KAP-MA001-F
γ-H2A.X (Ser_{139})	Abcam	ab11174
HA tag (GRA16)	Santa Cruz Biotechnology	sc-7392
PP2A-B55	Santa Cruz Biotechnology	sc-365282
HAUSP	Abcam	ab264422
c-Myc	Santa Cruz Biotechnology	sc-40
PTEN	Santa Cruz Biotechnology	sc-7974
Phospho-PTEN (Ser_{380}/$Thr_{382/383}$)	Santa Cruz Biotechnology	sc-377573
P53	Santa Cruz Biotechnology	sc-126
Phospho-P53 (Ser_{15})	Abcam	ab1431
NF-kB p65	Cell Signaling Technology	#8242
Phospho-NF-kB p65 (Ser_{536})	Cell Signaling Technology	#3033S
STAT3	Santa Cruz Biotechnology	sc-8019
Phospho-STAT3 (Tyr_{705})	Cell Signaling Technology	#9131
AKT	Cell Signaling Technology	#9272
Phospho-AKT (Ser_{473})	Cell Signaling Technology	#9271
Phospho-AKT (Thr_{308})	Cell Signaling Technology	#9275
E2F1	Santa Cruz Biotechnology	sc-193

Table 2. Antibodies used in immunofluorescence and western blotting (Continued)

Primary antibody	Source	Cat. No.
hTERT	GenTex	GTX124242
Phospho-hTERT (Ser_{824})	Abcam	ab63558
β-Actin	Santa Cruz Biotechnology	sc-47778
Lamin B	Santa Cruz Biotechnology	sc-6217
Secondary antibody	**Source**	**Cat. No.**
m-IgG_K BP-HRP	Santa Cruz Biotechnology	sc-516102
Goat anti-Mouse IgG (H+L)-HRP	Santa Cruz Biotechnology	sc-2005
Donkey anti-Goat IgG (H+L)-HRP	Santa Cruz Biotechnology	sc-2020
Chicken anti-Rabbit IgG (H+L)-HRP	Santa Cruz Biotechnology	sc-2357
Goat anti-Rabbit IgG (H+L)-HRP	Invitrogen	32460
Donkey anti-Rabbit IgG (H+L)-Alexa Fluor 488	Invitrogen	A-21206
Goat anti-Mouse IgG (H+L)-Alexa Fluor 546	Invitrogen	A-11030
Donkey anti-Mouse IgG (H+L)-Alexa Fluor 594	Invitrogen	A-21203

3. Results

3.1. Study-I. Inhibitory effect of *Toxoplasma gondii* GRA16 on host NF-kB pathway and parasitic enhancement of anticancer effect in combination with drug.

3.1.1. GRA16 expressing H1299 cells and binding of GRA16 and PP2A-B55

The *gra16* gene incorporated into the pBABE-HAII retroviral vector plasmid was transfected into the H1299 cells (Figure 1A). Using western blotting, the GRA16 protein expression was confirmed in the nucleus and cytoplasm of the H1299 cells (H1299 GRA16 cells). GRA16 was detected more in the nucleus than in the cytoplasm of H1299 cells (Figure 1B). The increased PP2A-B55 in H1299 GRA16 cells was supported by the change in the mRNA levels of transcriptional factors of PP2A-B55, including cAMP responsive element binding protein 1 (CREB1), stable protein 1 (SP1), and transcription factor activating enhancer binding protein 4 (TFAP4) (Figures 1C and 1D). The expression levels of CREB1 and SP1, which promote transcription of PP2A-B55, were significantly increased in the H1299 GRA16 cells (Figure 1D). The expression levels of TFAP4, which downregulate transcription of PP2A-B55, were significantly decreased in the H1299 GRA16 cells (Figure 1D). The red fluorescence images of PP2A-B55 protein expression in the H1299 stable cells (control, vector, and GRA16) at 48 h (Figure 1E). H1299 GRA16 cells showed high PP2A-B55 protein expression during the 60 h study period; the GRA16 protein expression was maintained (Figures 1F-1H). Also, the co-immunoprecipitation (Co-IP) assay showed a sustained binding between GRA16 and PP2A-B55 in H1299 GRA16 cells (Figure 1I).

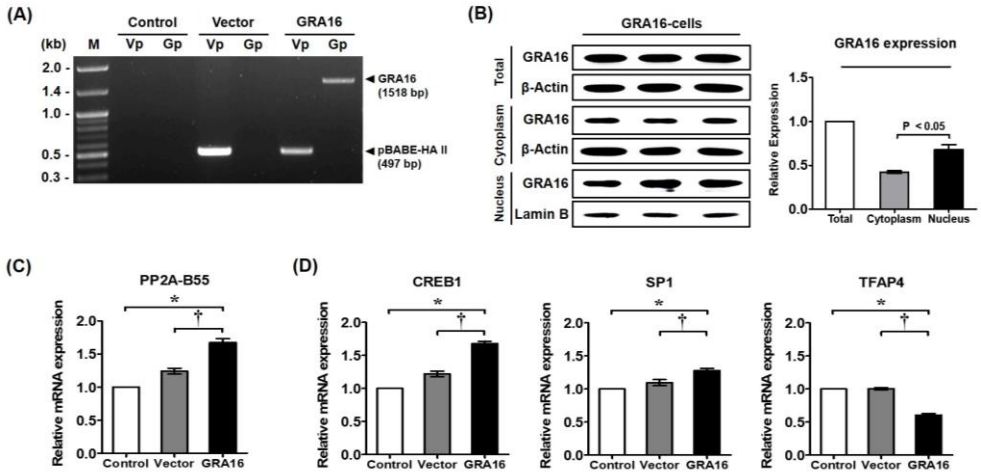

Figure 1. Ectopic expression of GRA16 in H1299 cells and confirmation of binding between GRA16 and PP2A-B55. (A) PCR result of cells (Control, Vector, and GRA16) using primers Vp (Vector primer) and Gp (GRA16 primer). (B) Western blots showing GRA16 distribution in cell fractions (Cytoplasm and nucleus) and relative GRA16 protein expression between the cytoplasm and nucleus. (C) Relative mRNA expression levels of PP2A-B55. (D) Expression of the transcriptional factor genes (*CREB1, SP1,* and *TFAP4*) in vector and GRA group compared with control group. Differences in PP2A-B55 expression among control, vector, and GRA16 group, with the expression value of control set at "1". * Significant at $p < 0.05$ between control and GRA16 group; † Significant at $p < 0.05$ between vector and GRA16 group.

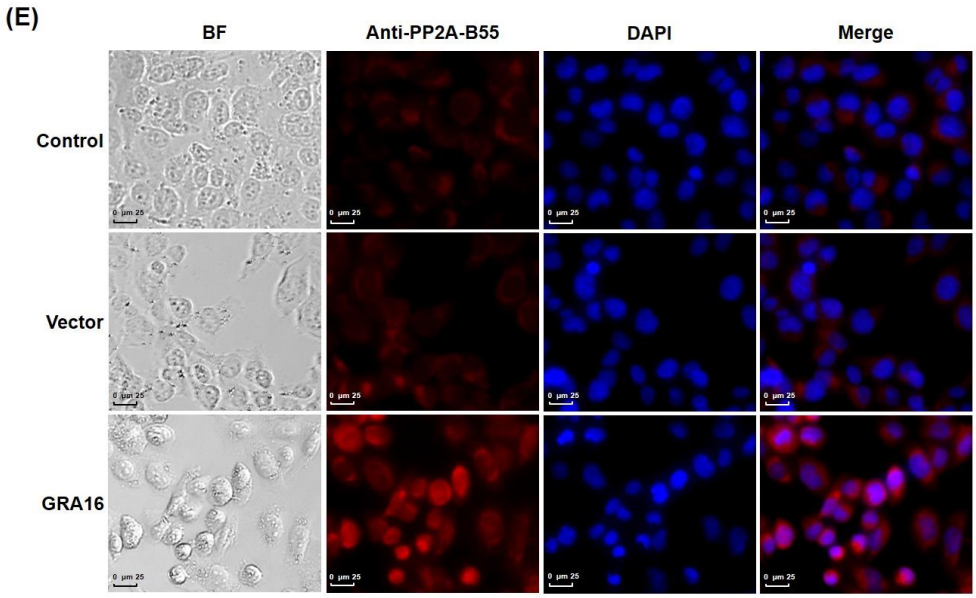

Figure 1. (Continued) Ectopic expression of GRA16 in H1299 cells and confirmation of binding between GRA16 and PP2A-B55. (E) Immunofluorescence assay (IFA) for PP2A-B55 expression in control, vector, and GRA16 cells. BF: bright field, DAPI: nucleus staining. Scale bar represents 25 μm.

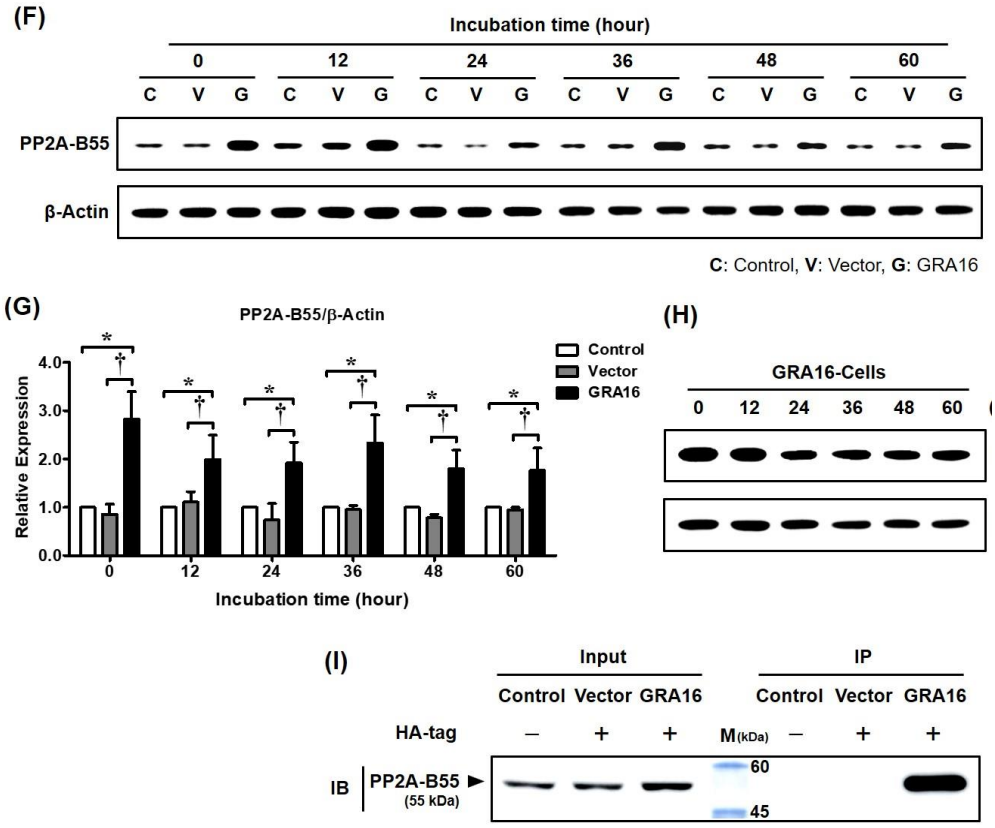

Figure 1. (Continued) Ectopic expression of GRA16 in H1299 cells and confirmation of binding between GRA16 and PP2A-B55. (F) Western blot showing PP2A-B55 expression in control, vector, and GA16 group during 60 h after cell synchronization. (G) Differences in PP2A-B55 expression among control, vector, and GRA16 group, with the expression value of control set at "1". (H) Western blots confirming sustained GRA16 expression in H1299 GRA16 cells during the 60 h experiment period. (I) Co-immunoprecipitation (Co-IP) confirming the interaction between GRA16 and PP2A-B55. Input: immunobinding of PP2A-B55 in total protein before Co-IP analysis; IP: Western blots stained with anti-PP2A-B55 Ab for the protein fraction (GRA16) extracted using anti-HA tag Ab at 48 h of cell incubation. Differences in PP2A-B55 expression among control, vector, and GRA16 group, with the expression value of control set at "1". * Significant at $p < 0.05$ between control and GRA16 group; † Significant at $p < 0.05$ between vector and GRA16 group.

3.1.2. Changes of tumor growth in xenograft mouse model

To determine whether GRA16 expression had an anticancer effect, tumor growth and body weight changes in xenograft mouse models were monitored for 44 days. Mouse xenografts with H1299 control and H1299 vector cells showed a progressive increase in tumor volume and weight. However, the tumor volume and weight of mouse xenografts with H1299 GRA16 cells were significantly lower than those of mouse xenografts with H1299 control and H1299 vector cells (Figures 2A–2D).

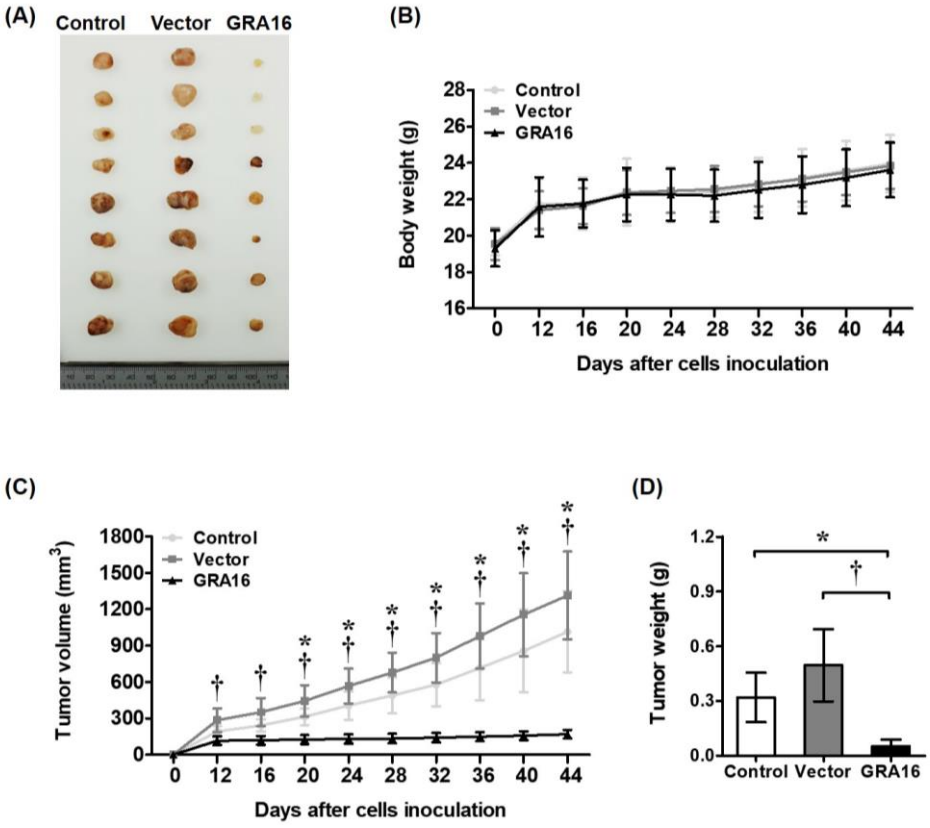

Figure 2. Anticancer effect in xenograft mice transplanted with H1299 GRA16 cells. (A) Images of tumors in control, vector, and GA16 group transplantation to xenograft model mice. (B) Tumor sizes (tumor volumes were calculated as A × $B^2/2$ (A: length; B: width)). (C) Body weights. (D) Tumor weights. * Significant at $p < 0.05$ between control and GRA16 group; † Significant at $p < 0.05$ between vector and GRA16 group.

3.1.3. Effect of irinotecan treatment on the NF-kB signaling pathway and drug resistance markers in H1299 cells

To determine if GRA16 can be used as a complement for the anticancer drug to block NF-kB-mediated chemoresistance, we examined the chemoresistance of irinotecan, as reflected by NF-kB activation (Figure 3). The half-maximal inhibitory concentration (IC_{50}) of irinotecan was 16.64 ± 1.31 μM (Figures 3A and 3B). Therefore, the concentration for treatment was determined to be 17 μM. Using irinotecan, the NF-kB pathway-related protein or phosphorylation levels were examined, including inhibitory kappa B kinase beta (IKKβ), ratios of phospho-inhibitor of kappa B alpha (p-IkBα), and translocation of NF-kB from the cytoplasm to the nucleus (Figures 3C and 3D). Irinotecan treatment increased the levels of IKKβ and p-IkBα but simultaneously maintained the nucleus localization of NF-kB p65 (Figure 3D). This result suggested that irinotecan does not inhibit NF-kB nucleus translocation. Moreover, the expression levels of resistance markers related to the augmentation of NF-kB activation, such as Cbp/p300 interacting transactivator with Glu/Asp rich carboxy-terminal domain 2 (CITED2), ATP-binding cassette subfamily G member 2 (ABCG2), and catenin alpha-like 1 (CTNNAL1), increased over time following irinotecan treatment (Figure 3E). However, the expression levels of breast cancer susceptibility gene 1 (BRCA1), a tumor suppressor gene related to NF-kB inhibition, were decreased following irinotecan treatment (Figure 3E). These results suggested that the anticancer effects of irinotecan are limited because it does not affect NF-kB activity, which may be a fundamental reason for chemoresistance to irinotecan.

(A)

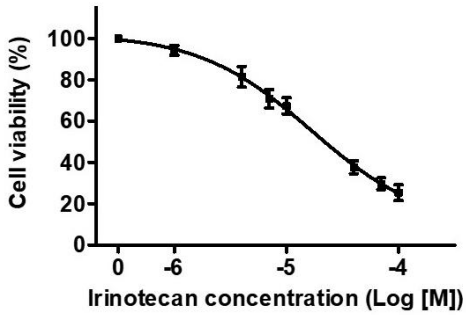

(B)

Cell	IC_{50} ± SD (μM)
Control	16.64 ± 1.306

Figure 3. IC_{50} determination of irinotecan in H1299 cells and its effects on NF-kB pathway and chemoresistance markers. (A) When cells were treated with 0-100 μM of irinotecan, the viability (%) decreased in an irinotecan concentration-dependent manner. (B) IC_{50} value of irinotecan was 16.64 μM and I determined concentration for treatment as 17 μM.

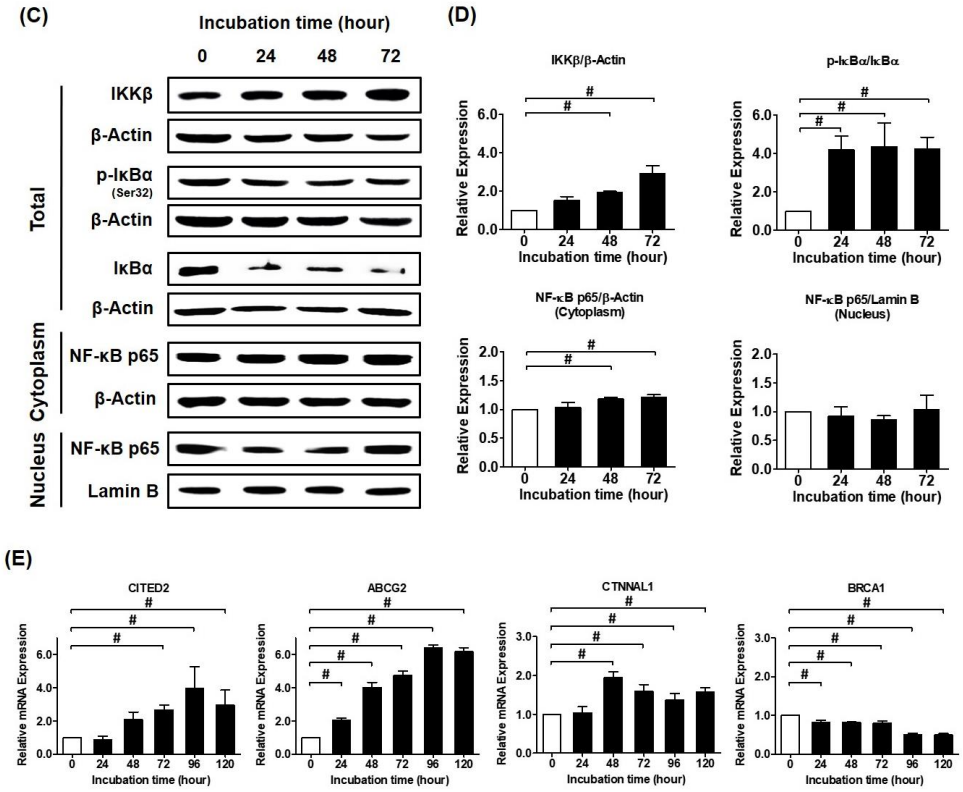

Figure 3. (Continued) IC_{50} of irinotecan in H1299 cells and its effects on NF-kB pathway and chemoresistance markers. (C) Proteins expression of IKKβ, p-IkBα, and NF-kB p65 after treatment with 17 μM irinotecan. (D) Relative protein expressions of IKKβ, p-IkBα, and NF-kB p65 (cytoplasm and nucleus) compared with those before treatment. (E) Changes in chemoresistance factors (CITED2, ABCG2, and CTNNAL1) and sensitivity (BRCA1) after irinotecan treatment. # Significant difference at each time point after irinotecan treatment ($p < 0.05$).

3.1.4. GRA16 regulates cell-cycle arrest and apoptosis via the PP2A-B55/GWL/ENSA pathway and CyclinB1, AKT and ERK dephosphorylation

Increased PP2A-B55 expression levels in H1299 GRA16 cells are required for Greatwall (GWL) dephosphorylation, leading to Endosulfine Alpha (ENSA) dephosphorylation. When activated, GWL induces ENSA phosphorylation, which inhibits PP2A-B55 activity via direct interaction. In these results, increased PP2A-B55 levels were followed by reduced GWL protein levels in the H1299 GRA16 cells (Figures 4A and 4B). Following the cascade reaction, ENSA phosphorylation significantly decreased in the H1299 GRA16 cells (Figures 4A and 4B), possibly leading to maintained PP2A-B55 activity and mitosis inhibition. The G_2/M-specific CyclinB1 is necessary for entry into mitosis. As key regulators of PP2A-B55 activity, GWL and ENSA expression and protein levels were inhibited by GRA16 but not by irinotecan (Figures 4C and 4D). CyclinB1 expression was reduced irrespective of irinotecan treatments in GRA16 cells (Figures 4A and 4C). The decrease in cyclinB1 expression was higher with GRA16 and irinotecan than with GRA16 alone (Figures 4B and 4D). Phosphorylated AKT and ERK signaling promote cellular survival and inhibit apoptosis. These processes are essential regulatory hallmarks of cancers and are required for unregulated cell growth. Therefore, the PP2A-mediated regulation of AKT and ERK is likely a central mechanism to the anticancer effects of GRA16. As expected, H1299 GRA16 cells showed decreased p-AKT(T308) (Figures 4E-4H). However, p-ERK was not changed by GRA16 alone (Figures 4E and 4F) but was decreased by the synergistic action of GRA16 and irinotecan (Figures 4G and 4H). These molecular signals indicated that GRA16, which augments PP2A protein expression, showed an anticancer effect via a decrease in cell survival and an increase in G_2/M arrest in H1299 GRA16 cells.

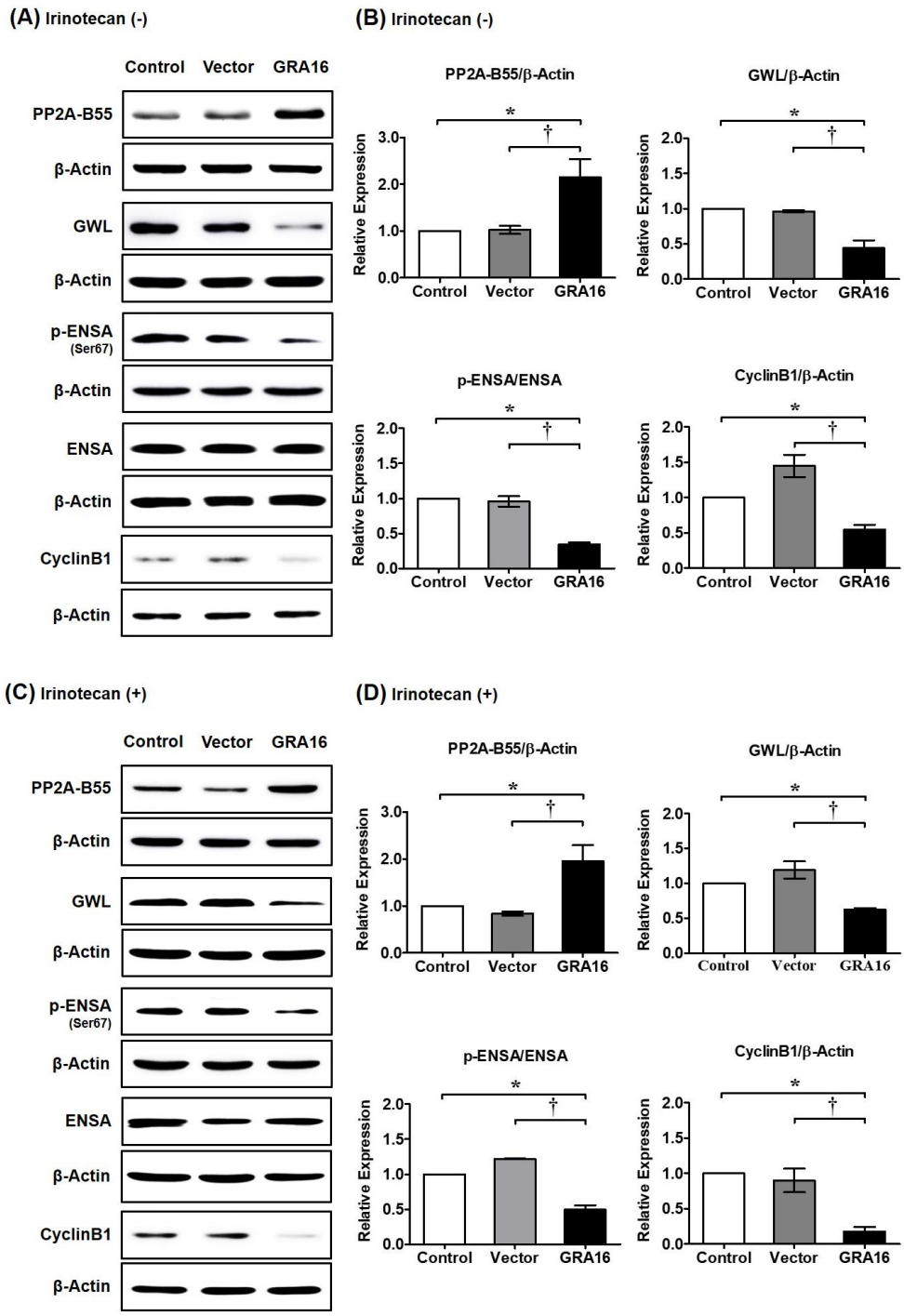

Figure 4. Inhibition of GWL and CyclinB1 and dephosphorylation of ENSA, AKT, and ERK by the augmentation of PP2A-B55 in H1299 GRA16 cells. (A) Proteins expression of PP2A-B55, GWL, p-ENSA, and CyclinB1 in cells without irinotecan treatment. (B)

Relative expression levels of these proteins in vector and GRA16 group compared with control group. (C) Expression levels of each protein under irinotecan treatment compared with those in (A). (D) Relative expression levels of these proteins under irinotecan treatment compared with those in (B). * Significant at $p < 0.05$ between control and GRA16 group; † Significant at $p < 0.05$ between vector and GRA16 group.

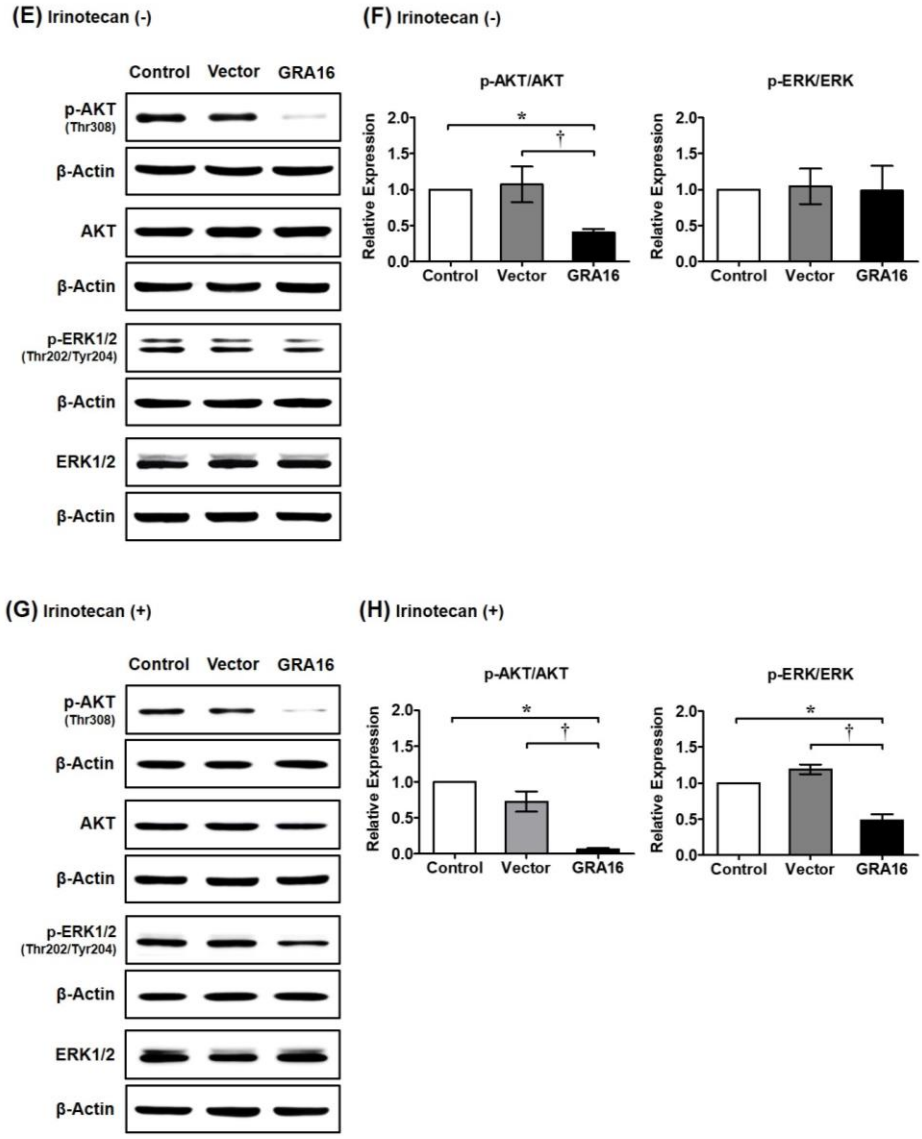

Figure 4. (Continued) Inhibition of GWL and CyclinB1 and dephosphorylation of ENSA, AKT, and ERK by the augmentation of PP2A-B55 in H1299 GRA16 cells. (E) Phosphorylation of AKT and ERK without irinotecan treatment. (F) Ratios of p-AKT(T308) and p-ERK expression without irinotecan treatment. (G) Phosphorylation of AKT and ERK under irinotecan treatment. (H) Ratios of p-AKT and p-ERK expression under irinotecan treatment. * Significant at $p < 0.05$ between control and GRA16 group; † Significant at $p < 0.05$ between vector and GRA16 group.

3.1.5. Induction of cell apoptosis and cell-cycle arrest and simultaneous inhibition of cell proliferation by GRA16

Since the anticancer effect is related to the inhibition of cancer cell proliferation and cell death, I determined the effects of GRA16 on cell apoptosis by FACS analysis and cell proliferation using the CCK-8 assay and trypan blue exclusion test without or with irinotecan treatment (Figures 5A-5D). The results showed that H1299 GRA16 cells induced cell apoptosis based on the significant increase of apoptotic and necrotic cells stained with annexin V and propidium iodide (PI) compared with H1299 control and H1299 vector cells (Figure 5A). The increase in apoptotic cells was higher under irinotecan treatment (Figure 5B). With the increase of apoptotic and necrotic cells, H1299 GRA16 cells significantly lower cell proliferation compared to H1299 control cells and H1299 vector cells regardless of irinotecan treatment (Figure 5C). Under irinotecan treatment, the proliferation of H1299 GRA16 cells was decreased further (Figure 5D). Moreover, in FACS analysis of cell-cycle arrest (Figures 5E and 5F), H1299 GRA16 cells showed significantly increased G_2/M arrest compared to the cells of other groups (Figure 5E). The G_2/M arrest was increased by irinotecan treatment in H1299 GRA16 cells, suggesting the synergistic effects of GRA16 and irinotecan (Figure 5F). Irinotecan treatment also significantly increased the proportion of cells in the sub-G_1 phase in cells of all groups at 48 h after cell synchronization, suggesting increased apoptosis (Figure 5F). Moreover, the proportion of cells in the sub-G_1 phase of cell-cycle (%) was higher in the GRA16 group (18.20% ± 1.85%) than in control (1.64% ± 0.20%) and vector groups (2.91% ± 0.29%) (Figure 5F). These results indicated that GRA16 induces G_2/M cell-cycle arrest and that irinotecan treatment accelerates entry into the apoptotic sub-G_1 phase (Figure 5F). This synergistic effect of irinotecan and GRA16 could be applied to treating H1299 cells.

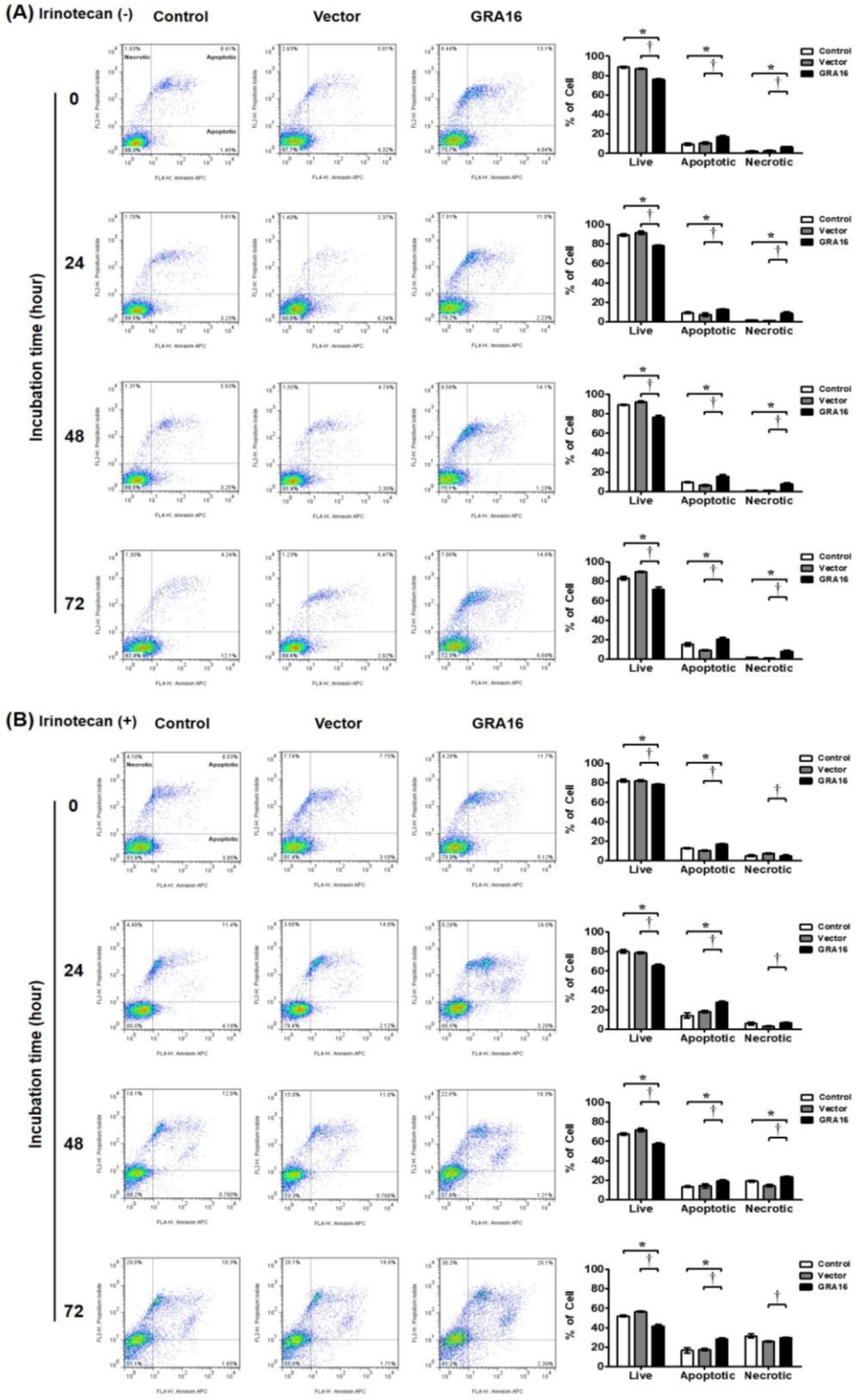

Figure 5. Effects of GRA16 and irinotecan on the induction of

apoptosis and cell-cycle arrest in H1299 cells. (A) Annexin V and propidium iodide (PI) staining without irinotecan treatment. (B) Annexin V and PI staining under irinotecan treatment. * Significant at $p < 0.05$ between control and GRA16 gorup; † Significant at $p < 0.05$ between vector and GRA16 group.

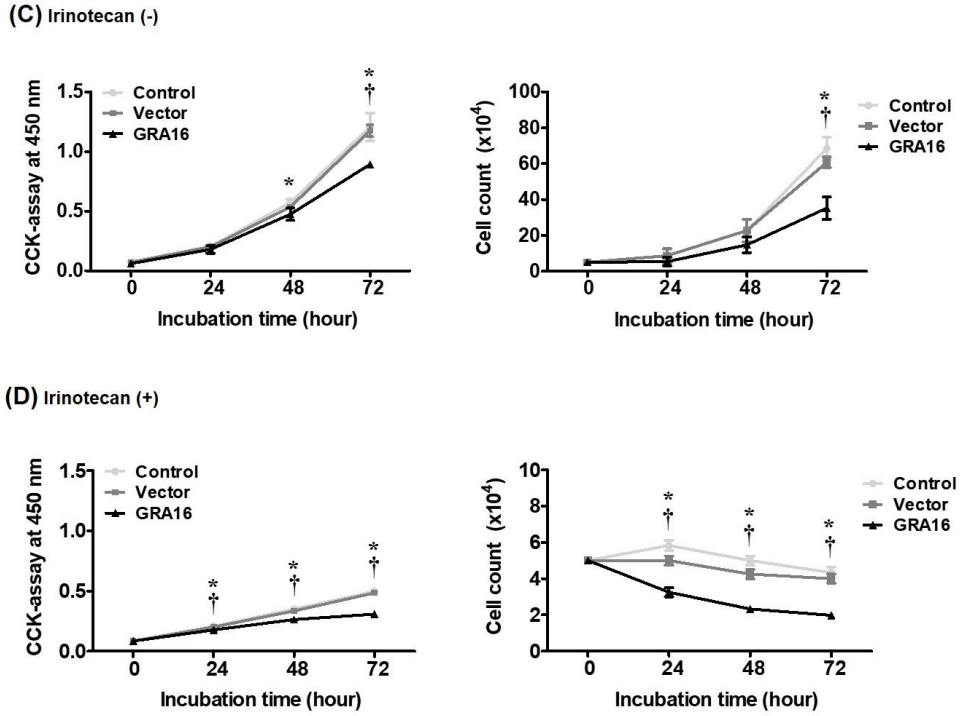

Figure 5. (Continued) Effects of GRA16 and irinotecan on the induction of apoptosis and cell-cycle arrest in H1299 cells. (C) Cell viability and cell count (trypan blue exclusion test) without irinotecan treatment. (D) Cell viability and cell count under irinotecan treatment. * Significant at $p < 0.05$ between control and GRA16 group; † Significant at $p < 0.05$ between vector and GRA16 group.

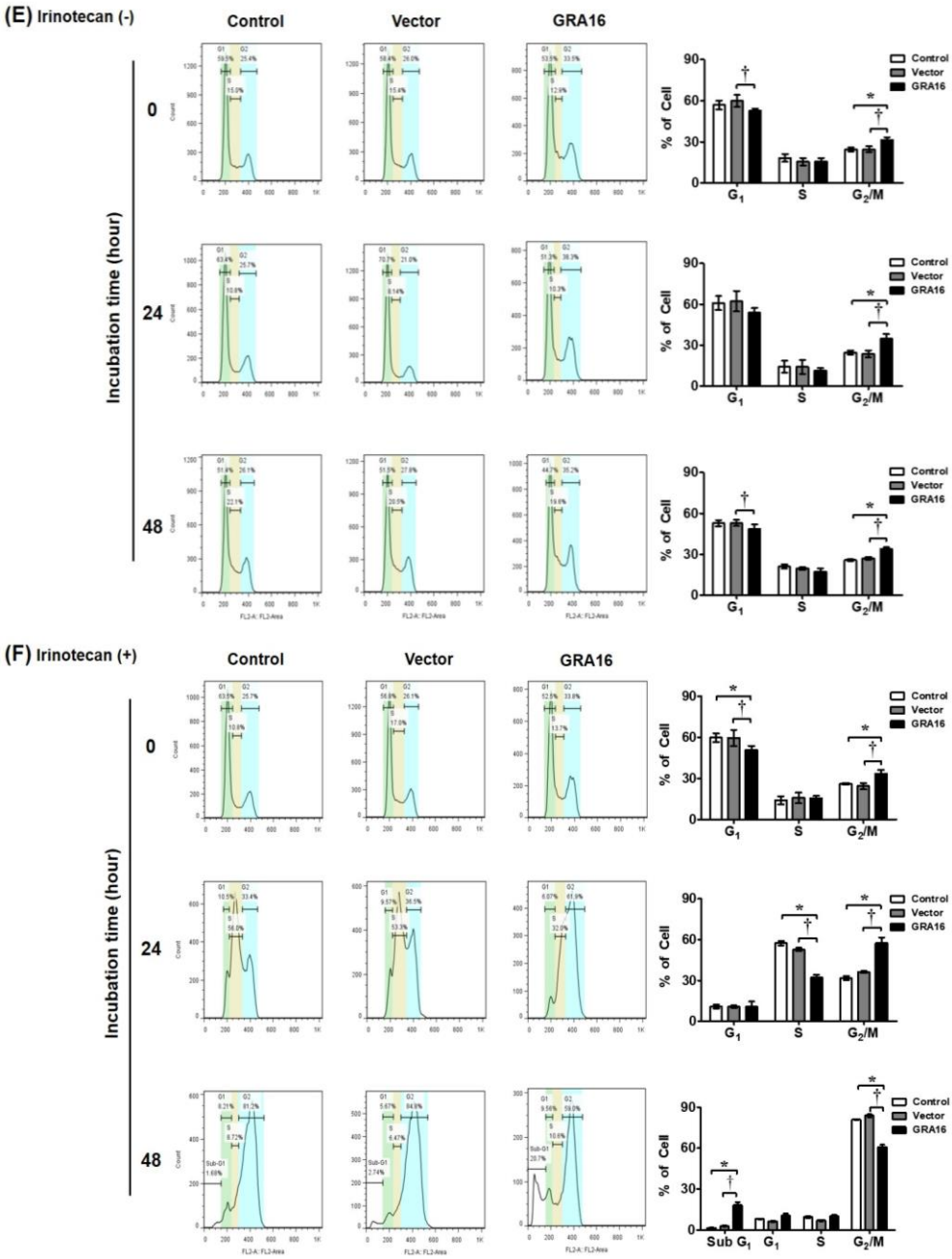

Figure 5. (Continued) Effects of GRA16 and irinotecan on the induction of apoptosis and cell-cycle arrest in H1299 cells. (E) Cell-cycle analysis via FACS without irinotecan treatment. (F) Cell-cycle analysis via FACS under irinotecan treatment. * Significant at $p < 0.05$ between control and GRA16 group; † Significant at $p < 0.05$ between vector and GRA16 group.

3.1.6. NF-kB inhibition in H1299 GRA16 cells regardless of irinotecan treatment

To investigate the effects of GRA16 and/or irinotecan on NF-kB activity, I examined changes in IKKβ, p-IkBα, and NF-kB p65 nucleus translocation in the control, vector, and GRA16 cells (Figure 6). In immunofluorescence experiments, nucleus translocation of NF-kB p65 protein was decreased in H1299 GRA16 cells compared with those in the control and vector groups (Figures 6A and 6B). In western blotting, the GRA16 group showed significantly decreased IKKβ, p-IkBα, and nuclear NF-kB p65 expression regardless of irinotecan treatment (Figures 6C-6F). These results indicated irinotecan does not affect NF-kB p65 expression regardless of irinotecan treatment. Therefore, as an inhibitor of NF-kB activation, GRA16 may overcome resistance to irinotecan chemotherapy, potentially leading to changes in the expression levels of chemoresistance markers (Figures 6G and 6H). The chemoresistance marker genes ABCG2 and CTNNAL1's relative mRNA expression were significantly reduced in the GRA16 cells (Figures 6G and 6H). The tumor suppresses gene BRCA1 was highly expressed in H1299 GRA16 cells compared with that in the control and vector groups (Figures 6G and 6H). The expression levels of these marker genes, which govern NF-kB activities, were affected by GRA16 but not by irinotecan in H1299 cells, suggesting that GRA16 prevents the development of chemoresistance (Figures 6G and 6H). Also, I investigated the relative mRNA expression of apoptosis-related genes among the various NF-kB target genes (Figures 6I and 6J). At this time, anti-apoptosis-related genes (c-Myc and BCL-2) were reduced, and pro-apoptosis-related genes (BAX and ARHGEF7) were conversely increased regardless of irinotecan treatment (Figures 6I and 6J). These results highlighted that GRA16 regulates the NF-kB target gene expression related to apoptosis via the inhibition of NF-kB p65 nuclear localization.

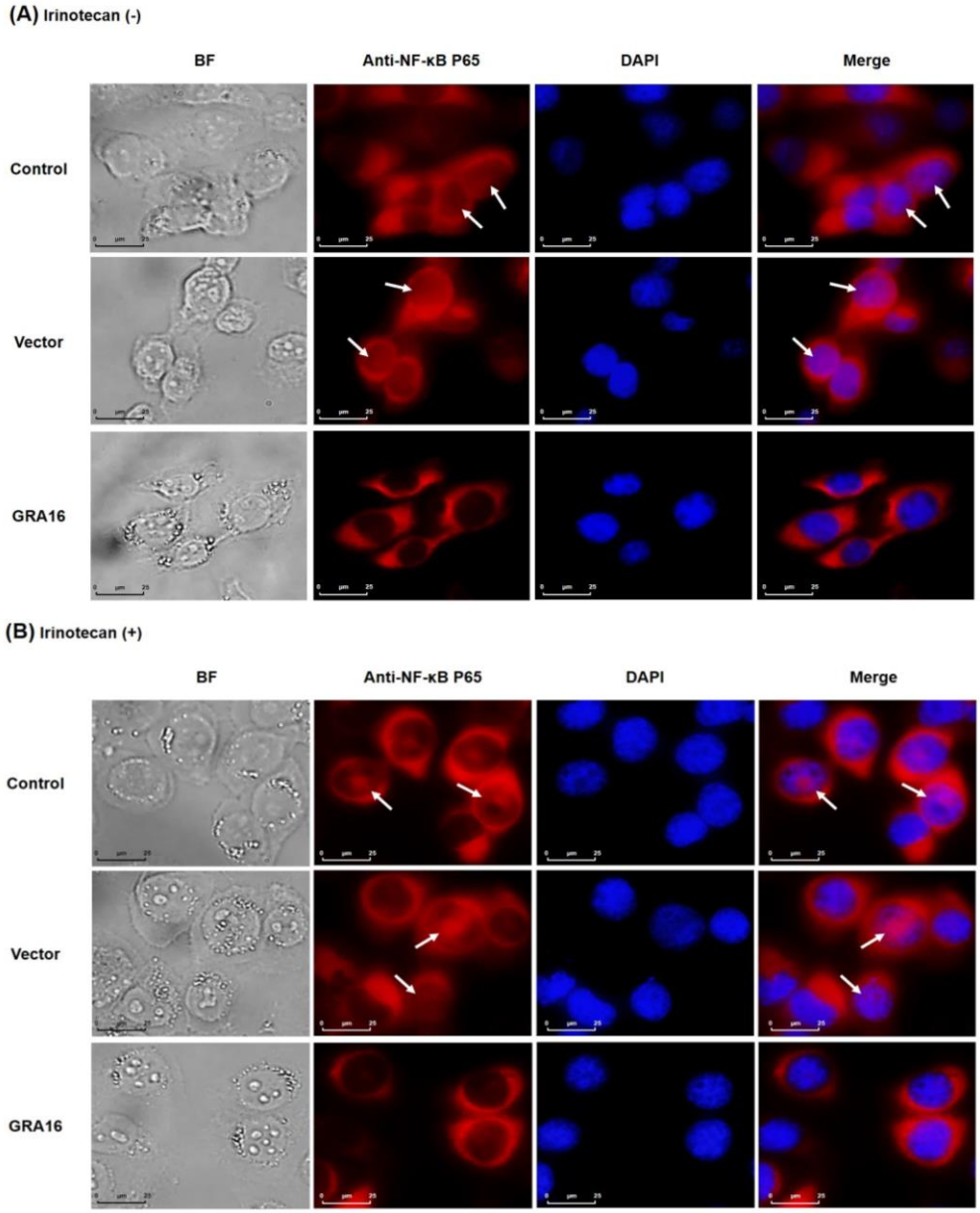

Figure 6. NF-kB inhibition induced by GRA16 in H1299 cells regardless of irinotecan treatment. Immunofluorescence assay (IFA) for NF-kB expression in control, vector, and GRA16 group without (A) and with (B) irinotecan treatment. BF: bright field, DAPI: nucleus staining. White arrows represent NF-kB p65 protein in the nucleus. Scale bar represents 25 μm. * Significant at $p < 0.05$ between control and GRA16 group; † Significant at $p < 0.05$ between vector and GRA16 group.

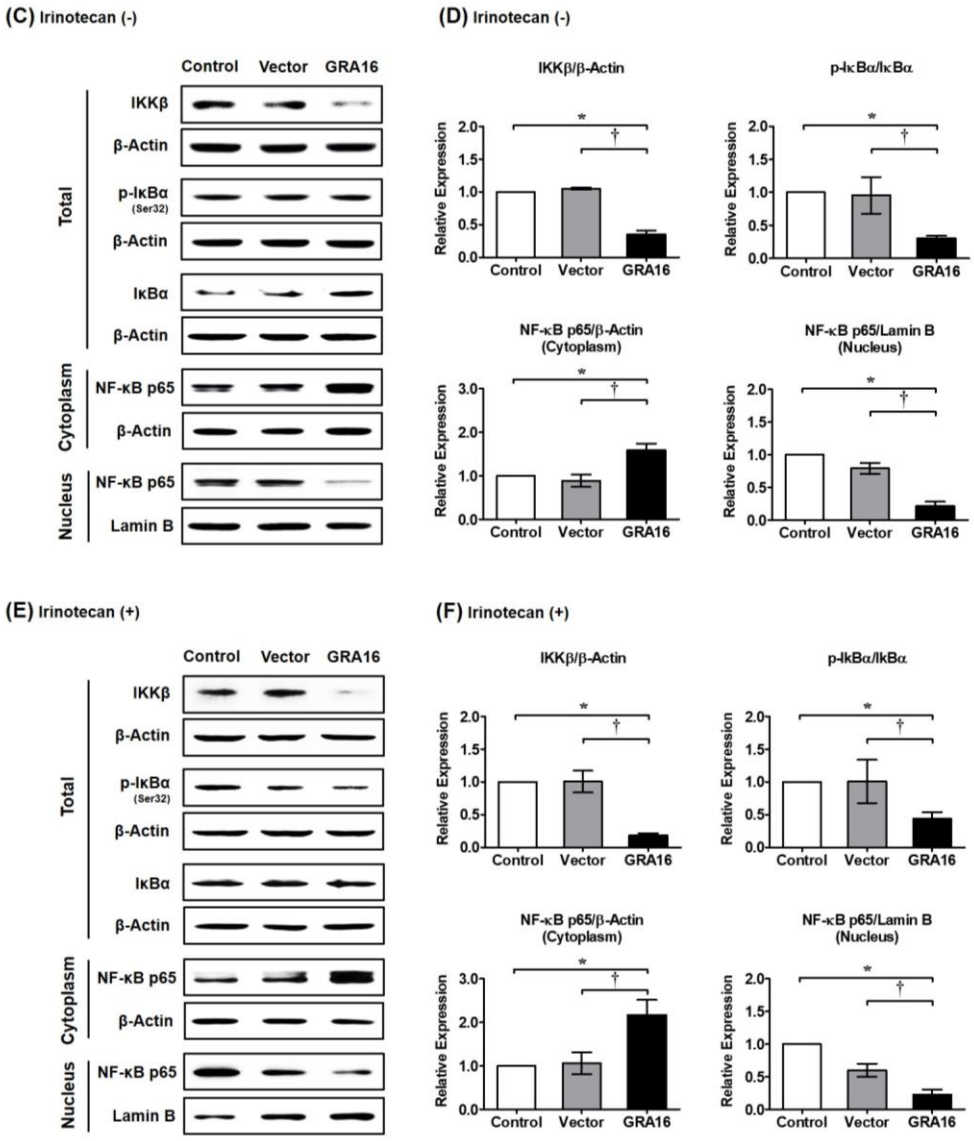

Figure 6. (Continued) NF-kB inhibition induced by GRA16 in H1299 cells regardless of irinotecan treatment. Western blots of IKKβ, p-IkBα, IkBα, and NF-kB p65 without (C) and with (E) irinotecan treatment and their relative expressions of protein in the cytoplasm and nucleus without (D) and with (F) irinotecan treatment. * Significant at $p < 0.05$ between control and GRA16 group; † Significant at $p < 0.05$ between vector and GRA16 group.

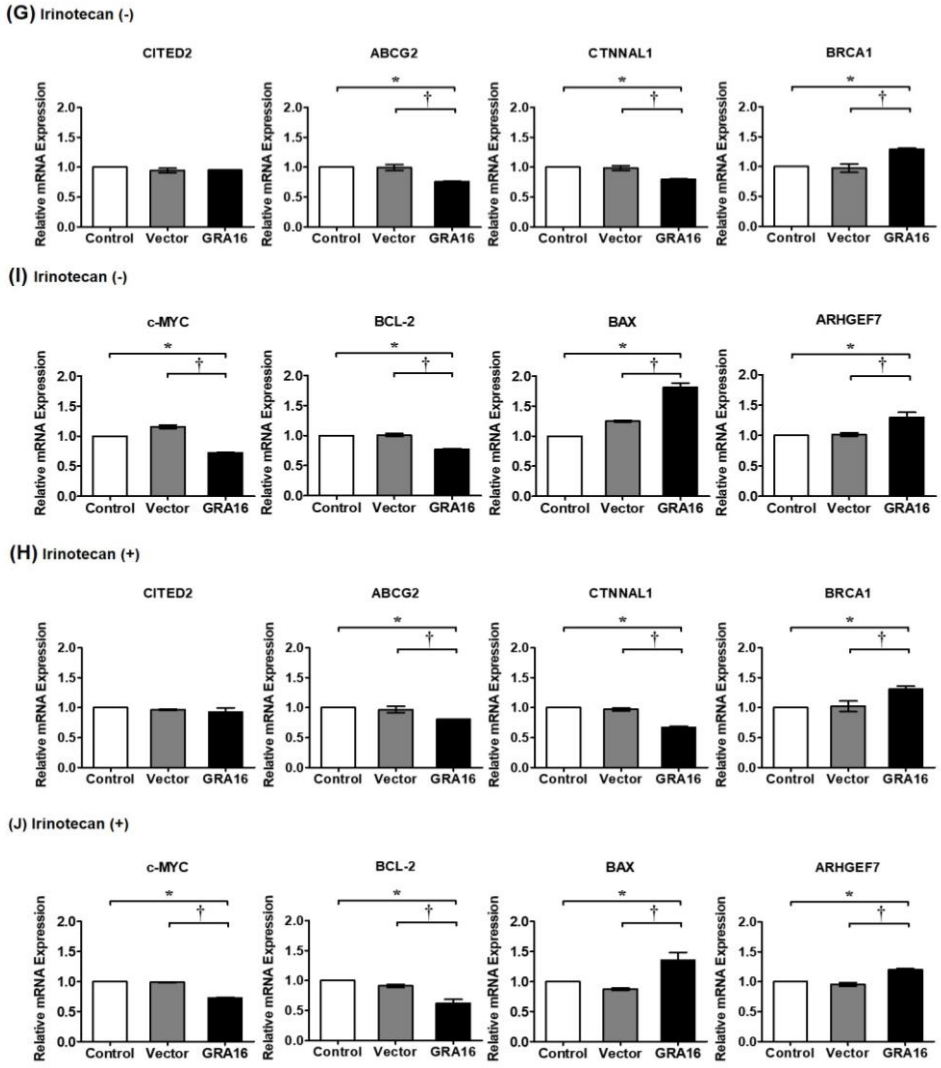

Figure 6. (Continued) NF-kB inhibition induced by GRA16 in H1299 cells regardless of irinotecan treatment. Changes in chemoresistance (CITED2, ABCG2, and CTNNAL1) and sensitivity (BRCA1) markers without (G) and with (H) irinotecan treatment. Changes in NF-kB target genes related with anti-apoptosis (c-Myc and BCL-2) and pro-apoptosis (BAX and ARHGEF7) markers without (I) and with (J) irinotecan treatment. * Significant at $p < 0.05$ between control and GRA16 group; † Significant at $p < 0.05$ between vector and GRA16 group.

3.1.7. GRA16-induced apoptosis and NF-kB inhibition was reversed by the LB-100, a PP2A inhibitor

The results showed that GRA16 increases PP2A-B55 and decreases p-AKT(T308), leading to NF-kB inhibition. To understand PP2A-B55's dependency on NF-kB inhibition, I treated H1299 control cells, H1299 vector cells, and H1299 GRA16 cells with the specific PP2A inhibitor LB-100 (Figure 7). In these experiments, the IC_{50} concentration of LB-100 was determined by 7 μM (Figure 7A). In LB-100, cell proliferation and NF-kB activity were not reduced in GRA16 cells (Figures 7B and 7C). Similarly, the relative protein expression levels of p-AKT, IKKβ, and p-IkBα were slightly increased in GRA16 cells, and the nucleus translocation of NF-kB was no longer inhibited (Figures 7D and 7E).

(A)

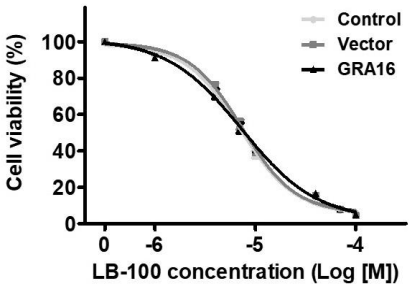

Cells	IC_{50} ± SD (μM)
Control	7.03 ± 1.039
Vector	7.38 ± 1.036
GRA16	7.35 ± 1.049

(B) LB-100 (+)

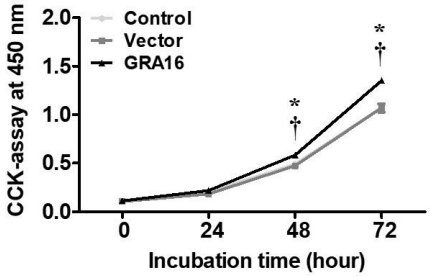

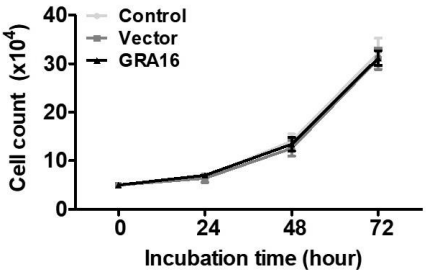

Figure 7. LB-100 (PP2A inhibitor) reversed the reduced cell viability, AKT dephosphorylation, and NF-kB inactivation induced in H1299 GRA16 cells. (A) IC_{50} of LB-100 in NSCLC cells. (B) Cell viability and cell count after treatment with 7 μM (as determined by the IC_{50} result) LB-100. * Significant at $p < 0.05$ between control and GRA16 group; † Significant at $p < 0.05$ between vector and GRA16 group.

(C) LB-100 (+)

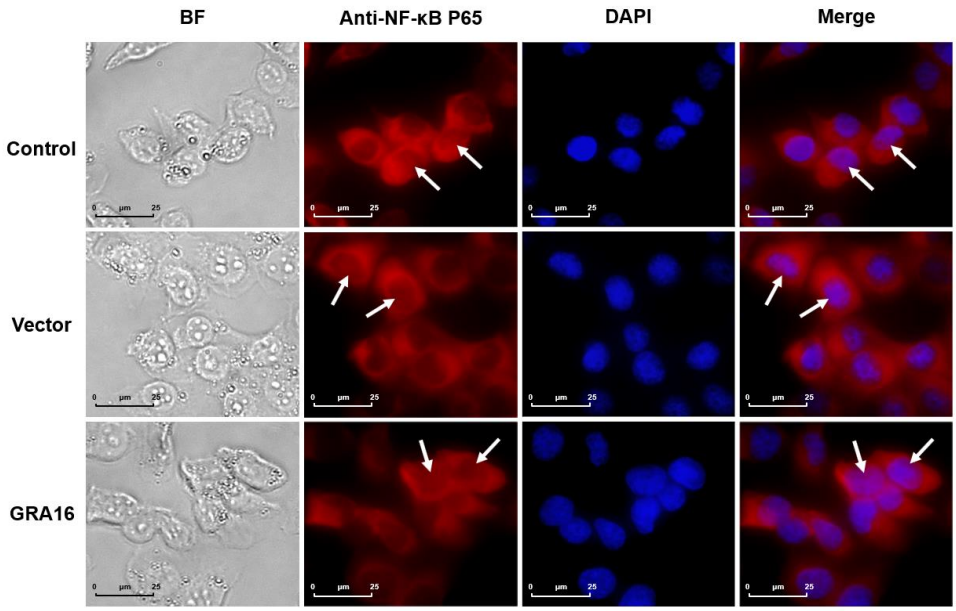

Figure 7. (Continued) LB-100 (PP2A inhibitor) reversed the reduced cell viability, AKT dephosphorylation, and NF-kB inactivation induced in H1299 GRA16 cells. (C) Immunofluorescence images of NF-kB distribution in the cytoplasm and nucleus. BF: bright field, DAPI: nucleus staining. White arrows represent NF-kB p65 protein in the nucleus. Scale bar represents 25 μm.

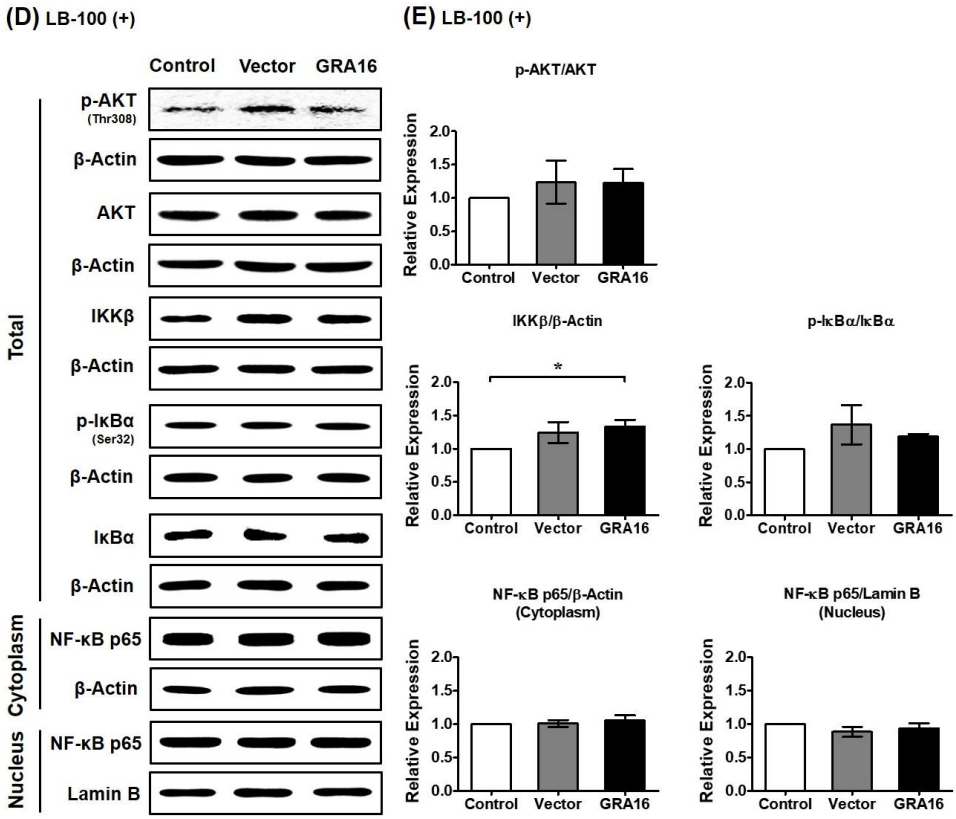

Figure 7. (Continued) LB-100 (PP2A inhibitor) reversed the reduced cell viability, AKT dephosphorylation, and NF-kB inactivation induced in H1299 GRA16 cells. Western blots of p-AKT, AKT, IKKβ, p-IkBα, IkBα, and NF-kB p65 in control, vector, and GRA16 group (D) and their relative expressions (E). * Significant at $p < 0.05$ between control and GRA16 group; † Significant at $p < 0.05$ between vector and GRA16 group.

3.2. Study-II. Telomerase inhibition and telomere shortening of *Toxoplasma gondii* GRA16 in cancer cell

3.2.1. Production of GRA16 expressing HCT116 cells and changes in cell signaling molecules related to hTERT regulation induced by GRA16

To investigate the telomere regulatory mechanism of GRA16 in colorectal cancer cells, the HCT116 cells were transfected with a GRA16-expressing viral vector (Figure 8A). Briefly, the *gra16* gene was successfully incorporated into the pBABE-HAII-Vector, and the resulting GRA16-expressing plasmid was transfected into the HCT116 cells (Figure 8A). The expression of GRA16 was confirmed using the HA-tag antibody (Figure 8B). The relative T/S ratio was calculated during the cell culture of 20 times passages in experimental groups to determine the appropriate experimental conditions associated with telomere length and telomerase. Telomere shortening (Reduced T/S ratio), which was observed by telomere quantitative polymerase chain reaction (PCR), was consistently and significantly observed in GRA16 expressing HCT116 (HCT116 GRA16) cells during cell culture of 20 times passages (Figure 8C). In these results, telomere-related molecular experimental results were comprehensively evaluated at the time point of 10 passages of cell culture (P10). When GRA16 was expressed, the changes in the cell signaling pathway in the HCT116 GRA16 cells were compared with those in the control and vector groups. The HAUSP expression and PTEN phosphorylation were significantly decreased, with PP2A-B55 expression significantly increased, and the phosphorylation of NF-kB p65 was significantly decreased (Figure 8D) in HCT116 cells. Furthermore, it was followed by an increase in the phosphorylation of P53, a decrease in the phosphorylation of AKT (S473 and T308) and STAT3, and a decrease in the expression of the hTERT transcriptional factors (E2F1 and c-Myc) (Figure 8E). Also, GRA16 significantly decreased the expression of shelterin complex factors to decrease

hTERT activation and hTERT transcriptional factors and increased the expression of hTERT repressors (HIF-2α and MAD1) (Figure 8F). Also, GRA16 eventually decreased the expression and phosphorylation of hTERT (Figure 8G). These results suggested that GRA16 expression in HCT116 cells induces telomere shortening and hTERT inactivation.

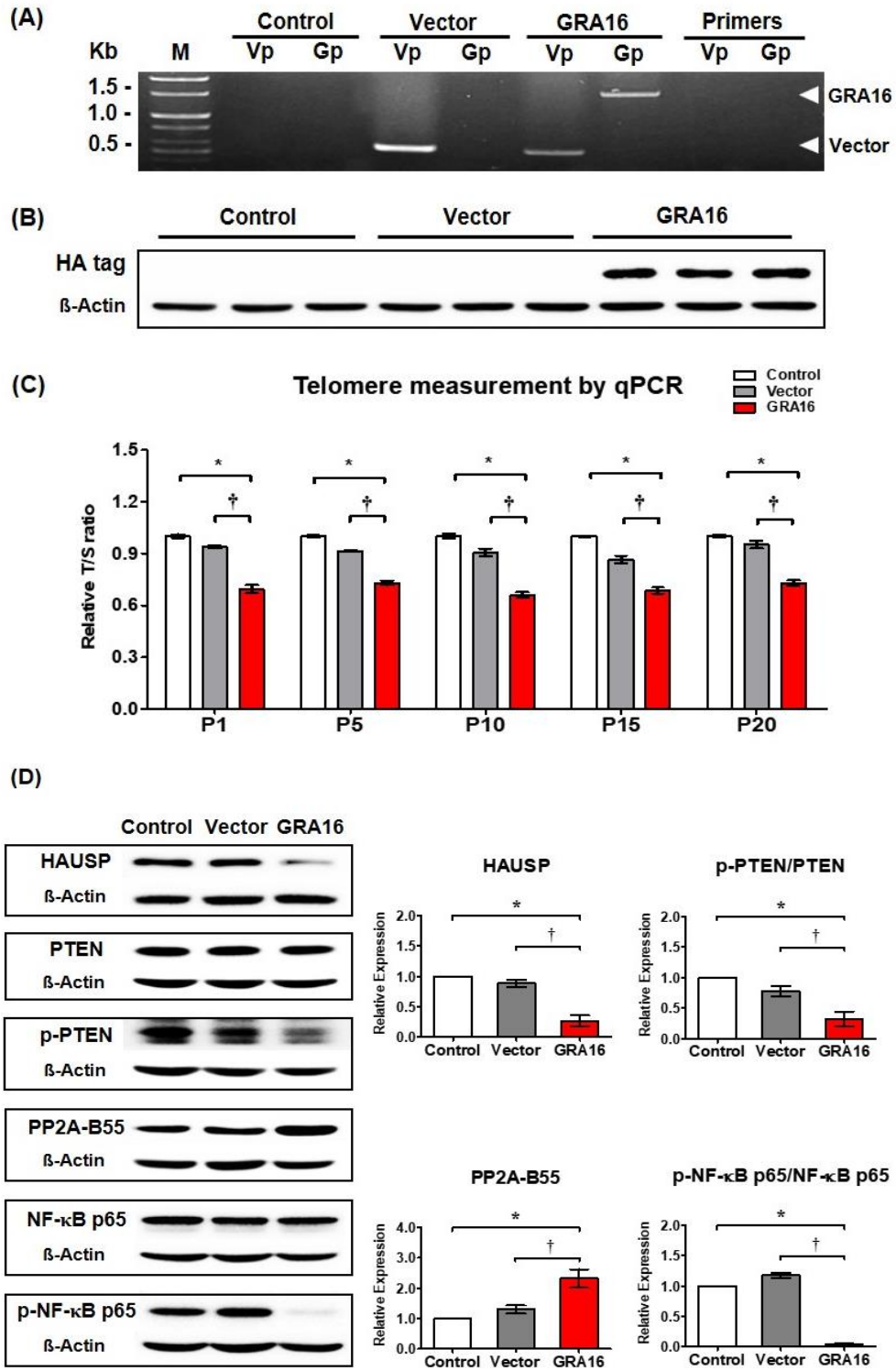

Figure 8. Production of GRA16 expressing HCT116 cells and expression of signaling molecules involved in hTERT transcription

and decrease in hTERT-expression and -phosphorylation in HCT116 GRA16 cells. (A) PCR results for vector gene *(pBABE-HAII)* or *gra16* gene *(pBABE-HAII-gra16)* using primers for vector (Vp) and GRA16 (Gp). (B) HA-tagged GRA16 expression in experimental groups (control, vector, and GRA16). (C) Telomere length analyzed by qPCR using telomere-specific primers (Tel1/2) and single-copy gene primers (36B4u/d). Their ratio (T/S) was used for the calculation of telomere length (n = 16). (D) Expressions of signaling molecules (HAUSP, PP2A-B55, p-PTEN, and p-NF-kB p65) in experimental groups (n = 3). Data represent mean ± standard deviation (SD). Each expression value of protein or mRNA of signaling molecules in the control group was fixed at "1", after which the relative expression of each signaling molecule in vector and GRA16 group was calculated. * Significant difference between control and GRA16 group ($p < 0.05$); † Significant difference between vector and GRA16 group ($p < 0.05$).

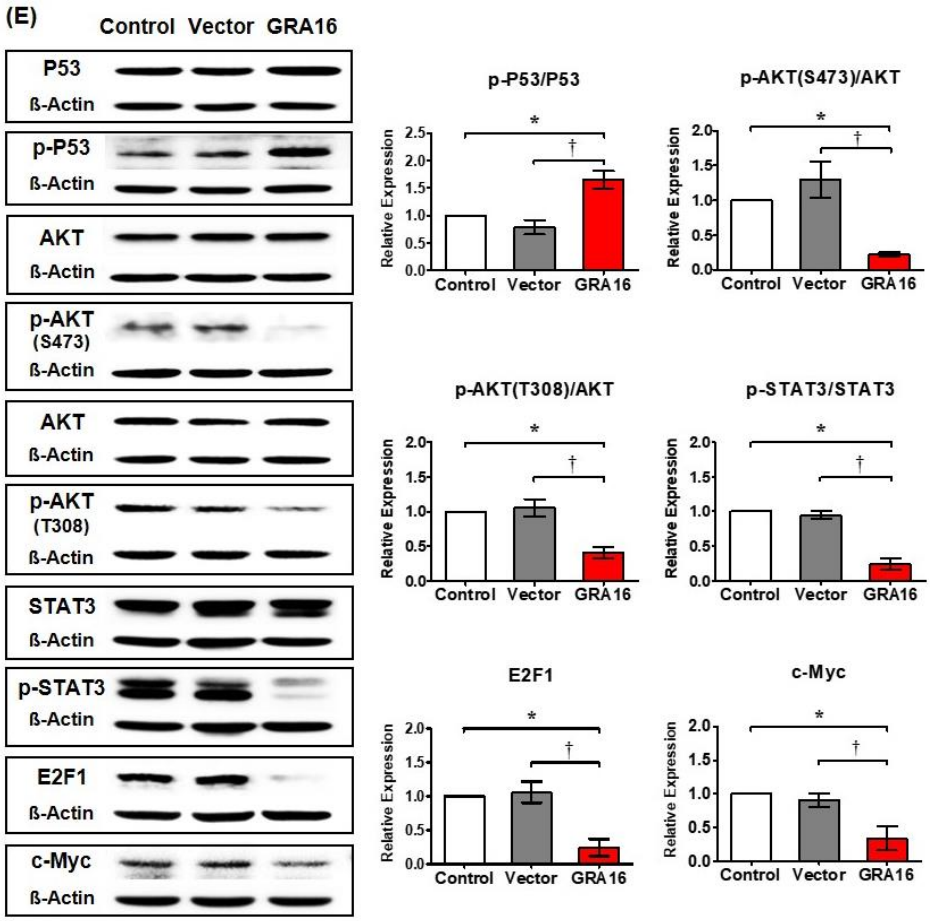

Figure 8. (Continued) Production of GRA16 expressing HCT116 cells and expression of signaling molecules involved in hTERT transcription and decrease in hTERT-expression and -phosphorylation in HCT116 GRA16 cells. (E) Expressions of signaling molecules involved in the transcription and activation of hTERT (p-P53, p-AKT(S473), p-AKT(T308), p-STAT3, E2F1, and c-Myc) (n = 3). Data represent mean ± standard deviation (SD). Each expression value of protein of signaling molecules in the control group was fixed at "1", after which the relative expression of each signaling molecule in vector and GRA16 group was calculated. * Significant difference between control and GRA16 group ($p < 0.05$); † Significant difference between vector and GRA16 group ($p < 0.05$).

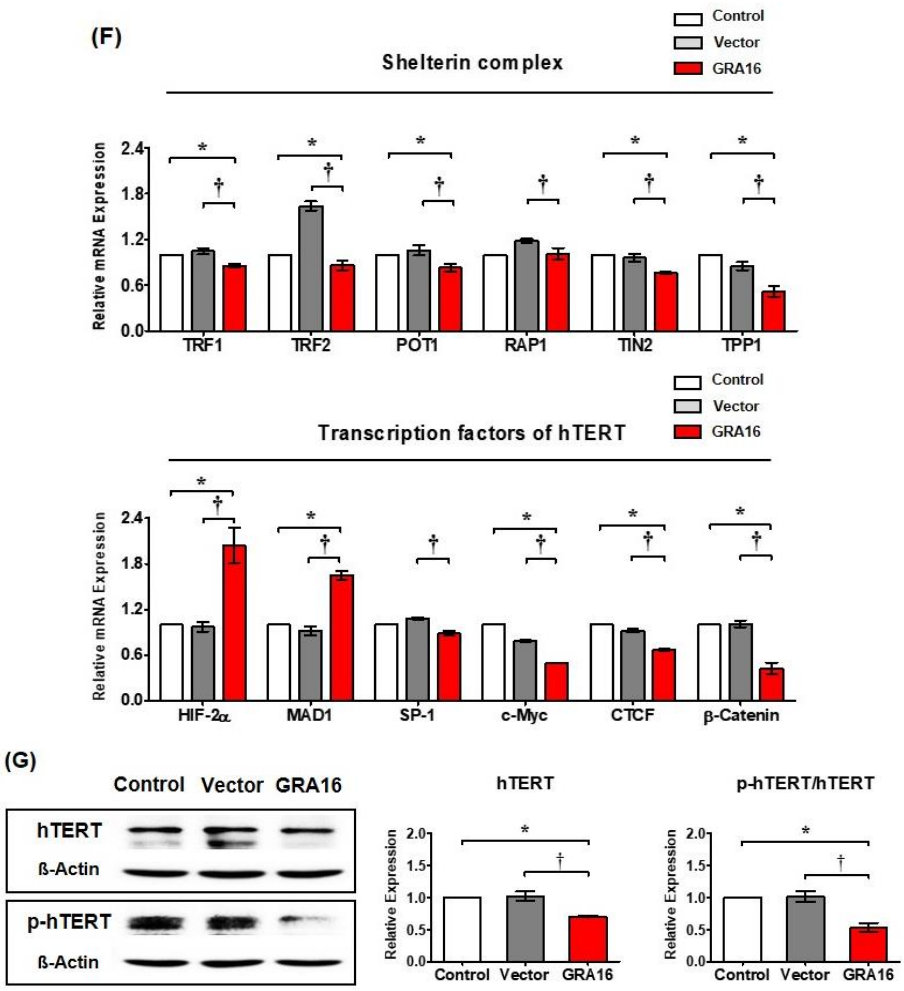

Figure 8. (Continued) Production of GRA16 expressing HCT116 cells and expression of signaling molecules involved in hTERT transcription and decrease in hTERT-expression and -phosphorylation in HCT116 GRA16 cells. (F) mRNA expressions of shelterin complex factors and hTERT transcriptional factors in experimental groups (n = 3). (G) hTERT expressions and p-hTERT levels in experimental groups (n = 3). Data represent mean ± standard deviation (SD). Each expression value of protein or mRNA of signaling molecules in the control group was fixed at "1", after which the relative expression of each signaling molecule in vector and GRA16 group was calculated. * Significant difference between control and GRA16 group ($p < 0.05$); † Significant difference between vector and GRA16 group ($p < 0.05$).

3.2.2. Expression of GRA16 in HCT116 cells results in an increase in PTEN nuclear localization and a simultaneous decrease in NF-kB p65 nuclear localization

As presented in Figure 9, GRA16 induced PTEN and NF-kB p65 dephosphorylation. This result indicated the stabilization and activation of PTEN and suppression of NF-kB p65, respectively. Nucleus localization of PTEN was expected to increase, and nucleus localization of NF-kB p65 was expected to decrease. To demonstrate this, I performed immunofluorescence analysis and western blotting (Figure 9). In immunofluorescence staining, PTEN was evenly distributed in the cytoplasm and nucleus in HCT116 control and HCT116 vector cells, but it was intensively distributed in the nucleus in HCT116 GRA16 cells (Figure 9A). The western blotting results were similar to those of immunofluorescence analysis (Figure 9B), namely an increase in nuclear PTEN expression and a simultaneous decrease in cytoplasmic PTEN expression in HCT116 GRA16 cells (Figure 9B). By contrast, cytoplasmic NF-kB p65 significantly increased, and the nuclear expression of NF-kB p65 decreased in HCT116 GRA16 cells in immunofluorescence analysis and western blotting (Figures 9C and 9D). These results suggested that GRA16 stabilizes PTEN via nucleus localization and simultaneously suppresses the transcriptional function of NF-kB p65 by blocking its nucleus localization.

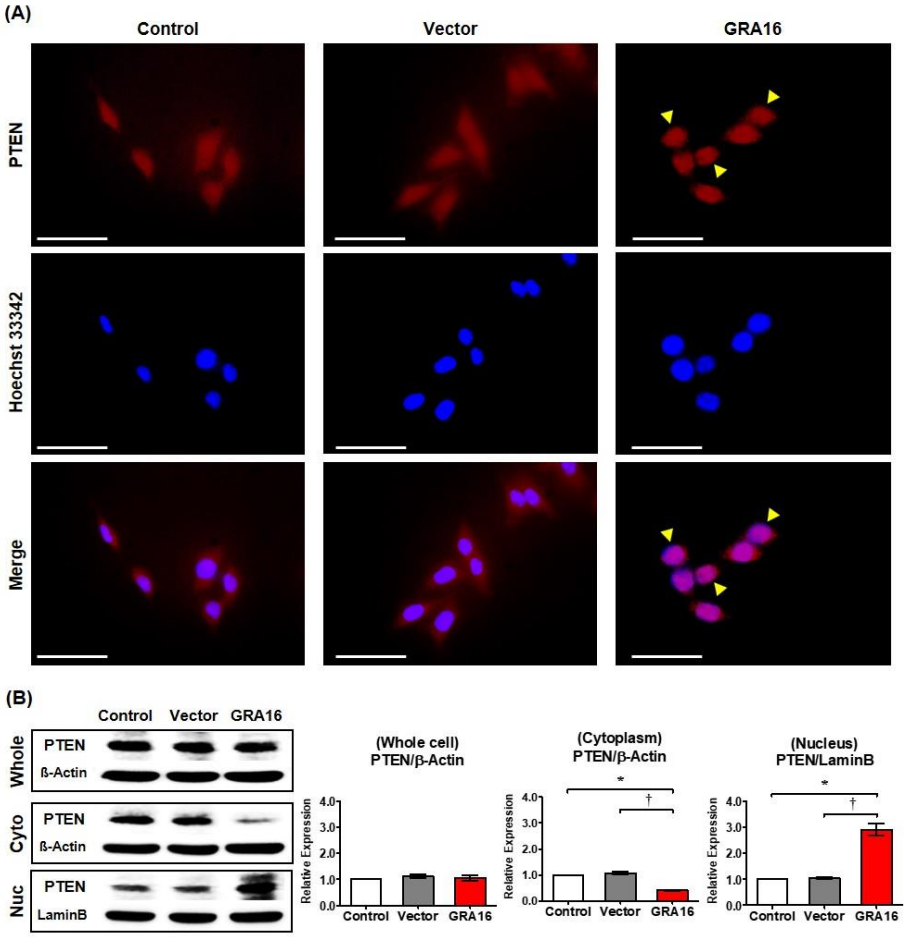

Figure 9. Increase in the nuclear localization of PTEN and decrease in the nuclear localization of NF-kB p65 in HCT116 GRA16 cells. (A) Immunofluorescence images illustrated the increased translocation of PTEN into the nuclei of HCT116 GRA16 cells. Scale bars represent 50 μm. Yellow arrows indicate PTEN translocated into the nucleus of HCT116 GRA16 cells (n = 3). (B) PTEN expression in the whole cell (Whole), cytoplasmic (Cyto), and nuclear fractions (Nuc) of HCT116 stable cells. Data are presented as the mean ± SD. Results in bar graphs present the relative protein expression (PTEN or NF-kB p65) in vector and GRA16 group relative to the value in control group, which was fixed at "1". * Significant difference between the control and GRA16 group ($p < 0.05$); † Significant difference between the vector and GRA16 group ($p < 0.05$).

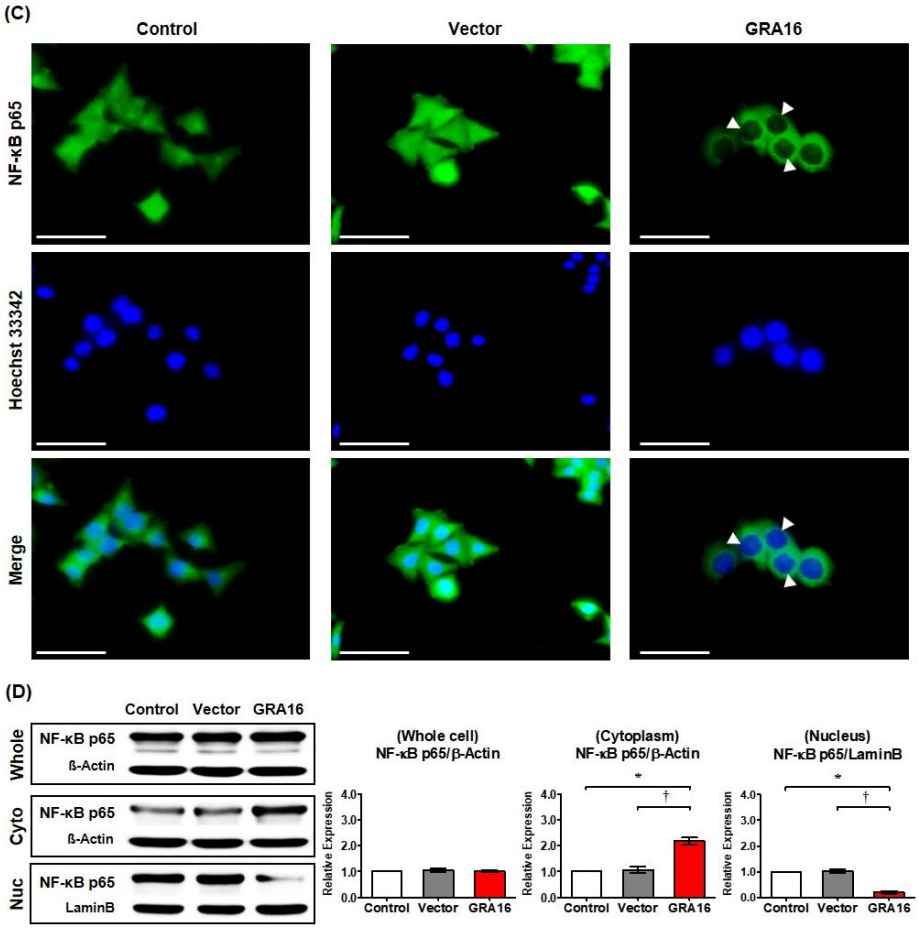

Figure 9. (Continued) Increase in the nuclear localization of PTEN and decrease in the nuclear localization of NF-kB p65 in HCT116 GRA16 cells. (C) Immunofluorescence images presenting the decreased nuclear expression of NF-kB p65 in HCT116 GRA16 cells. Scale bars represent 50 μm. White arrows indicate NF-kB p65 translocated to the nucleus of HCT116 GRA16 cells (n = 3). (D) Western blot images of NF-kB p65 expression in Whole, Cyto, and Nuc lysates in the control, vector, and GRA16 group. Data are presented as the mean ± SD. Results in bar graphs present the relative protein expression (PTEN or NF-kB p65) in vector and GRA16 group relative to the value in control group, which was fixed at "1". * Significant difference between the control and GRA16 group ($p < 0.05$); † Significant difference between the vector and GRA16 group ($p < 0.05$).

3.2.3. Increased γ-H2A.X-stained nucleus and nucleus size and decreased telomerase activity in HCT116 GRA16 cells

To investigate the cellular changes caused by the reduced telomere length in HCT116 GRA16 cells, double-stranded DNA breaks (DSBs) and enlargement of the nucleus were investigated by immunofluorescence Hoechst33342 DNA staining dye and DSBs/telomere shortening-specific marker antibody γ-H2A.X (Figure 10A). The features that merged between the blue-colored nucleus and green-colored γ-H2A.X-stained nucleus indicated that the nucleus of HCT116 GRA16 cells underwent DNA break, including DNA fragmentation (Figure 10A). Moreover, the nucleus in HCT116 GRA16 cells was enlarged compared with the control and vector groups, as shown by yellow arrows in Figure 10, and the nucleus size was significantly increased in HCT116 GRA16 cells (Figure 10B). Briefly, the mean nucleus size increased from 133.51 ± 29.23 and 133.11 ± 43.47 μm^2 in the control and vector groups, respectively, to 220.05 ± 111.71 μm^2 in the GRA16 group (Figure 10B). Simultaneously, the telomerase activity significantly decreased in HCT116 GRA16 cells compared with the control and vector groups (Figure 10C). Briefly, the relative telomerase activity (RTA) decreased to 68.33% ± 4.17% in HCT116 GRA16 cells compared with HCT116 control cells (Figure 10C). Altogether, the decrease in telomerase activity and telomere shortening and the increase in γ-H2A.X-stained nucleus result in DNA damage and telomere dysfunction, indicating a hallmark of senescence, it may drive genomic instability with the enlargement of the nucleus in cancer cells. Accordingly, these results indicate that the induction of telomere shortening by telomerase inactivation is a process that results in apoptosis when GRA16 is expressed in cancer cells. This effect may be induced by changes in the cell signaling pathway regulating hTERT activity, as shown in Figure 8.

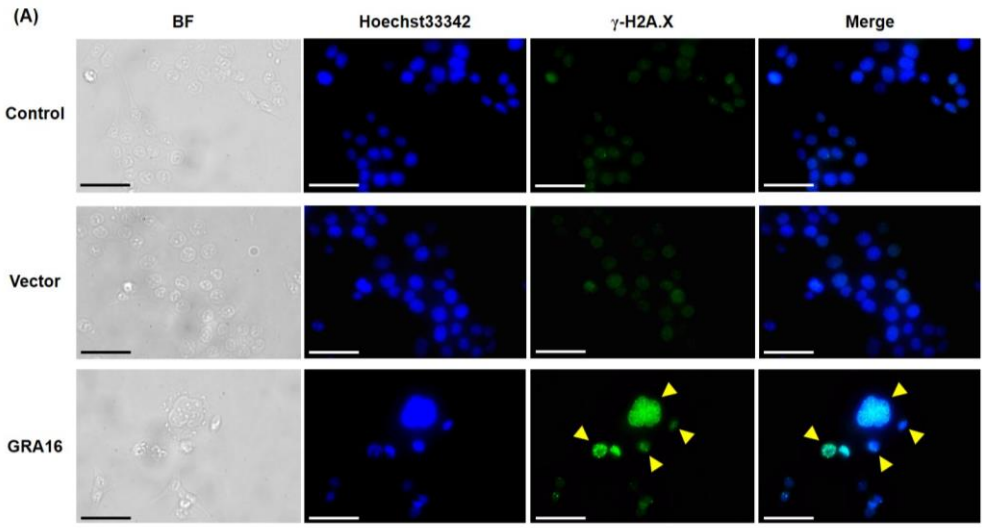

Figure 10. Comparison of DNA damage (γ-H2A.X-stained nucleus), nucleus size, and telomerase activity among the experimental groups of HCT116 cells. (A) Immunofluorescence images of double-strand breaks (γ-H2A.X-stained DSBs) of the cell nucleus indicated by yellow arrows (n = 3). Scale bars represent 50 μm.

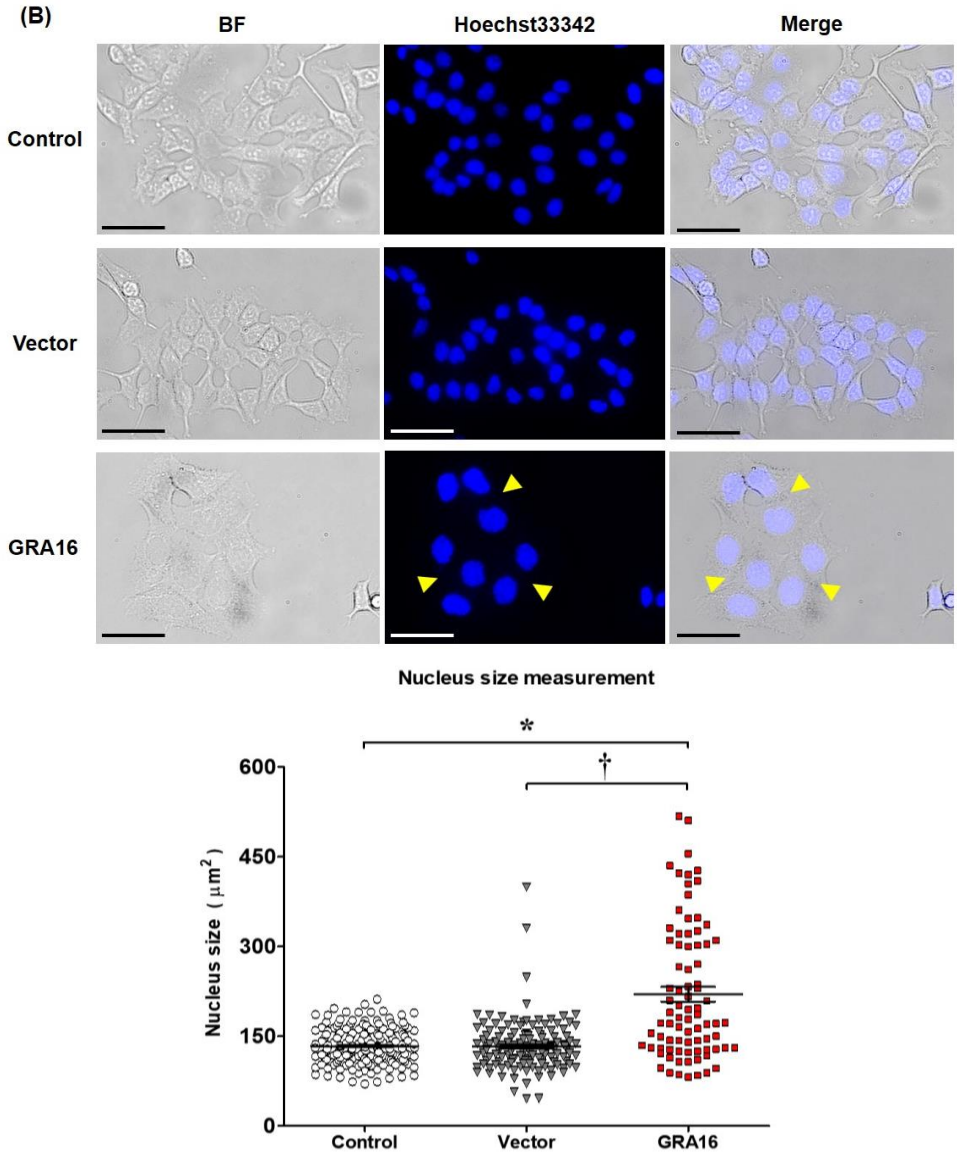

Figure 10. (Continued) Comparison of DNA damage (γ-H2A.X-stained nucleus), nucleus size, and telomerase activity among the experimental groups of HCT116 cells. (B) Immunofluorescence images of the enlarged nucleus indicated by yellow arrows. Scale bars represent 50 μm. Nucleus size was calculated by tracking pixel area using ImageJ. Data represent mean ± standard error (SE) (HCT116 Control cells; n = 185, HCT116 Vector cells; n = 132, HCT116 GRA16 cells; n = 82). * Significant at $p < 0.05$ between the control and GRA16 group; † Significant at $p < 0.05$ between the vector and GRA16 group.

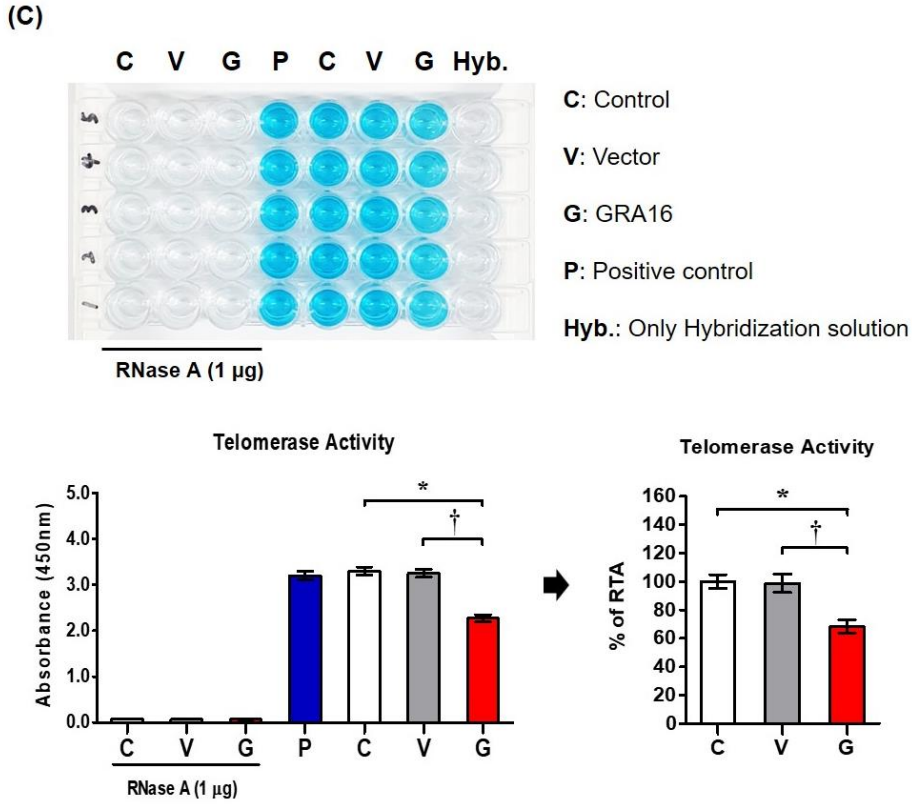

Figure 10. (Continued) Comparison of DNA damage (γ-H2A.X-stained nucleus), nucleus size, and telomerase activity among the experimental groups of HCT116 cells. (C) Telomerase activity was analyzed using the TeloTAGGG^{TM} Telomerase PCR ELISA kit, and the value was measured at 450 nm; their relative telomerase activity (RTA) among experimental groups was calculated using the percentage of telomerase activity in HCT116 GRA16 cells compared with that in HCT116 control cells (100%) (n = 5). Data represent mean ± SD. * Significant at $p < 0.05$ between the control and GRA16 group; † Significant at $p < 0.05$ between the vector and GRA16 group.

3.2.4. Cell-cycle arrest and apoptosis were induced in GRA16 cells

It was speculated that the subsequent cell-cycle arrest and apoptosis would increase due to γ-H2A.X increase and telomerase inactivation in HCT116 GRA16 cells. To confirm this, we investigated cell proliferation, cell-cycle, and apoptosis in HCT116 GRA16 cells using the CCK assay, trypan blue exclusion test, and cell-cycle analysis with apoptosis analysis by FACS at passage 10 of subculture (P10) (Figure 11). HCT116 GRA16 cells showed significant decreases in cell proliferation and the number of live cells compared with the control and vector group after 48 h of incubation (Figure 11A). At 48 h after incubation, significantly increased sub-G_1 phase and decreased G_1, S, and G_2/M phases were observed in HCT116 GRA16 cells compared with the vector group (Figure 11B). Meanwhile, the number of live cells decreased, and apoptotic cells increased in HCT116 GRA16 cells (Figure 11C). The expression of the key factors for cell-cycle arrest (PP2A-B55, GADD45A, P21, P27, and Wee1) increased, whereas the expression of cell-cycle activators (CyclinB1, CDC2, TELO2, and CDC25c) decreased (Figure 11D). The expression of anti-apoptotic factors (HAUSP, MDM2, BCL-2, Survivin, and Wnt3A) decreased, whereas the expression of pro-apoptotic factors (P53, PUMA, NOXA, and BAX) increased (Figure 11E). During the subculture of 20 passages of HCT116 GRA16 cells in which GRA16 was expressed sustainably, the sub-G_1 phase was strikingly increased, and necrotic and late apoptotic cells were continuously increased (Figures 11F-11G). Decreased cell proliferation and increased cell-cycle arrest were induced in HCT116 GRA16 cells. The results were sufficiently predicted from the induced hTERT telomerase inactivation and telomere shortening, as shown in Figures 8 and 10.

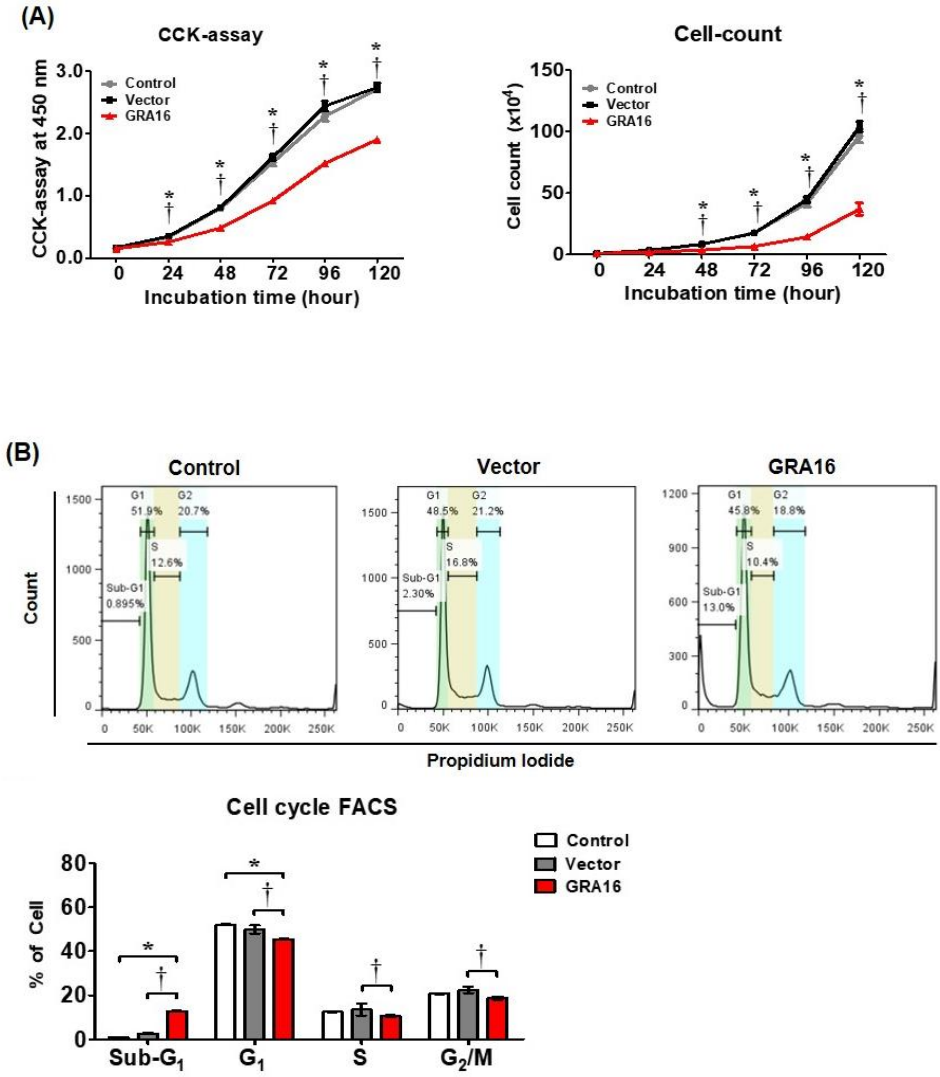

Figure 11. Cell-cycle arrest and apoptosis were increased in HCT116 GRA16 cells. (A) Changes in cell proliferation in control, vector, and GRA16 group (n = 6). (B) Cell-cycle was analyzed by flow cytometry (sub-G_1, G_1, S, and G_2/M phases) (n = 3). All data in this figure represent mean ± SD. * Significant difference at $p < 0.05$ between control and GRA16 group; † Significant difference at $p < 0.05$ between vector and GRA16 group.

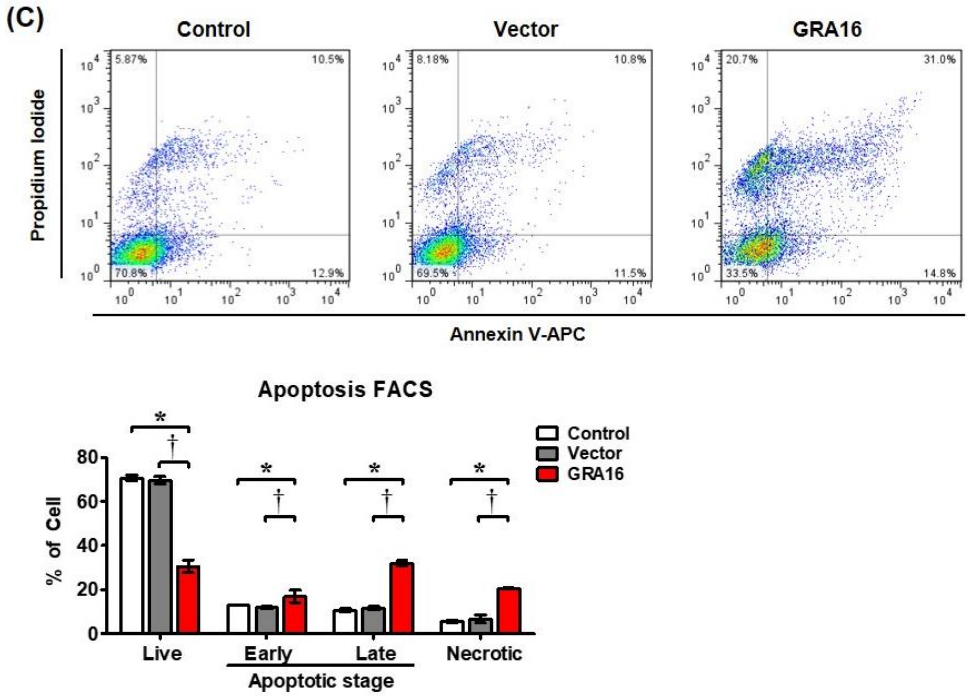

Figure 11. (Continued) Cell-cycle arrest and apoptosis were increased in HCT116 GRA16 cells. (C) Apoptosis was analyzed by flow cytometry (live, early apoptotic, late apoptotic, and necrotic stages of cells) (n = 3). All data in this figure represent mean ± SD. * Significant difference at $p < 0.05$ between control and GRA16 group; † Significant difference at $p < 0.05$ between vector and GRA16 group.

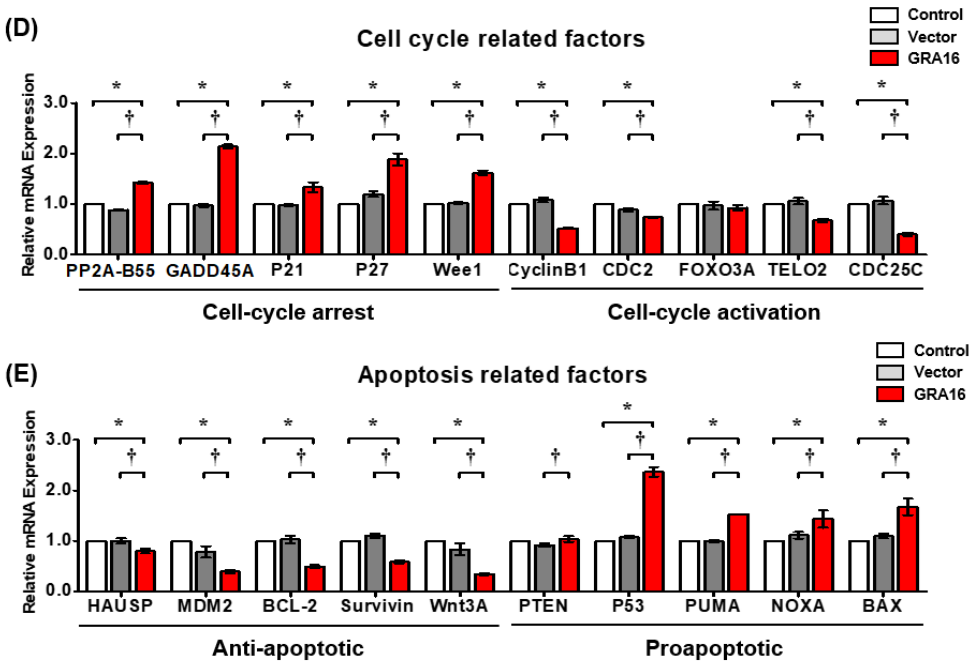

Figure 11. (Continued) Cell-cycle arrest and apoptosis were increased in HCT116 GRA16 cells. (D, E) mRNA expressions of cell-cycle-related factors (D) and apoptosis-related factors (E) in control, vector, and GRA16 group (n = 3). The relative mRNA expressions were calculated by comparing the expression values of each signaling molecule in vector and GRA16 group, with the mRNA expression value of each signaling molecule in HCT116 control cells set to "1". All data in this figure represent mean ± SD. * Significant difference at $p < 0.05$ between control and GRA16 group; † Significant difference at $p < 0.05$ between vector and GRA16 group.

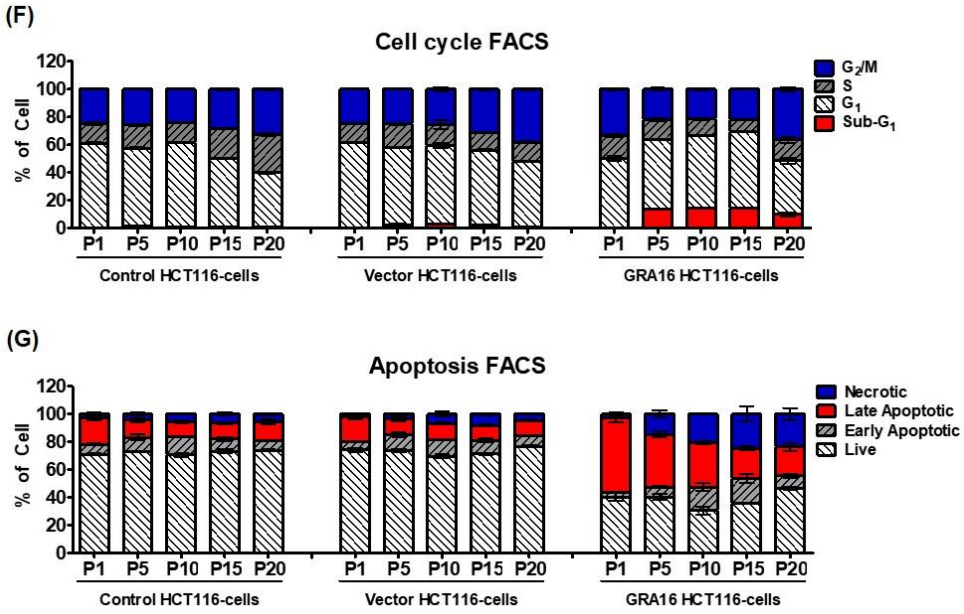

Figure 11. (Continued) Cell-cycle arrest and apoptosis were increased in HCT116 GRA16 cells. (F) Cell-cycle analysis and (G) apoptosis analysis were performed during subcultures from P1 to P20 (n = 3). All data in this figure represent mean ± SD. * Significant difference at $p < 0.05$ between control and GRA16 group; † Significant difference at $p < 0.05$ between vector and GRA16 group.

3.2.5. Confirmation of signaling molecules causing the induction of telomerase inactivation in GRA16 cells using the inhibitors of PTEN and/or PP2A-B55

As described earlier, GRA16 binds to two host enzymes, HAUSP and PP2A-B55, and this study demonstrated that their subsequent signaling pathways resulted in cell-cycle arrest, apoptosis, and telomere shortening. Among these two host enzymes, we investigated the enzymatic signaling pathway directly involved in telomerase inactivation and shortening (Figure 12). When SF1670, an inhibitor of PTEN, and LB-100, an inhibitor of PP2A-B55, were added to the HCT116 GRA16 cells, the enzymatic signaling pathway showed changes (Figures 12A and 12B). SF1670 treatment increased the protein levels of signaling molecules, such as HAUSP, E2F1, and c-Myc, and increased the phosphorylation of PTEN, AKT(S473), STAT3, and NF-kB p65 (Figures 12A and 12B). As phosphorylated STAT3, phosphorylated NF-kB p65, E2F1, and c-Myc comprise the hTERT transcriptional factors, the increase in these signaling molecules resulted in the increased relative expression of p-hTERT in SF1670-treated HCT116 GRA16 cells (Figures 12A-12C). However, treatment with LB-100, the PP2A inhibitor, decreased PP2A-B55 expression and p53 phosphorylation and increased the phosphorylation of STAT3, NF-kB p65, and AKT(T308) (Figures 12A and 12B). However, PP2A-B55 inhibition had no significant changes in the relative expression of p-hTERT compared with PTEN inhibition (Figure 12C). The shelterin complex contributes to its interaction with telomeric DNA and maintenance, and this interaction is involved in inhibiting DNA damage response. Furthermore, the transcription of hTERT is required for telomere maintenance to prevent cellular senescence. Therefore, the significant increase in the shelterin complex and hTERT transcription factors observed in SF1670-treated HCT116 GRA16 cells compared with LB-100-treated HCT116 GRA16 cells suggested the role of PTEN signaling pathway in the HCT116 GRA16 cells associated with hTERT inhibition (Figure 12D). Briefly,

the expression of the transcriptional suppressors, HIF-2α and MAD1, of hTERT decreased in SF1670- and LB-100-treated HCT116 GRA16 cells, but the expression of the transcriptional activators of hTERT significantly increased in SF1670-treated HCT116 GRA16 cells and not in LB-100-treated HCT116 GRA16 cells (Figure 12D). Moreover, SF1670-treated HCT116 GRA16 cells showed significantly decreased relative mRNA expression of cell-cycle arrest-inducing factors, GADD45A, P21, and P27, but significantly increased relative mRNA expression of cell-cycle activators (Figure 12E). These changes in cell-cycle arrest-related factors were more significant in SF1670-treated HCT116 GRA16 cells than in LB-100-treated HCT116 GRA16 cells (Figure 12E). Regarding apoptosis-related factors, SF1670-treated HCT116 GRA16 cells showed a significant increase in the expression of apoptosis suppressors, MDM2, BCL-2, Survivin, and Wnt3A (Figure 12E). The expression of apoptosis-related factors in LB-100-treated HCT116 GRA16 cells remained unchanged (Figure 12E). Altogether, SF1670-treated HCT116 GRA16 cells showed increased phosphorylation of AKT(S473), STAT3, and hTERT and increased relative mRNA expression of hTERT transcription factors, followed by an increase in the expression of cell-cycle activators and apoptosis suppressors. However, LB-100-treated HCT116 GRA16 cells showed no significant changes in hTERT-related factors and apoptosis compared to the SF1670-treated HCT116 GRA16 cells. These results strongly suggested that the PTEN-induced hTERT inactivation is a dominant mechanism underlying the inhibition of hTERT activity among the two host enzymes GRA16 binds.

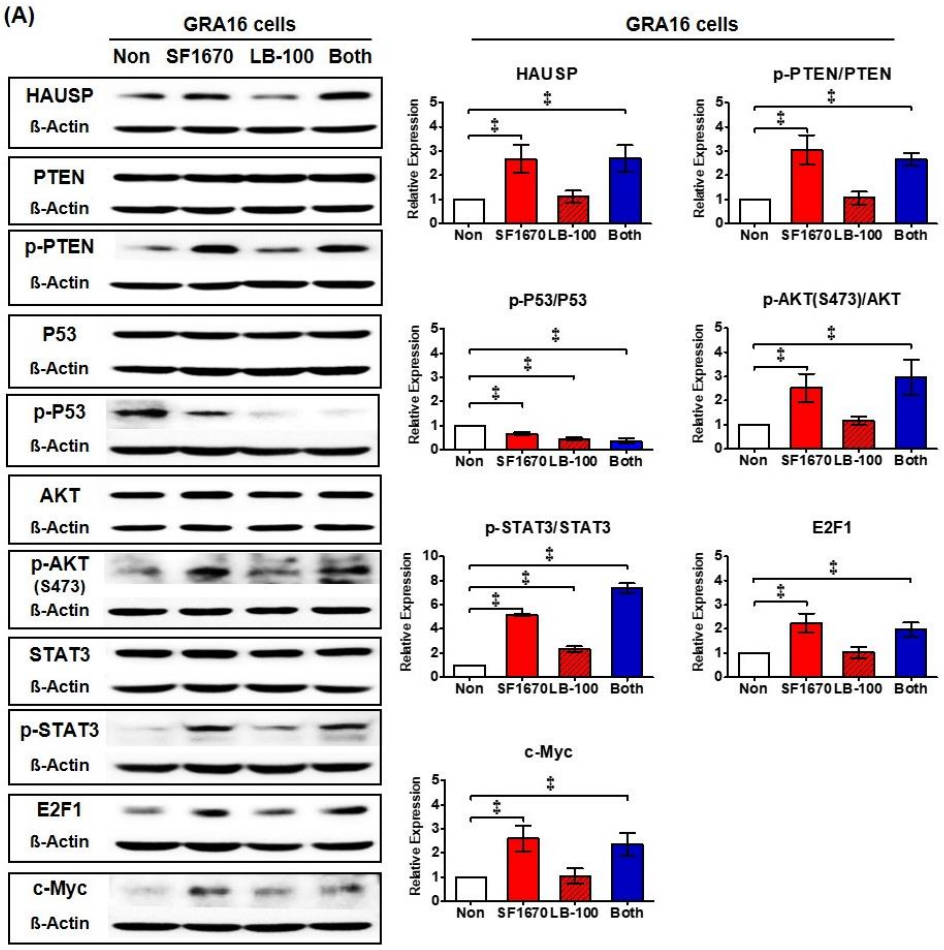

Figure 12. Identification of signaling pathway to induce hTERT inactivation in HCT116 GRA16 cells using inhibitors of PTEN and PP2A-B55 (SF1670 and LB-100, respectively). (A) Western blot images of GRA16/HAUSP/PTEN/AKT(S473) signaling pathway molecules when HCT116 GRA16 cells were treated with SF1670, LB-100, or both inhibitors and their relative protein expression (n = 3). Relative expressions of proteins were calculated by comparing each expression value in HCT116 GRA16 cells treated with each inhibitor when their expression value in nontreated HCT116 GRA16 cells (non) was set to "1". Data in this figure represent mean ± SD. ‡ Significant difference between nontreated HCT116 GRA16 cells and SF1670- and/or LB-100-treated HCT116 GRA16 cells ($p < 0.05$).

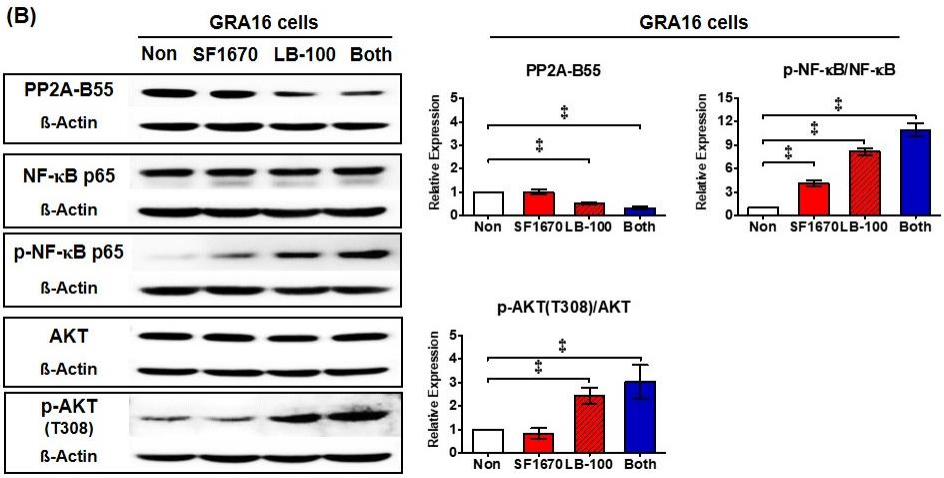

Figure 12. (Continued) Identification of signaling pathway to induce hTERT inactivation in HCT116 GRA16 cells using inhibitors of PTEN and PP2A-B55 (SF1670 and LB-100, respectively). (B) Western blot images of GRA16/PP2A-B55/p-NF-kB p65/p-AKT(T308) signaling pathway molecules when GRA16-stable cells were treated with SF1670, LB-100, or both inhibitors and their relative protein expressions (n = 3). Relative expressions of proteins were calculated by comparing each expression value in HCT116 GRA16 cells treated with each inhibitor when their expression value in nontreated HCT116 GRA16 cells (non) was set to "1". Data in this figure represent mean ± SD. ‡ Significant difference between nontreated HCT116 GRA16 cells and SF1670- and/or LB-100-treated HCT116 GRA16 cells ($p < 0.05$).

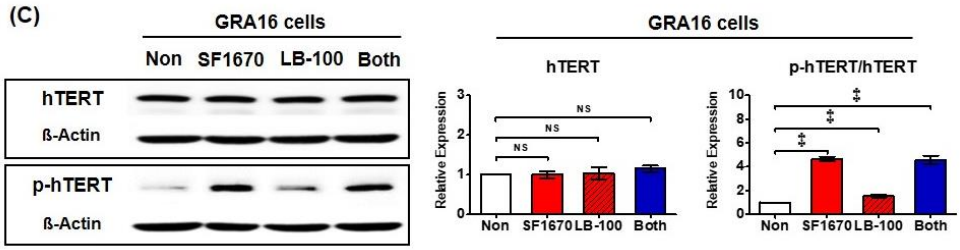

Figure 12. (Continued) Identification of signaling pathway to induce hTERT inactivation in HCT116 GRA16 cells using inhibitors of PTEN and PP2A-B55 (SF1670 and LB-100, respectively). (C) Western blot images of hTERT and p-hTERT and their relative protein expressions (n = 3). Relative expressions of proteins were calculated by comparing each expression value in HCT116 GRA16 cells treated with each inhibitor when their expression value in nontreated HCT116 GRA16 cells (Non) was set to "1". Data in this figure represent mean ± SD. ‡ Significant difference between nontreated HCT116 GRA16 cells and SF1670- and/or LB-100-treated HCT116 GRA16 cells ($p < 0.05$).

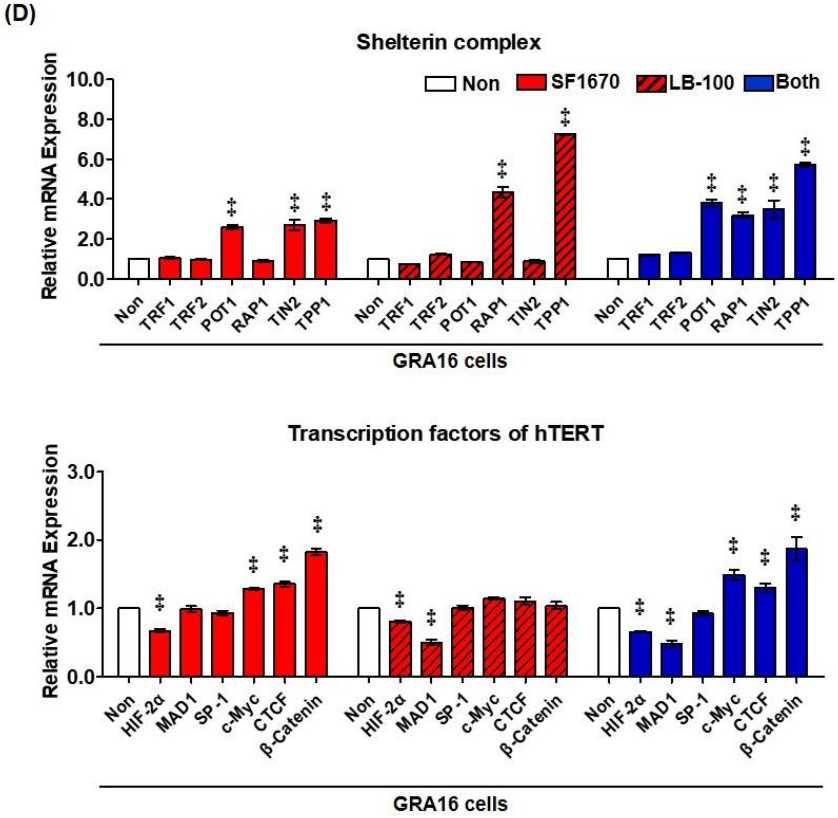

Figure 12. (Continued) Identification of signaling pathway to induce hTERT inactivation in HCT116 GRA16 cells using inhibitors of PTEN and PP2A-B55 (SF1670 and LB-100, respectively). (D) Relative mRNA expressions of shelterin complex factors and hTERT transcriptional factors responding to inhibitors of PTEN and PP2A-B55 (SF1670 and LB-100, respectively) in HCT116 GRA16 cells when the expression value of each molecule in nontreated HCT116 GRA16 cells (non) was set to "1" (n = 3). Relative expressions of mRNAs were calculated by comparing each expression value in HCT116 GRA16 cells treated with each inhibitor when their expression value in nontreated HCT116 GRA16 cells (Non) was set to "1". Data in this figure represent mean ± SD. ‡ Significant difference between nontreated HCT116 GRA16 cells and SF1670- and/or LB-100-treated HCT116 GRA16 cells ($p < 0.05$).

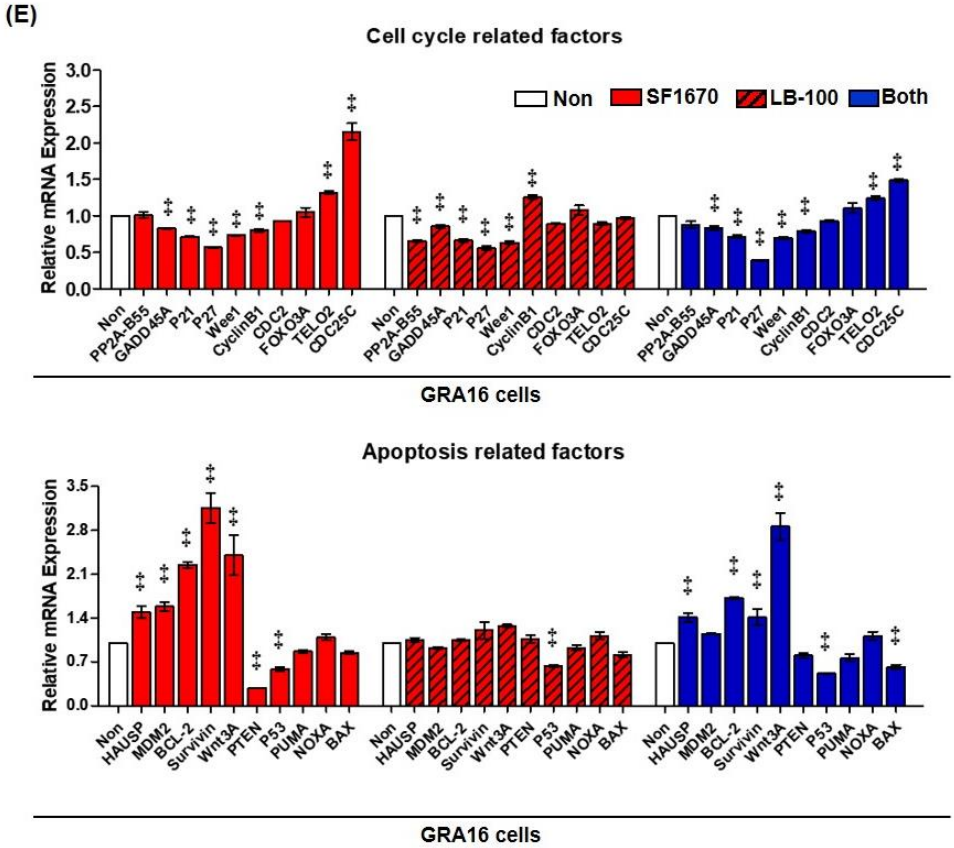

Figure 12. (Continued) Identification of signaling pathway to induce hTERT inactivation in HCT116 GRA16 cells using inhibitors of PTEN and PP2A-B55 (SF1670 and LB-100, respectively). (E) Relative mRNA expressions of cell-cycle-related factors and apoptosis-related factors responding to inhibitors of PTEN and PP2A-B55 (SF1670 and LB-100, respectively) (n = 3). Relative expressions of mRNAs were calculated by comparing each expression value in HCT116 GRA16 cells treated with each inhibitor when their expression value in nontreated HCT116 GRA16 cells (Non) was set to "1". Data in this figure represent mean ± SD. ‡ Significant difference between nontreated HCT116 GRA16 cells and SF1670- and/or LB-100-treated HCT116 GRA16 cells ($p < 0.05$).

3.2.6. Changes in telomerase-related signaling pathway in HCT116 GRA16 cells with gene silencing to PTEN or PP2A-B55

Using inhibitors, PTEN rather than PP2A-B55 blocking significantly increased the levels of p-hTERT, implying that the PTEN signaling pathway is essential for hTERT inactivation in the HCT116 GRA16 cells. To confirm these results, the gene silencing technique was used to elucidate the molecular mechanisms responsible for hTERT inactivation. When PTEN siRNA was transfected into HCT116 GRA16 cells, the PTEN expression was blocked entirely compared to the mock and siRNA control groups (Figure 13A). When PP2A-B55 siRNA was transfected, the PP2A-B55 expression was completely blocked (Figure 13B). The changes in crucial factors regulating the expression of hTERT among the downstream signaling molecules triggered after GRA16 binding to HAUSP or PP2A-B55 under blocked expression of PTEN or PP2A-B55 are shown in Figure 13. The expression of p-P53 decreased, and the expression of p-NF-kB p65 increased in PTEN siRNA-transfected and PP2A-B55 siRNA-transfected groups compared with the mock and siRNA control groups (Figures 13A and 13B). Regarding other signaling molecules, when PTEN siRNA was transfected into HCT116 GRA16 cells, the expression of p-AKT(S473), p-STAT3, E2F1, and c-Myc increased (Figure 13A). However, when PP2A-B55 siRNA was transfected into HCT116 GRA16 cells, the expression of p-AKT(T308) increased, but that of other molecules, such as p-AKT(S473), p-STAT3, E2F1, and c-Myc, remained unchanged compared to the mock and siRNA control groups (Figures 13A and 13B). Meanwhile, hTERT expression and the relative expression of p-hTERT increased in PTEN siRNA-transfected HCT116 GRA16 cells but not in PP2A-B55 siRNA-transfected GRA16 cells (Figure 13C). This result suggested that the primary pathway inducing hTERT inactivation is HAUSP/PTEN/AKT(S473)/STAT3/NF-kB signaling pathway in the HCT116 GRA16 cells.

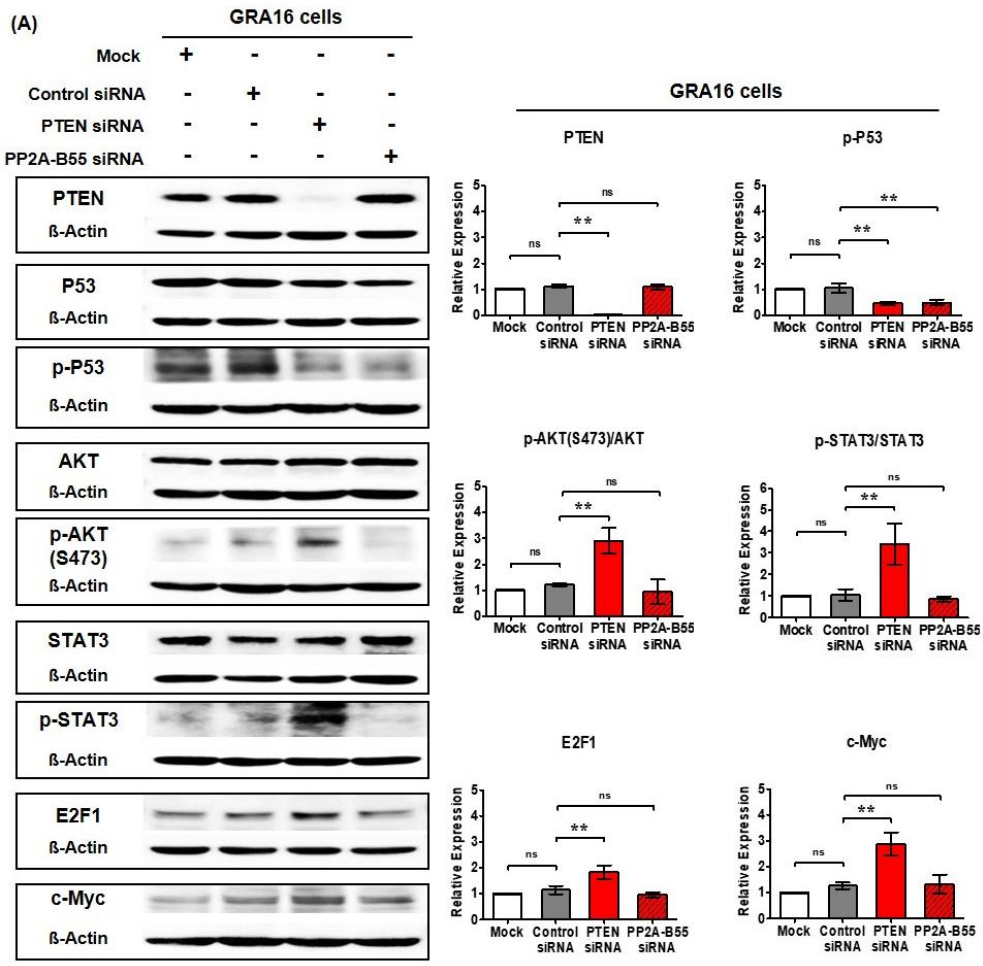

Figure 13. Changes in hTERT-related signaling molecules in HCT116 GRA16 cells transfected with PTEN siRNA or PP2A-B55 siRNA. (A) Western blot images and their relative protein expressions for GRA16/HAUSP/PTEN/AKT(S473) signaling pathway molecules and hTERT transcription factors in PTEN siRNA- or PP2A-B55 siRNA-transfected HCT116 GRA16 cells (n = 3). The expression value of each molecule in the nontransfection group (mock) was set to "1", and then the relative expression of each molecule in HCT116 GRA16 cells transfected with PTEN siRNA or PP2A-B55 siRNA was calculated. Data represent mean ± SD. ** Significant difference at $p < 0.05$ between control siRNA transfection and PTEN siRNA or PP2A-B55 siRNA transfection.

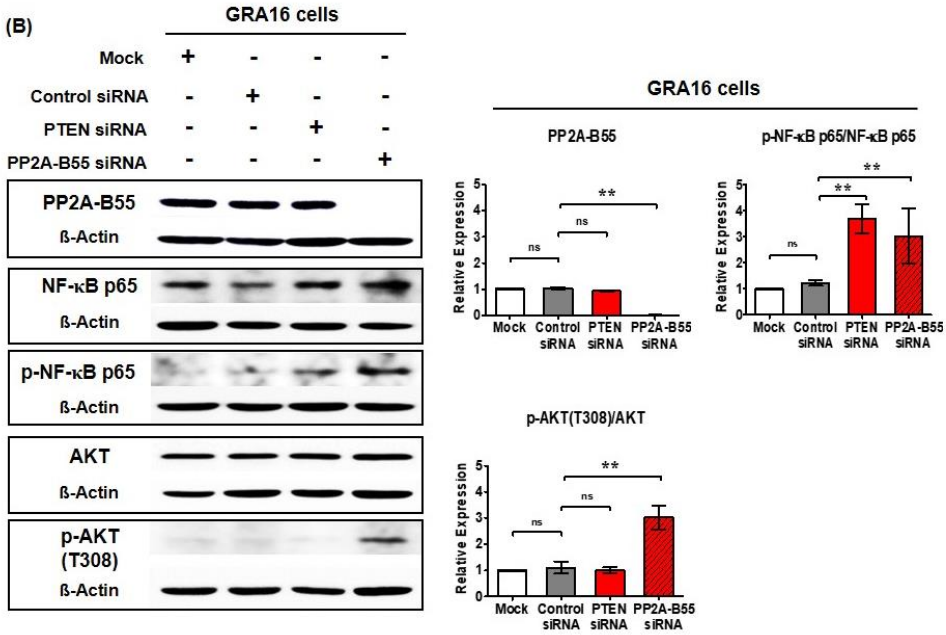

Figure 13. (Continued) Changes in hTERT-related signaling molecules in HCT116 GRA16 cells transfected with PTEN siRNA or PP2A-B55 siRNA. (B) Western blot images and their relative protein expressions for PP2A-B55/NF-kB/AKT(T308) signaling pathway molecules in PTEN siRNA- or PP2A-B55 siRNA-transfected HCT116 GRA16 cells (n = 3). The expression value of each molecule in the nontransfection group (Mock) was set to "1", and then the relative expression of each molecule in HCT116 GRA16 cells transfected with PTEN siRNA or PP2A-B55 siRNA was calculated. Data represent mean ± SD. ** Significant difference at $p < 0.05$ between control siRNA transfection and PTEN siRNA or PP2A-B55 siRNA transfection.

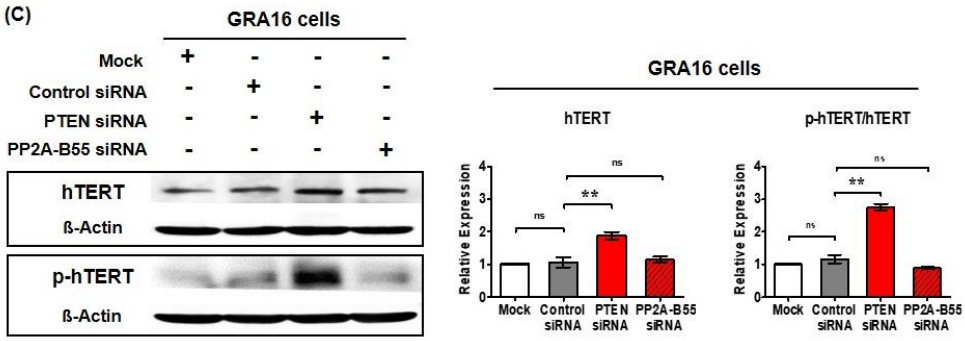

Figure 13. (Continued) Changes in hTERT-related signaling molecules in HCT116 GRA16 cells transfected with PTEN siRNA or PP2A-B55 siRNA. (C) Western blot images and their relative protein expressions for hTERT and p-hTERT in PTEN siRNA- or PP2A-B55 siRNA-transfected HCT116 GRA16 cells (n = 3). The expression value of each molecule in the nontransfection group (Mock) was set to "1", and then the relative expression of each molecule in HCT116 GRA16 cells transfected with PTEN siRNA or PP2A-B55 siRNA was calculated. Data represent mean ± SD. ** Significant difference at $p < 0.05$ between control siRNA transfection and PTEN siRNA or PP2A-B55 siRNA transfection.

3.2.7. Increases in the γ-H2A.X and the decrease in the phosphorylation of hTERT in *T. gondii*-infected HCT116 cells

GRA16 is a dense granule protein secreted within *T. gondii;* therefore, I explored whether the hTERT-related cellular phenomena observed in HCT116 GRA16 cells were observed in *T. gondii*-infected HCT116 cells (Figure 14). Furthermore, I investigated the expression of phosphorylated histone H2A.X (γ-H2A.X) for DNA DSB analysis (Figure 14A). The results showed an increase in the expression of γ-H2A.X (phosphorylated histone H2A.X) in *T. gondii*-infected HCT116 cells (Figure 14A); the white arrows in the figure indicated nucleus, and the yellow arrows indicated *T. gondii* tachyzoites. *T. gondii* infection was successfully established in the HCT116 cells as shown by TP3 protein expression, and simultaneously, the protein expression of γ-H2A.X significantly increased 48 h after infection under the amplified *T. gondii* (Figure 14B). I investigated whether hTERT is affected by GRA16 in *T. gondii*-infected HCT116 cells and observed that the phosphorylation of hTERT significantly decreased after *T. gondii* infection (Figure 14C). Meanwhile, the *gra16* gene expression was confirmed in *T. gondii*-infected HCT116 cells (Figure 14D). Overall, because the increase in H2A.X phosphorylation and the decrease in hTERT phosphorylation were commonly observed in HCT116 GRA16 and *T. gondii*-infected HCT116 cells, I concluded that GRA16 has a role in inducting hTERT inactivation in cancer cells.

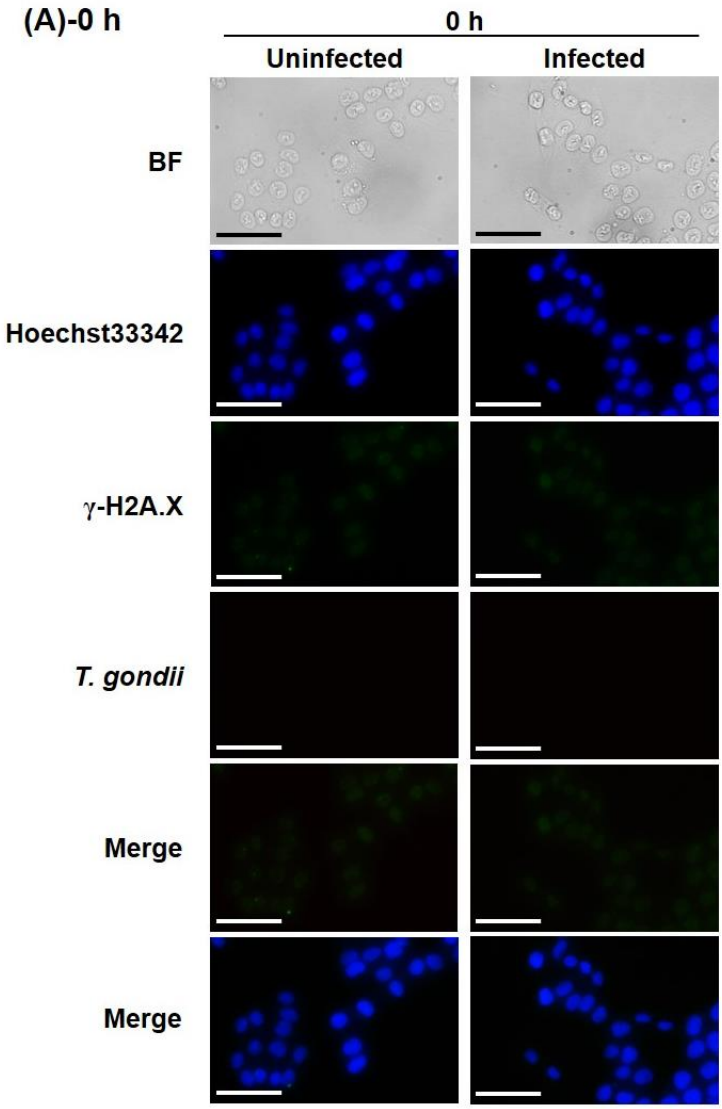

Figure 14. Increase in DNA damage (γ-H2A.X-stained nucleus) and inactivation of hTERT in *T. gondii*-infected HCT116 cells. (A)-0 h Immunofluorescence images showing the increase in γ-H2A.X-stained nucleus at 0 h after *T. gondii* infection. Scale bars represent 50 μm.

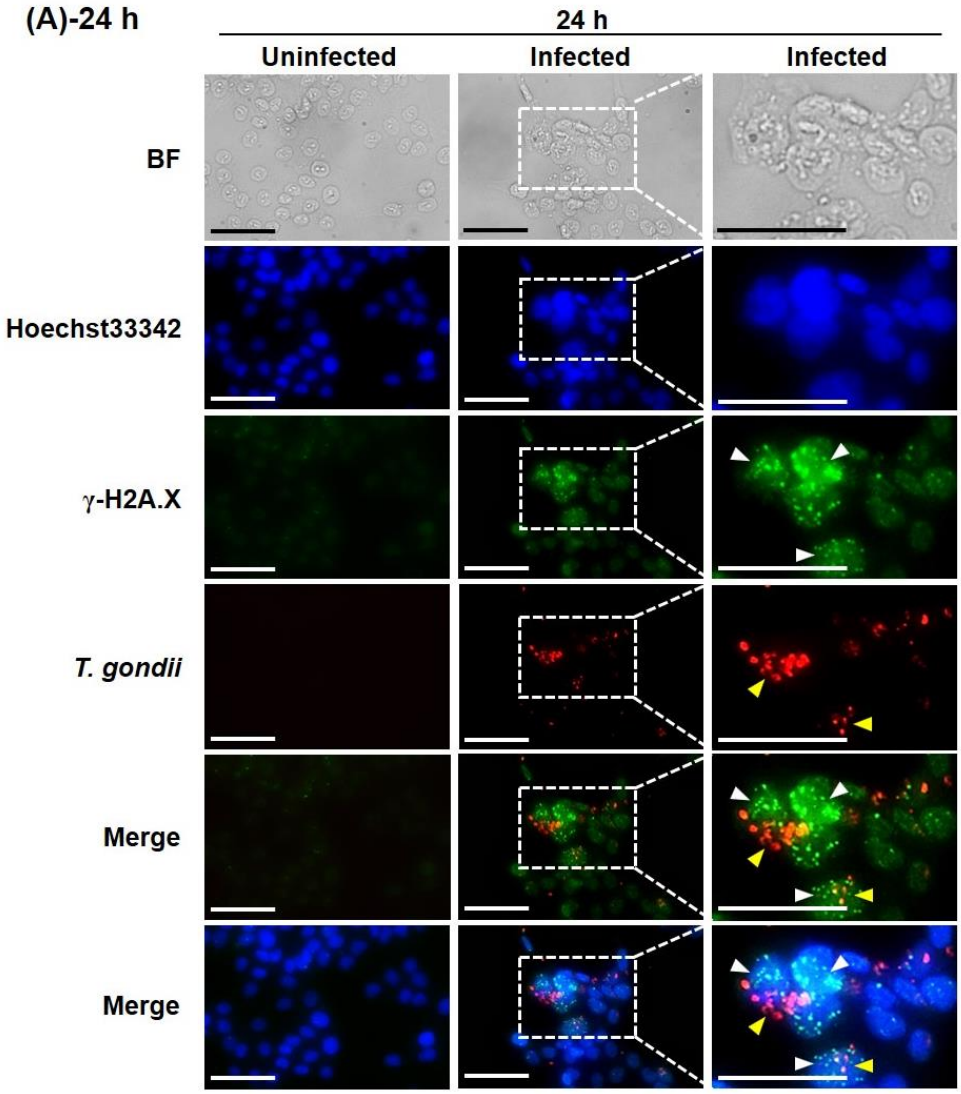

Figure 14. (Continued) Increase in DNA damage (γ-H2A.X-stained nucleus) and inactivation of hTERT in *T. gondii*-infected HCT116 cells. (A)-24 h Immunofluorescence images showing the increase in γ-H2A.X-stained nucleus at 24 h after *T. gondii* infection. Scale bars represent 50 μm. White arrows indicate γ-H2A.X- stained nuclei. Yellow arrows indicate *T. gondii* tachyzoites stained with TP3, a *T. gondii*-specific marker, antibody in the cytoplasm of HCT116 cells (n = 3).

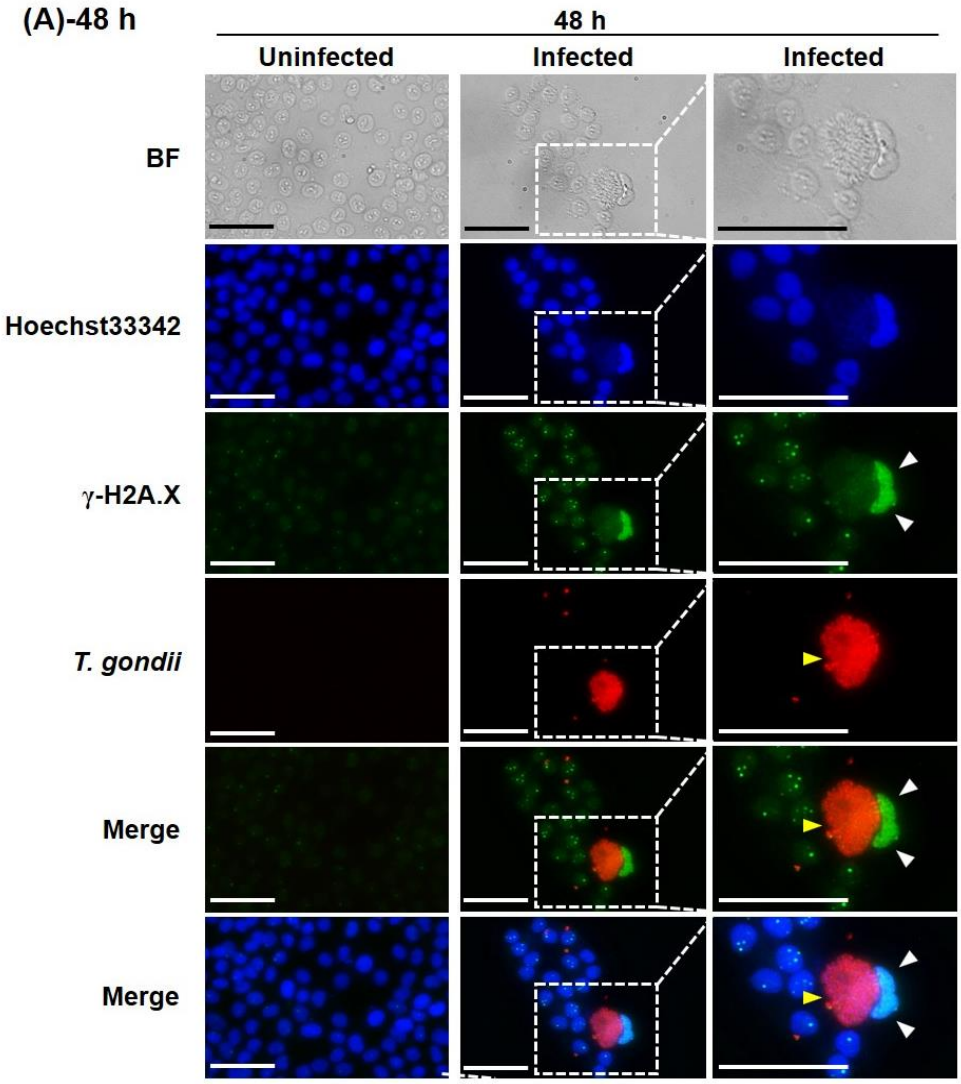

Figure 14. (Continued) Increase in DNA damage (γ-H2A.X-stained nucleus) and inactivation of hTERT in *T. gondii*-infected HCT116 cells. (A)-48 h Immunofluorescence images showing the increase in γ-H2A.X-stained nucleus at 48 h after *T. gondii* infection. Scale bars represent 50 μm. White arrows indicate γ-H2A.X- stained nuclei. Yellow arrows indicate *T. gondii* tachyzoites stained with TP3, a *T. gondii*-specific marker, antibody in the cytoplasm of HCT116 cells (n = 3).

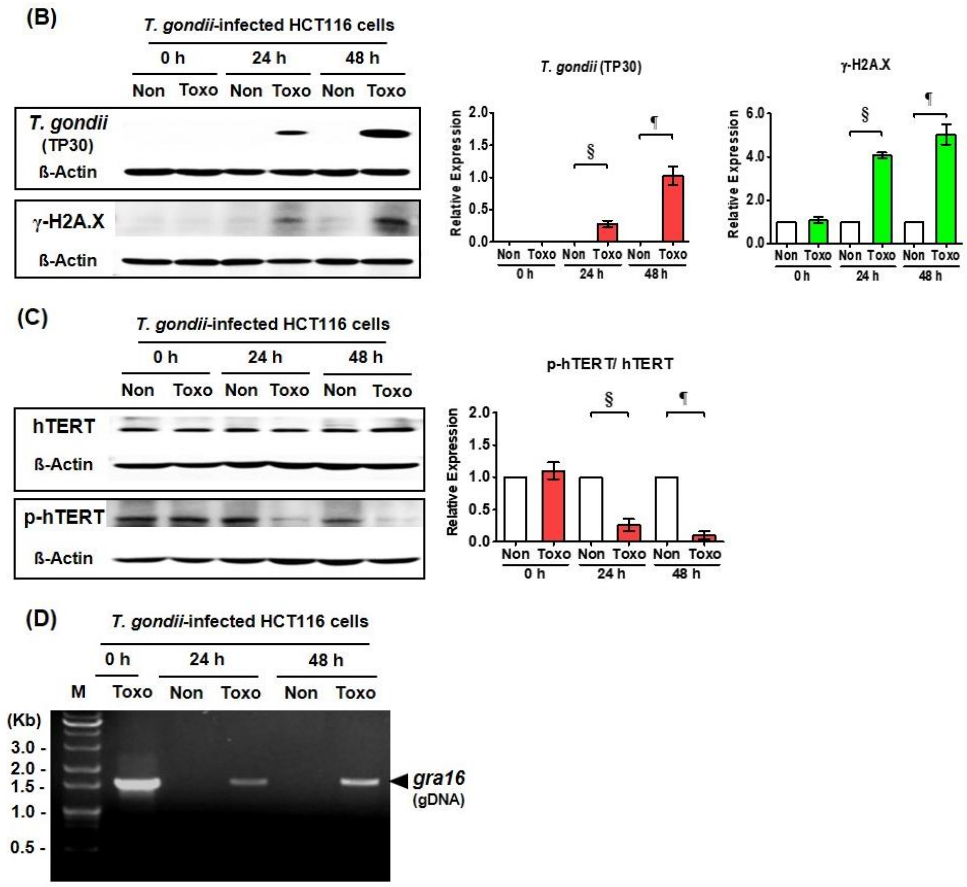

Figure 14. (Continued) Increase in DNA damage (γ-H2A.X-stained nucleus) and inactivation of hTERT in *T. gondii*-infected HCT116 cells. (B) The positive relationship between *T. gondii* infection and the increased γ-H2A.X in western blot images and their relative expression analysis (n = 3). (C) Decrease in p-hTERT expression in HCT116 cells at 24 and 48 h after *T. gondii* infection (n = 3). (D) *gra16* gene expression in *T. gondii*-infected HCT116 cells at 24 and 48 h after *T. gondii* infection (n = 3). Data represent mean ± SD. The relative expressions of proteins in each experiment were calculated by comparing each expression value in *T. gondii*-infected HCT116 cells, with their expression value in noninfected HCT116 cells (Non) set to "1". § Significant difference at 24 h after infection and ¶ Significant difference at 48 h after infection between noninfected HCT116 cells and *T. gondii*-infected HCT116 cells ($p < 0.05$).

4. Discussion

In this study, I demonstrated that GRA16, a dense granule protein secreted by *T. gondii* for its intracellular parasitism and trafficking to the infected host cell nucleus, exerts anticancer effects by stabilization of PTEN and P53, and inhibition of NF-kB and hTERT, after binding HAUSP and PP2A-B55 in the NSCLC and CRC cells. The protozoan parasite, *T. gondii*, invades the host cells and resides in the PVs surrounded by PVMs. Once inside the PV, tachyzoites secrete GRA16 and are transported beyond the PVM via putative translocon [9, 30]. In the chronic stage, *T. gondii* converts from tachyzoites to bradyzoites, and tissue cysts are formed to maintain a dormant state until reactivation [31]. GRA16 is secreted from tachyzoites and bradyzoites; however, it does not pass through the cyst wall and accumulates within the cyst [30].

GRA16 binds HAUSP and PP2A-B55 in the host cells [9]. However, the regulatory mechanism after binding to the corresponding proteins or their mechanism of action in cancer cells has not been studied until recently. HAUSP and PP2A-B55 bind to GRA16 and are essential for cancer cell's activation and inhibition. HAUSP is highly expressed in several types of cancer and is a crucial deubiquitinase that regulates cell-cycle, DNA repair, chromatin remodeling, and epigenetic regulation. Abnormal activity and overexpression of HAUSP promote oncogenesis, making it a target for therapeutic intervention [32]. Serine/Threonine phosphatase PP2A-B55 is a master cell-cycle regulator that acts as a gatekeeper from mitotic entry to exit cell division [33]. PP2A-B55 deficiency is also associated with poor prognosis in cancer patients [25]. The results of previous studies showed that GRA16 binds to HAUSP and PP2A-B55 in host cells, supporting the possibility of applying GRA16 for the target-specific anticancer candidate in this study [9, 34].

Study-I confirmed that GRA16 increased PP2A-B55, inhibited AKT phosphorylation (T308), and blocked nucleus translocation of NF-kB, a transcriptional factor in *p53*-null NSCLC cells (H1299).

This indicated that inhibiting the transcription of essential factors for cancer cell proliferation and metastasis induces cancer cell-cycle arrest and cancer cell apoptosis in the pathways. Herein, I showed that GRA16, which modulates the PP2A-B55/AKT/NF-kB signaling cascade, could be used as an alternative adjuvant therapy to reduce the chemoresistance of *p53*-mutant NSCLC with irinotecan as a chemotherapeutic agent. The topoisomerase-I inhibitor, irinotecan, is used as a chemotherapeutic agent for various types of cancer, including lung cancer [35]. However, long-term use of irinotecan or AKT and NF-kB activation, which are not irinotecan targets, reduce the effectiveness of irinotecan by inducing cancer cell survival and chemoresistance [25, 36].

Furthermore, AKT upregulates NF-kB to induce translocation to the nucleus. NF-kB enters the nucleus and increases the expression of crucial factors for cancer cell proliferation and metastasis as a transcription factor [37].

In NSCLC without P53 expression, since the binding of GRA16 and HAUSP does not affect the activation of P53, it is possible to analyze the changes in the mechanism of cancer cells caused by the binding of GRA16 and PP2A-B55. My study results confirmed that GRA16 in H1299 cells binds to PP2A-B55 and inhibits AKT to block the nuclear translocation of NF-kB. In addition, from a lung cancer xenograft mouse model, the results were obtained in which tumor growth was inhibited when GRA16 was expressed in the tumor cells, which showed that GRA16 could induce cell-cycle arrest and apoptosis by regulating the PP2A/AKT/NF-kB pathway. The study-I results showed that GRA16 could be used as an adjuvant to compensate for the inability to inhibit the NF-kB pathway, a limitation of irinotecan. These data suggested that GRA16 could act as a novel AKT/NF-kB modulating adjuvant chemotherapy for irinotecan-resistant NSCLC.

Study II showed that *p53* and *nf-kb* wild-type colorectal cancer cells (HCT116) were used to induce apoptosis via the two binding mechanisms of GRA16 in cancer cells. I focused on telomerase as a new crucial factor that positively affects the uncontrolled

proliferation of cancer cells under conditions where AKT inhibition is essential for the anticancer action of GRA16 [38]. Among the AKTs distributed in the cytoplasm and nucleus, the question of whether GRA16 can regulate cytoplasmic AKT in the process of translocation from the PVM to the host nucleus could be resolved by confirming that GRA16 is localized in the nucleus and cytoplasm of GRA16 expressing cancer cells (Figure 1B) [31, 39]. This is significant because GRA16, which aims to identify the anticancer effects, can regulate all AKTs in the cytoplasm and nucleus of cancer cells.

Meanwhile, telomerase activation is the biggest difference between normal and cancer cells. In more than 90% of cancers, telomerase activity is high, and hTERT, which plays a functional role of telomerase as a telomerase catalytic subunit, is highly expressed in cancer cells [40]. In cancer cells, telomerase blocks the natural telomere shortening by continuously maintaining a repeating sequence (TTAGGG) located at the end of the telomere [40]. As a result, abnormal gene expression and continuous cell division proceeds, and cancer cells proliferate indefinitely. It is emerging as a therapeutic strategy targeting telomerase while developing anticancer drugs, but no commercially available anticancer drugs inhibit telomerase [41]. hTERT, which AKT directly regulates, is activated through phosphorylation and leads to the functional activity of telomerase. AKT-dependent signaling is essential for telomere length maintenance, including telomerase activation, telomere protection, and telomere-binding shelterin complex stability [42, 43]. The representative transcriptional regulators of hTERT, include STAT3, c-Myc, NF-kB, HIF-2α, MAD1, and P53, respectively, with transcriptional activation (STAT3, c-Myc, and NF-kB) and transcriptional suppression (HIF-2α, MAD1, and P53). As identified by previous studies and study-I, GRA16 inhibits AKT by binding HAUSP and PP2A-B55. In the case of GRA16/HAUSP, p-AKT(S473) was inhibited, whereas in the case of GRA16/PP2A-B55, p-AKT(T308) was inhibited. Although AKT phosphorylation (S473 and T308) is

required for maximal activation of the protein kinase, the main consideration for validating the signaling pathway of AKT for hTERT regulation is to evaluate the two AKT mechanisms. It is the reduction of p-AKT(S473) in a PTEN-dependent manner and the reduction of p-AKT(T308) in a PP2A-B55-dependent manner in GRA16-expressing cancer cells [44-46].

Therefore, in study II, I confirmed whether AKT inhibition had a negative effect on hTERT expression and telomerase activity in cancer cells concerning the anticancer effects of GRA16. In addition, I analyzed the telomere shortening, increased DNA damage indicator factors, and increased nuclear size as precursors of cancer cell apoptosis. Finally, the central mechanism that directly affects hTERT regulation among the two mechanisms of GRA16 in cancer cells was identified using inhibitors of PTEN and PP2A or through gene silencing using siRNA transfection of PTEN and PP2A-B55. The function of the PP2A enzyme depends on which regulatory subunit binds to PP2A. The regulatory subunits are classified as B (PR55; B55), B' (PR56/61), B'' (PR59, PR72, PR130), and B''' (PR93/PR110) [47]. Currently, there is no PP2A-B55-specific inhibitor. However, LB-100 and other PP2As, can also inhibit PP2A-B55 increased by GRA16. Therefore, in this study, both LB-100 treatment and *pp2A-b55* gene-specific silencing were performed, and the results were similar.

In HCT116 GRA16 cells, PTEN and P53 were activated, and both NF-kB and AKT were suppressed with the decrease of HAUSP and increase of PP2A-B55. The results were similar to those confirmed in a previous study and study-I. In addition, STAT3, E2F1, c-Myc, SP-1, CTCF, and β-catenin, the transcriptional activators of hTERT, decreased, while HIF-2α and MAD1, the transcriptional repressors of hTERT, increased during the expression of GRA16. However, in the case of c-Myc, a recently published article showed that *T. gondii* uses GRA16 for host c-Myc up-regulation [48]. In the article, the cells were infected with *gra16*-transfected *Neospora caninum (N. caninum)*. As a result, GRA16-expressing *N. caninum* induced c-Myc activation in the host cells [48]. However,

the role of GRA16 and the effects of the parasite cannot be ignored. It is difficult to compare the two opposite results directly; therefore, I confirmed the suppression of c-Myc by expressing GRA16 alone.

GRA16 significantly decreased the expression and phosphorylation of hTERT, which led to a decrease in telomerase activity and telomere shortening. From the results of telomerase inhibition via AKT down-regulation of GRA16, we analyzed the main signaling pathways that regulate the direct activity of hTERT via GRA16-regulated PTEN and PP2A inhibitors (SF1670 and LB-100). As a result, when PTEN was inhibited, the expression of the transcriptional regulators of hTERT and hTERT was remarkably changed. These results were more evident in the *pten* knock-down and *pp2a-b55* knock-down through gene silencing. In study II, I confirmed that GRA16 could decrease telomerase activity and induce telomere shortening via the HAUSP/PTEN/AKT(S473)/P53/NF-kB signaling pathway as a pre-apoptosis stage in cancer cells.

Overall, in this study, GRA16 can induce apoptosis by binding to HAUSP and PP2A-B55 in cancer cells and can induce synergistic effects of commercial anticancer drugs. In addition, the results of telomerase inhibition and telomere shortening centering on AKT in the HAUSP and PP2A-B55 regulatory pathways of GRA16 highlight the need for detailed studies in the future as a target-specific anticancer candidate of GRA16. I summarized these results as a schematic diagram (Figure 15).

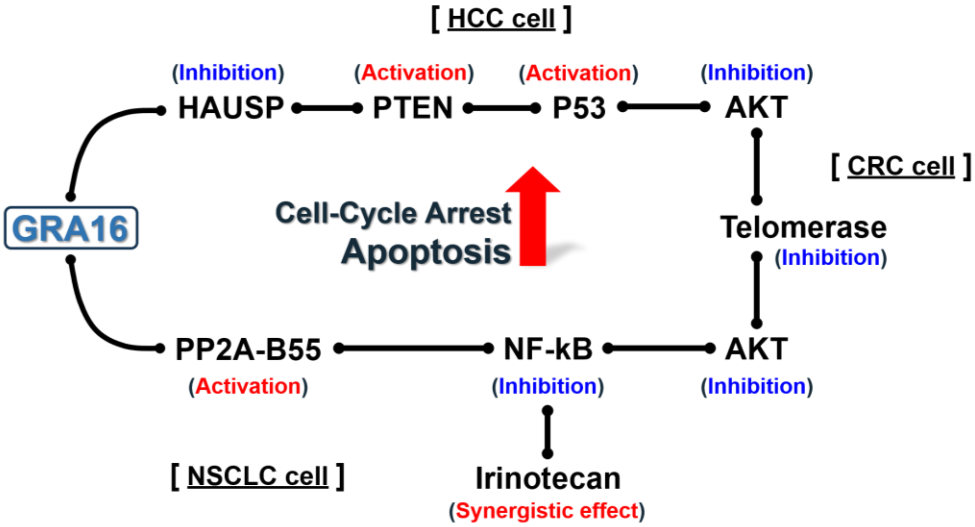

Figure 15. Summary of this study. *T. gondii* GRA16 induces cancer cell-cycle arrest and apoptosis via the PTEN/P53/AKT mechanism by binding HAUSP in the HCC cells. Also, GRA16 inhibits the NF-kB/AKT mechanism by binding PP2A-B55 in the NSCLC cells and enhancing irinotecan's synergistic effects. GRA16 inhibits telomerase, induces telomere shortening, and causes DNA damage in the CRC cells, the stages before cancer cell apoptosis.

5. Bibliography

1. Botelho, M.C. and Richter, J. "parasites and cancer." *Frontiers in medicine* 6 (2019): 55.
2. Zhao, X.Y. and Ewald, S.E. "The molecular biology and immune control of chronic *Toxoplasma gondii* infection." *The Journal of Clinical Investigation* 130.7 (2020): 3370-3380.
3. Tender, A.M., Heckeroth, A.R., and Weiss, L.M. "*Toxoplasma gondii:* from animals to humans." *International Journal for Parasitology* 30.12-13 (2000): 1217-1258.
4. Hakimi, M.A., Olias, P., and Sibley, L.D. "Toxoplasma effectors targeting host signaling and transcription." Clinical microbiology reviews 30.3 (2017): 615-645.
5. Rezaei, F., et al. "A systematic review of *Toxoplasma gondii* antigens to find the best vaccine candidates for immunization." *Microbial Pathogenesis* 126 (2019): 172-184.
6. Dogga, S.K., et al. "Importance of Aspartyl Protease 5 in the establishment of the intracellular niche during acute and chronic infection of *Toxoplasma gondii*." *Molecular microbiology* (2022).
7. Mercer, H.L., et al. "*Toxoplasma gondii* dense granule protein GRA24 drives MyD88-independent p38 MAPK activation, IL-12 production and induction of protective immunity." *PLoS Pathogens* 16.5 (2020): e1008572.
8. Arne, L., et al. "The *Toxoplasma* effector GRA28 promotes parasite dissemination by inducing dendritic cell-like migratory properties in infected macrophages." *Cell Host & Microbe* 30.11 (2022): 1570-1588.
9. Bougdour, A., et al. "Host cell subversion by *Toxoplasma* GRA16, an exported dense granule protein that targets the host cell nucleus and alters gene expression." *Cell host & microbe* 13.4 (2013): 489-500.
10. Callejas, B.E., Martinez-Saucedo, D., and Terrazas, L.I. "Parasites as negative regulators of cancer." *Bioscience reports* 38.5 (2018).
11. Statistics Korea. "Statistics on causes of death in 2021." *Vital*

Statistics Division, Social Statistics Bureau (2022).
12. Van Tong, H., et al. "Parasite infection, carcinogenesis and human malignancy." *EBioMedicine* 15 (2017): 12-23.
https://www.kostat.go.kr/portal/korea/kor_nw/1/6/2/index.board.
13. Hunter, C.A., et al. "Cutting edge: systemic inhibition of angiogenesis underlies resistance to tumors during acute toxoplasmosis." *The Journal of Immunology* 166.10 (2001): 5878-5881.
14. Hafez, E.N., et al. "Gamma radiation-attenuated toxoplasma gondii provokes apoptosis in Ehrlich ascites carcinoma-bearing mice generating long-lasting immunity." *Technology in Cancer Research & Treatment* 19 (2020): 1533033820926593.
15. Kim, J.O., et al. "Inhibition of Lewis lung carcinoma growth by *Toxoplasma gondii* through induction of Th1 immune responses and inhibition of angiogenesis." *Journal of Korean medical science* 22.Suppl (2007): S38-S46.
16. Zhu, S., et al. "Anti-Tumoral Effect and Action Mechanism of Exosomes Derived From *Toxoplasma gondii*-Infected Dendritic Cells in Mice Colorectal Cancer." *Frontiers in oncology* 12 (2022): 870528-870528.
17. Kim, Y.R., et al. "*Toxoplasma gondii* GRA8 induces ATP5A1-SIRT3-mediated mitochondrial metabolic resuscitation: a potential therapy for sepsis." *Experimental & molecular medicine* 50.3 (2018): e464-e464.
18. Wei, R., et al. "Deubiquitinases in cancer." *Oncotarget* 6.15 (2015): 12872.
19. Trotman, L.C., et al. "Ubiquitination regulates PTEN nuclear import and tumor suppression." *Cell* 128.1 (2007): 141-156.
20. Nakanishi, A., et al. "The tumor suppressor PTEN interacts with p53 in hereditary cancer." *International Journal of Oncology* 44.6 (2014): 1813-1819.
21. Davis, M.I. and Anton S. "Ubiquitin-specific proteases as druggable targets." *Drug target review* 2.3 (2015): 60.
22. Tavana, O. and Wei G. "Modulation of the p53/MDM2 interplay by HAUSP inhibitors." *Journal of Molecular Cell Biology* 9.1

(2017): 45-52.
23. Barisic, S., et al. "Identification of PP2A as a crucial regulator of the NF-kB feedback loop: its inhibition by UVB turns NF-kB into a pro-apoptotic factor." *Cell Death & Differentiation* 15.11 (2008): 1681-1690.
24. Ikeda, R., et al. "Establishment and characterization of irinotecan-resistant human non-small cell lung cancer A549 cells." *Molecular Medicine Reports* 3.6 (2010): 1031-1034.
25. Nader, C.P., et al. "Protein phosphatase 2A (PP2A): a key phosphatase in the progression of chronic obstructive pulmonary disease (COPD) to lung cancer." *Respiratory Research* 20.1 (2019): 1-18.
26. Kim, S.G. and Seo, S.H., et al. "Increase in the nuclear localization of PTEN by the *Toxoplasma* GRA16 protein and subsequent induction of p53-dependent apoptosis and anticancer effect." *Journal of Cellular and Molecular Medicine* 23.5 (2019): 3234-3245.
27. Qiu, G.H., et al. "Distinctive pharmacological differences between liver cancer cell lines HepG2 and Hep3B." *Cytotechnology* 67.1 (2015): 1-12.
28. Cawthon, R.M. "Telomere measurement by quantitative PCR." *Nucleic acids research* 30.10 (2002): e47-e47.
29. Carlsson, G., Gullberg, B., Hafström L.O. "Estimation of liver tumor volume using different formulas—an experimental study in rats." Journal of cancer research and clinical oncology 105.1 (1983): 20-23.
30. Krishnamurthy, S. and Jeroen P.J.S. "*Toxoplasma* does not secrete the GRA16 and GRA24 effectors beyond the parasitophorous vacuole membrane of tissue cysts." *Frontiers in cellular and infection microbiology* 8 (2018): 366.
31. Sinai, A.P., et al. "Reexamining chronic *Toxoplasma gondii* infection: surprising activity for a "dormant" parasite." *Current Clinical Microbiology Reports* 3.4 (2016): 175-185.
32. Wang, Z. et al. "USP7: novel drug target in cancer therapy." *Frontiers in Pharmacology* 10 (2019): 427.

33. Wlodarchak, N. and Yongna X. "PP2A as a master regulator of the cell cycle." *Critical reviews in biochemistry and molecular biology* 51.3 (2016): 162-184.
34. Krishnamurthy, S. and Saeij, J.P.J. "*Toxoplasma* does not secrete the GRA16 and GRA24 effectors beyond the parasitophorous vacuole membrane of tissue cysts." *Frontiers in cellular and infection microbiology* 8 (2018): 366.
35. Denes, A. "The role of irinotecan in non-small cell and small-cell lung cancer." *Oncology Research and Treatment* 23.Suppl. 6 (2000): 25-27.
36. Ruvolo, P.P. "The broken "Off" switch in cancer signaling: PP2A as a regulator of tumorigenesis, drug resistance, and immune surveillance." BBA clinical 6 (2016): 87-99.
37. Dimitrakopoulos, F.I.D., et al. "The Fire Within: NF-kB Involvement in Non-Small Cell Lung Cancer." *Cancer Research* 80.19 (2020): 4025-4036.
38. Sasaki, T., et al. "AKT activation and telomerase reverse transcriptase expression are concurrently associated with prognosis of gastric cancer." *Pathobiology* 81.1 (2014): 36-41.
39. Rosner, M., et al. "Nuclear/cytoplasmic localization of Akt activity in the cell cycle." *Amino acids* 32.3 (2007): 341-345.
40. Jafri, M.A., et al. "Roles of telomeres and telomerase in cancer, and advances in telomerase-targeted therapies." *Genome medicine* 8.1 (2016): 1-18.
41. Berei, J. et al. "Potential telomere-related pharmacological targets." *Current Topics in Medicinal Chemistry* 20.6 (2020): 458-484.
42. Sánchez-Vázquez, R., Paula M., and Maria, A.B. "AKT-dependent signaling of extracellular cues through telomeres impact on tumorigenesis." *PLoS genetics* 17.3 (2021): e1009410.
43. Sasaki, T., et al. "AKT activation and telomerase reverse transcriptase expression are concurrently associated with prognosis of gastric cancer." *Pathobiology* 81.1 (2014): 36-41.
44. Kang, S.S., Taegun K., and Su I.D. "Akt protein kinase enhances human telomerase activity through phosphorylation of telomerase

reverse transcriptase subunit." *Journal of Biological Chemistry* 274.19 (1999): 13085-13090.
45. Manning, B.D., and Alex T. "AKT/PKB signaling: navigating the network." *Cell* 169.3 (2017): 381-405.
46. Kuo, Y.C, et al. "Regulation of phosphorylation of Thr-308 of Akt, cell proliferation, and survival by the B55α regulatory subunit targeting of the protein phosphatase 2A holoenzyme to Akt." *Journal of Biological Chemistry* 283.4 (2008): 1882-1892.
47. Seshacharyulu, P., et al. "Phosphatase: PP2A structural importance, regulation and its aberrant expression in cancer." *Cancer letters* 335.1 (2013): 9-18.
48. Panas, M.W. and John C.B. "*Toxoplasma* uses GRA16 to upregulate host c-Myc." *Msphere* 5.3 (2020): e00402-20.

Abstract in Korean

암세포에서 톡소포자충 과립단백질 16 (GRA16)이 유도하는 세포주기 억제와 세포사멸에 대한 기전 규명 연구

기생충을 활용한 항암효과 연구는 난치성중증질환 중 하나인 암의 치료 효과를 높이기 위한 새로운 접근방법으로써, 기생충과 암은 선행연구 결과를 바탕으로 그 관련성이 입증되고 있다. 본 연구에서 다루고자 하는 톡소포자충은 항암 기생충 중 하나로, 톡소포자충의 감염이 암의 증식을 억제시킬 수 있음이 밝혀졌으나, 어떠한 유래 물질 또는 기전은 아직까지 알려진 바 없다. 본 논문에서는 톡소포자충과 톡소포자충 용해 항원물이 암의 증식을 억제할 수 있다는 선행연구와 톡소포자충 유래 과립단백질 16 (GRA16)이 숙주세포 내에서 HAUSP와 PP2A-B55와 결합한다는 선행연구를 근거로, 톡소포자충을 활용한 항암효과 연구의 핵심 단백질로 GRA16을 선정하고, 다양한 암세포에서 GRA16이 발현될 때 어떤 신호 전달 메커니즘이 암세포 성장을 억제할 수 있는 분석했다. 첫번째로 간암세포 (HepG2)에서 GRA16은 HAUSP와 결합하여 PTEN의 핵 내 이동과 P53의 활성을 증가시키고 p-AKT(S473)를 억제함으로써 암세포의 증식을 억제할 수 있음을 밝혔다. 두번째로 폐암세포 (H1299)에서 GRA16은 PP2A-B55와의 결합을 통해 PP2A-B55를 활성화시키고 p-AKT(T308)를 억제했다. 또한 NF-kB의 핵 내 이동을 억제했다. 특히 GRA16의 NF-kB 억제는 상용중인 항암제 (Irinotecan)가 갖지 못하는 한계점을 보완함으로써 GRA16과 irinotecan을 병용했을 때 항암효과가 더욱 증가했다. 위 결과를 바탕으로 암세포에서 GRA16이 HAUSP/PTEN/AKT/P53 경로와 PP2A-B55/AKT/NF-kB 경로를 통해 세포주기 억제와 세포사멸을 유도하고 항암제의 민감성을 높일 수 있다는 것을 새롭게 규명했다. 한편 암세포

에서 AKT는 텔로머라제의 촉매 소단위인 hTERT의 활성을 증가시켜 암의 무한한 증식을 가능하도록 한다. 두 가지 선행 연구를 통해 GRA16이 AKT를 억제한다는 점에 착안하여 세번째로는 암세포 사멸을 유도하는 GRA16이 hTERT의 발현과 활성을 어떻게 조절할 수 있는지 확인하고 세포사멸 전 발생하는 텔로미어 길이 단축에 대해 어떠한 영향을 미치는지 분석했다. 대장암세포 (HCT116)에서 GRA16은 hTERT의 발현과 인산화를 억제하고 텔로머라제의 활성을 억제했으며, 텔로미어 길이 단축을 초래했다. 표적 단백질 억제제 (PTEN inhibitor, PP2A inhibitor)와 siRNA 유전자 침묵을 통해 GRA16의 두 가지 신호전달 기전 중 hTERT의 발현과 활성을 조절하는 중심 기전이 HAUSP/PTEN/AKT/STAT3/E2F1/c-Myc 경로라는 점을 새롭게 밝혔다. 이번 연구를 통해 HAUSP, PP2A-B55와 결합하는 *T. gondii*-derived GRA16이 암세포에서 PTEN, NF-kB, AKT, hTERT를 조절함으로써 세포주기 억제, 텔로미어 단축, 세포사멸을 유도한다는 것을 확인했다. 이는 숙주 암세포에서 암의 성장을 억제할 수 있는 GRA16의 새로운 작용기전 규명과 함께 항암 억제제로써 향후 암에 대한 새로운 치료전략으로 활용할 수 있음을 시사한다.

*** 본 학위 논문은 선행으로 출판된 본 저자의 논문을 기반으로 함.**

1. SEO, Seung-Hwan, et al. (2020) *International Journal of Molecular Sciences,* 21.18: 6642.
2. SEO, Seung-Hwan, et al. (2022) *Biomedicine & Pharmacotherapy,* 153: 113366.

주요어 : 톡소포자충 유래 조밀한 과립 16, 포스파타제 및 텐신 동족체, 핵인자-카파비, 단백질인산화효소-비, 사람 텔로머라아제 역전사 효소, 항암 효과

학 번 : 2018-32737